EMAG 2022:

Multidimensional Electron Microscopy

incorporating the 75th anniversary of EMAG

5 July 2022
London, UK

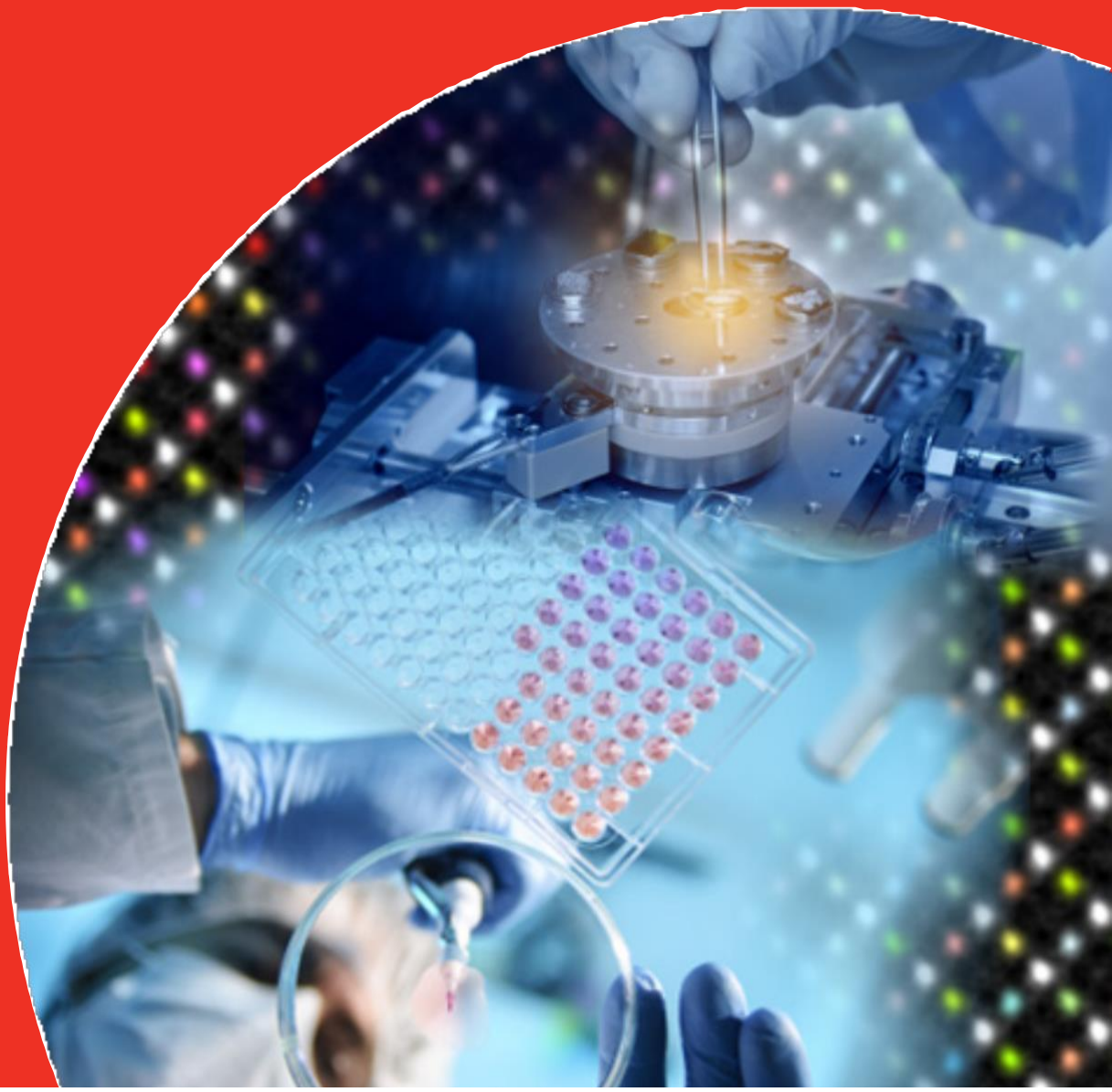

iop.org

IOP Institute of Physics

thermoscientific

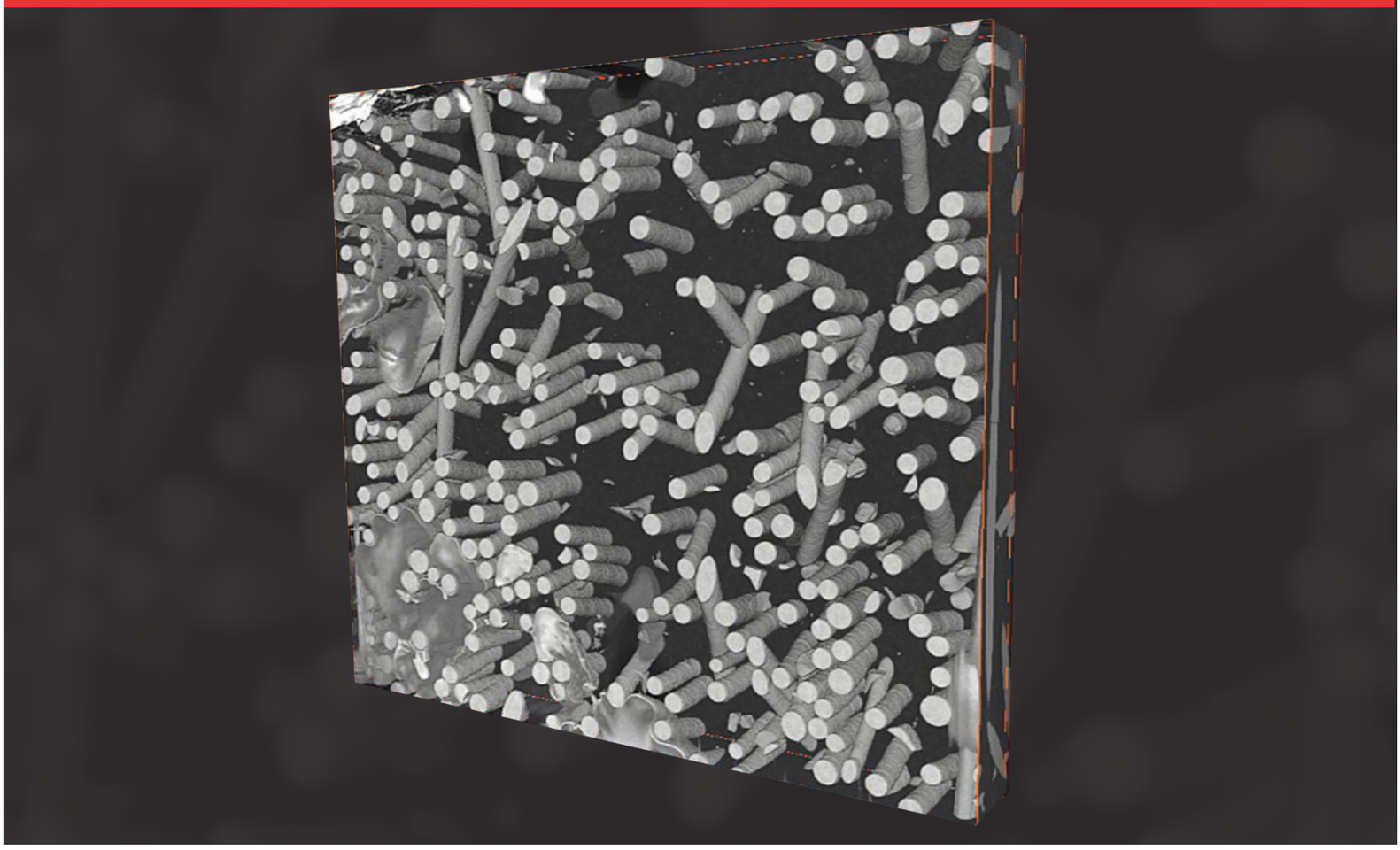

3D reconstruction of an automotive oil filter casing (polymer/glass fiber composite) acquired with a Helios Hydra CX DualBeam using O^+ focused ion beam and AS&V4 Software for automated serial sectioning (HFW is 350 µm).

Helios Hydra DualBeam

The new Thermo Scientific™ Helios™ Hydra™ DualBeam delivers four different ion species as the primary beam, allowing you to choose the ions that provide the best results for your samples and use cases, such as S/TEM sample preparation and 3D materials characterization. Switching between argon, nitrogen, oxygen and xenon is easy and can be done in under ten minutes without sacrificing performance. This unprecedented flexibility significantly expands the potential application space of FIB and enables research of ion-sample interactions to optimize the existing use cases.

Find out more at **thermofisher.com/helioshydra**

ThermoFisher SCIENTIFIC

IOP Institute of Physics

Table of Content

Welcome message from the EMAG Chair

On behalf of the EMAG committee of the Institute of Physics, I am honoured and delighted to welcome you to EMAG2022, our biennial focus meeting, with this year's theme on Multidimensional Electron Microscopy. This meeting is especially interesting on several accounts. Just over 75 year ago, the predecessor of the EMAG group, the electron microscopy group of the Institute of Physics was founded. As appropriate, our celebration part of the event will be taking place in the new headquarter of the Institute of Physics at Kings Cross, followed by a dinner at the nearby London Canal Museum.

The technical part of the focus meeting will be held at Imperial College, South Kensington. The first electron microscope produced in UK by Metropolitan Vickers in the UK was designed by Prof. L. C. Martin at Imperial College. This and other early electron microscopes set the scene for the birth of the electron microscopy community in the UK and the EMAG group in particular. It is therefore highly symbolic that Imperial College again acts as a host to EMAG meetings.

The EMAG committee has organized a rich and varied program covering many aspects of new development in multidimensional electron microscopy, covering not only spatial, but also temporal, diffractional and spectral dimensions and their applications in materials science and biology. We have invited 8 speakers to share their experience in these fields. The program is also bolstered by many abstract submissions. They will be presented as 18 oral talks and 49 posters, 16 of which will be highlighted in flash talks. We hope that they will simulate fruitful discussions.

This meeting will also be the first in-person meeting since the start of the pandemic. In addition to being able to talking to the participants about their oral or poster presentations, you will be able to visit a small but representative trade exhibit and talk to our commercial partners and sponsors face-to-face. The local organization team, with the support of our sponsor, will also organize a barbecue after the exhibit session on Wednesday to allow social interaction to continue into the evening. Last but not least, EMAG is co-sponsoring a 'town-hall'-style meeting Thursday afternoon, after the close of EMAG2022, together with Royal Microscopical Society and other national EM facilities, to start the consultation process for the next roadmap for UK's EM development in Physical and Enginnering Science, so stay on to contribute to EMAG's future.

Let me end this message by thanking the IOP conference team led by Jenny Griffiths and Clare Garland and our local organizers Catriona McGilvery and Michele Conroy for all the behind the scene pre-conference preparation and Imperial College for the kind hospitality. I would like to thank other committee members for the preparation of the scientific program and particularly Laura Clark for the 75 anniversary event. The EMAG committee would also like to thank you for your participation in EMAG2022 and hope you will enjoy the meeting as well as the scenery of London.

Jun Yuan.

Programme

75th Anniversary Event **Tuesday 5th July (Institute of Physics, London)**	
15:15	**Registration, tea and coffee**
	Join Zoom Meeting https://us02web.zoom.us/j/83005573873 Meeting ID: 830 0557 3873
16:00	**Welcome and Introduction**
16:15	**(Plenary)** A Brief History of EMAG Mick Brown, University of Cambridge, UK
17:00	**Research Slam**
17:30	**(Plenary)** Multidimensional electron microscopy at the rescue of materials science: probing spatial, time and spectral domains in novel low-dimensional nanostructures Valeria Nicolosi, Trinity College Dublin, Republic of Ireland
18:15	**Drinks Reception**
19:30	**Conference Dinner** The London Canal Museum (Pre-bookable)

EMAG Conference (Imperial College London) Wednesday 6th July	
08:30	*Registration, Tea and Coffee* *Location: City and Guilds Building (CAGB) outside Lecture Theatre 200*
	Join Zoom Meeting https://us02web.zoom.us/j/83005573873 Meeting ID: 830 0557 3873
09:00	**Introductions, Welcome to EMAG** Jun Yuan, University of York, UK and Catriona McGilvery, Imperial College London, UK EMAG Committee Chair and Local Organising Committee Chair
09:05	**(Invited)** The smaller the better? Small-scale mechanical testing of ceramics and composites Oriol Gavalda Diaz, University of Nottingham, UK
09:35	Session Chairs: Joanne Sharp and Catriona McGilvery Improving the sensitivity of off-axis electron holography for studying the in-situ heat treatment of double magnetic tunnel junctions Trevor Almeida, University of Glasgow, UK
	From Atom to Nanoparticle. Understanding exsolution through in situ scanning transmission electron microscopy, density functional theory and machine-learning analytics Eleonora Cali, Imperial College London, UK
	Direct visualisation of nucleation and synthesis of Ga2Se3 nanostructures from liquid coordination complexes studied by in-situ TEM Miryam Arredondo, Queen's University Belfast, UK
	The effect of hydrogen on the mechanical performance of La(Fe,Mn,Si)13 magnetocalorics studied by in situ SEM mechanical testing Siyang Wang, Imperial College London, UK
10:30	*Tea and Coffee*
11:00	Session Chair: Laura Clark and Andy Brown **(Invited)** Toward quantitative electron tomography of large volumes with preserved detail Sean Collins, University of Leeds, UK
11:30	Scanning Electron Nanobeam Diffraction experiments: from optical set-up to data handling and ML-assisted post-processing - case study for a battery cathode phase Mohsen Danaie, Diamond Light Source, UK

	Unsupervised machine learning applied on correlated 4DSTEM/EDS data to investigate the structural ordering of Co2FeSi thin films Ercin Duran, University of Manchester, UK
	3D-Multidimensional Analysis of Magnetoelectric Multiferroic Topologies via Scanning Transmission Electron Microscopy, Spectroscopy and Atom Probe Tomography Shelly Conroy, Imperial College London, UK
12:15	Flash presentations
	Classification of Fluctuating Gold Clusters using Convolutional Neural Networks Malcolm Dearg, Cardiff University, UK
	Deep neural network pipeline for statistically significant metrics of heterogeneous catalyst systems Kevin Treder, University of Oxford, UK
	Extracting the crystal orientation information from spectroscopic data for the EMCD experiments Hasan Ali, Stockholm University, Sweden
	Visualising surface chemistry variations across length scales using secondary electron hyperspectral imaging in LV-SEM James Nohl, University of Sheffield, UK
12:30	*Lunch and exhibition*
14:00	Session Chairs: Alex Eggeman and Jun Yuan **(Invited)** Structured illumination ptychography Andy Maiden, University of Sheffield, UK
14:30	Accessing Sub-Angstrom Ptychographic Information in a Scanning Electron Microscope at ≤ 30 kV Arthur Blackburn, University of Victoria, Canada
	Low Voltage Electron Ptychographic Imaging Christopher Allen, University of Oxford, UK
	A Correlative Microscopy Technique Development: Exploring 3D Chemistry and Grain Orientation in Ni-W Nanocrystalline alloys Saurabh Mohan Das, The Max-Planck-Institut für Eisenforschung, Germany
15:15	Flash Presentations
	Visualising beam-activated degradation processes in halide perovskite semiconductors using 4D-STEM nanoprobe diffraction Jordi Ferrer Orri, University of Cambridge, UK
	Imaging Structural Defects and Associated Oxygen Positions in Li-rich $Li_{1.2}Ni_{0.13}Mn_{0.54}Co_{0.13}O_2$ Weixin Song, University of Oxford, UK

15:30	*Tea and Coffee*
16:00	Session Chair: Miryam Arredondo-Arechavala and Shelly Conroy (Invited) EELS of low energy magnetic excitations Budhika Mendis, Durham University, UK
16:30	Revelation of electric dipole configurations on the subatomic scale in ferro-electric materials envisaged for quantum device Ursel Bangert, University of Limerick, Republic of Ireland
	Determining Atomic Structure of Grain Boundaries and Heterostructure Interfaces at Solid-State Electrode/Electrolyte Connor Murrill, University of York, UK
	In search of nothing: characterisation and quantification of vacancy clusters in thermoelectric half-Heusler alloys Ben Smith, University of Glasgow, UK
17:15	Flash Presentations
	Atomic resolution electric field mapping Ziyi Yuan, University of Oxford, UK
	Elucidating the mechanism responsible for swift heavy ion induced crystal rotation in NiO. Danielle Douglas-Henry, Trinity College Dublin, Republic of Ireland
	A New Approach for 3D Quantitative STEM Using Defocus Corrected Electron Ptychography Ali Mostaed, University of Oxford, UK
	Scanning Electron Diffraction of Pharmaceutical Amorphous Solid Dispersions Helen Leung, University of Cambridge, UK
17:30	*Drinks reception and exhibition* *Sponsored by* DENS solutions
17:30	**EMAG AGM**
19:00	*Dinner at Eastside Bar and Grill (included in registration, no prebooking required, all welcome)* *Sponsored by* JEOL

EMAG Conference (Imperial College London) **Thursday 7th July**	
09:00	***Refreshments and poster set up***
	Join Zoom Meeting https://us02web.zoom.us/j/83005573873 Meeting ID: 830 0557 3873
09:30	**Session Chairs: Donald MacLaren and Miryam Arredondo-Arechavala** **(Invited)** Atom-by-atom vibrational spectroscopy in the electron microscope. Fred Hage, University of Oslo, Norway
10:00	Quantum theory of ultra-low loss aloof beam EELS applied to molecular crystals Sabrina Wang, University of Oxford, UK
	Electron beam Induced deposition of Functional Magnetic Nanowires: A correlative EELS study of the link between Chemical variations and magnetic properties John Fullerton, University of Glasgow, UK
	ADF/EDS/EELS Characterization of Spontaneous Cathode/Electrolyte Reaction in Air- and Beam-sensitive Solid-state Li-ion Batteries Ruomu Zhang, University of Oxford, UK
10:45	**Flash Presentations**
	Improving the Noise Floor and Speed of Your Detector: A Modular Hardware Approach for Under £1000 Jonathan Peters, Trinity College Dublin, Republic of Ireland
	The Use of Advanced Electron Microscopy for the Characterisation and Structure-Property Correlation of $BaMnO_3$ for the Oxygen Reduction Reaction Lucia Hughes, Trinity College Dublin, Republic of Ireland
	Atomic Resolution Investigation of Ultra-Low Energy Ion-Implanted Monolayer TMDs Using Scanning Transmission Electron Microscopy Michael Hennessy, University of Limerick, Republic of Ireland
	Advanced TEM and STEM/EELS study of Zr and Nb doped Titanium dioxide Nanoparticles Fayzah Talbi, University of York, UK
	The User Adjustable Pole-piece - A TEM Heart Transplant Lewys Jones, Trinity College Dublin, Republic of Ireland
11:00	***Tea and Coffee and Poster Session***
12:00	***Lunch and Poster Session***

13:20	Session Chairs: Andy Brown and Catriona McGilvery **(Plenary)** High-resolution imaging of human viruses in liquid droplets Deb Kelly, Pennsylvania State University, USA

14:05	Revealing mechano-chemical interactions on the surface of polypropylene surgical mesh using Secondary Electron HyperSpectral Imaging Nicholas Farr, University of Sheffield, UK
	Optimization of (cryo-)FIB-SEM protocols to study interactions between Airborne Pollution Particles and Nasal Epithelial Cells Victoria Garcia Giner, Imperial College London, UK
	Cryogenic Electron Ptychographic Single Particle Analysis (Cryo-EPty SPA) Peng Wang, University of Warwick, UK
14:50	**Student Prizes and close of EMAG 2022**
15:00	*Tea and Coffee*
15:30	**EM Town Hall Meeting**

Posters

P1	Fast Ptychographic Reconstruction for Sparse Binary Ptychography data Emma Hedley, University of Oxford, UK
P2	Electron microscopy of crystalline and amorphous phases in model leaf waxes Emily Wynne, University of Leeds, UK
P3	Influence of Plasmon-excitation Electrons on Ptychography Phase Imaging Zhiyuan Ding, University of Oxford, UK
P4	Using Low-Dose Scanning Electron Diffraction Microscopy to Observe Hydration/Dehydration of Theophylline Natalia Koniuch, University of Leeds, UK
P5	In-situ environmental TEM study of the oxidation and reduction of Ni/NiO Arej Eid, University of York, UK
P6	Observing calcium sulfate crystallisation and phase transformation using in situ transmission electron microscopy techniques Martha Ilett, University of Leeds, UK
P7	Structural and electronic study of Cu doped NiO Ahmad Althumali, University of York, UK
P8	Mapping oxygen columns in magnetite crystals using differential phase contrast STEM imaging Xuyang Zhou, Max-planck-institut Fuer Eisenforschung Gmbh, Germany
P9	Automated sample alignment in the transmission electron microscope Zaeem Najeeb, Imperial College London, UK
P10	Spin-scattering function of confined magnons in magnetic interfaces. Júlio Do Nascimento, University of York, UK
P11	Exploring the Cryogenic Phase Changes within 2D MoTe2 via TEM, 4DSTEM and Electron Spectroscopy Techniques Samad Abdus, University of Limerick, Republic of Ireland
P12	Native state structural and chemical characterisation of Pickering emulsions Dario Luis Fernandez Ainaga, University of Leeds, UK
P13	Compressive Scanning Transmission Electron Microscopy Daniel Nicholls, University of Liverpool, UK
P14	Stability-limited Subsampled Scanning in Scanning Transmission Electron Microscopy Daniel Nicholls, University of Liverpool, UK
P15	Fast frame-rates from STEM interlacing: Two frames for the price of one? Jonathan Peters, Trinity College Dublin, Republic of Ireland

P16	Experimental Optimization and Data Analysis of In-Situ Electron Energy Loss Spectroscopy Eoin Moynihan, University of Limerick, Republic of Ireland
P17	A preliminary investigation into plasmons in topological insulator Bi2Se3 using electron energy loss spectroscopy Mairi McCauley, University of Glasgow, UK
P18	Atomic Study of Structural Changes of LiNiO2 Charged at High Voltage in Lithium Ion Batteries Jun Chen, University of Oxford, UK
P19	4D-STEM study of phospholipid microbubble microstructure Bing Han, University of Manchester, UK
P20	Understanding Wet Impregnation Synthesis for Sustainable Hydrogenation Catalysts via In-situ TEM Observation Rongsheng Cai, University of Manchester, UK
P21	3D reconstruction and correlative multidimensional characterisation of graphene nanocomposites Yuhan Li, Imperial College London, UK
P22	Analysing the SEI Layer Formation and Lithiation Processes of Si Nanowire Based Electrodes by Cryogenic STEM EELS and In-situ Liquid Cell Electrochemistry STEM Temilade Esther Adegoke, Imperial College London, UK
P23	Investigating the Ferroelasticity Governing the Dynamics of Improper Ferroelectric Domain Walls by In-Situ Biasing 4D-STEM Shelly Conroy, Imperial College London, UK
P24	Multi-dimensional electron microscopy data analysis assisted by deep learning Fanzhi Su, University of Cambridge, UK
P25	Electron microscopy studies on concentration gradient Ni-rich cathodes for lithium-ion batteries May Ching Lai, University of Cambridge, UK
P26	Investigating Avalanche Criticality in $LaAlO_3$: The Effect of Aspect Ratio John Scott, Queen's University Belfast, UK
P27	Characterising Surface Segregation in Bimetallic Precious Metal Catalysts using Analytical Scanning Transmission Electron Microscopy Sam Sullivan-Allsop, University of Manchester, UK
P28	Atomistic and electronic structures of CuCrMnO4 spinel studied by probe-corrected STEM, EELS, 4DSTEM and DFT modelling. Trung Dung Tran, Johnson Matthey Technology Centre, UK
P29	Multiscale microscopic characterization of 3D volume and metal-polymer interface using cutting edge multi scale electron microscopy technologies Min Wu, Thermo Fisher Scientific, Netherlands
P30	Nanoparticle Feature Analysis for Subsampled Images Using Deep Neural Networks William Pearson, University of Liverpool, UK

P31	Using atomistic modelling to assist ADF-STEM based strain measurements of nanoparticle alloys Tom Ellaby, Johnson Matthey Technology Centre, UK
P32	Properties of InGaAs metamorphic buffers on GaAs Nicholas Stephen, Queen's University Belfast, UK
P33	The next generation of in-situ open cell environmental double aberration corrected e-(S)TEM: ARTEMIS Leonardo Lari, University of York, UK
P34	Sizing fat globules and casein micelles in Milk using Cryo FIB-SEM Fraser Laidlaw, University of Edinburgh, UK
P35	Classification of Fluctuating Gold Clusters using Convolutional Neural Networks Malcolm Dearg, Cardiff University, UK
P36	Deep neural network pipeline for statistically significant metrics of heterogeneous catalyst systems Kevin Treder, University of Oxford, UK
P37	Extracting the crystal orientation information from spectroscopic data for the EMCD experiments Hasan Ali, Stockholm University, Sweden
P38	Visualising surface chemistry variations across length scales using secondary electron hyperspectral imaging in LV-SEM James Nohl, University of Sheffield, UK
P39	Visualising beam-activated degradation processes in halide perovskite semiconductors using 4D-STEM nanoprobe diffraction Jordi Ferrer Orri, University of Cambridge, UK
P40	Imaging Structural Defects and Associated Oxygen Positions in Li-rich $Li_{1.2}Ni_{0.13}Mn_{0.54}Co_{0.13}O_2$ Weixin Song, University of Oxford, UK
P41	Atomic resolution electric field mapping Ziyi Yuan, University of Oxford, UK
P42	Elucidating the mechanism responsible for swift heavy ion induced crystal rotation in NiO. Danielle Douglas-Henry, Trinity College Dublin, Republic of Ireland
P43	A New Approach for 3D Quantitative STEM Using Defocus Corrected Electron Ptychography Ali Mostaed, University of Oxford, UK
P44	Scanning Electron Diffraction of Pharmaceutical Amorphous Solid Dispersions Helen Leung, University of Cambridge, UK
P45	Improving the Noise Floor and Speed of Your Detector: A Modular Hardware Approach for Under £1000 Jonathan Peters, Trinity College Dublin, Republic of Ireland

P46	The Use of Advanced Electron Microscopy for the Characterisation and Structure-Property Correlation of $BaMnO_3$ for the Oxygen Reduction Reaction Lucia Hughes, Trinity College Dublin, Republic of Ireland
P47	Atomic Resolution Investigation of Ultra-Low Energy Ion-Implanted Monolayer TMDs Using Scanning Transmission Electron Microscopy Michael Hennessy, University of Limerick, Republic of Ireland
P48	Advanced TEM and STEM/EELS study of Zr and Nb doped Titanium dioxide Nanoparticles Fayzah Talbi, University of York, UK
P49	Multimodal In-Situ Spectrum Imaging with Synchronized and Automated Stimulus Control Liam Spillane, Gatan Inc, USA

Abstracts
75th Anniversary Event

(Plenary) HAPPY 75th BIRTHDAY EMAG!

Prof L. M. Brown

Conceived before the second world war, and delivered in the aftermath of it, the nascent group has since flourished. Its biennial conferences are an outstanding example of how to enable University-based research to provide education, scientific advance, and commercial opportunity.

(Plenary) Multidimensional electron microscopy at the rescue of materials science: probing spatial, time and spectral domains in novel low-dimensional nanostructures

Prof Valeria Nicolosi

Trinity College Dublin, Ireland

Low-dimensional nanostructured materials such as organic and inorganic nanotubes, nanowires and platelets are potentially useful in a number of areas of nanoscience and nanotechnology due to their remarkable mechanical, electrical and thermal properties. However, difficulties associated with their lack of processability have seriously hampered both. In the last decade dispersion and exfoliation methods have been developed and demonstrated to apply universally to 1D and 2D nanostructures of very diverse nature, offering a practical means of processing the nanostructures for a wide range of innovative technologies. To make real applications truly feasible, however, it is crucial to fully characterize the nanostructures on the atomic scale and correlate this information with their physical and chemical properties. Advances in aberration-corrected optics and in-situ techniques in electron microscopy have revolutionised the way to characterise nanomaterials, opening new frontiers for materials science. With the recent advances in nanostructure processability, electron microscopes are now revealing the structure of the individual components of nanomaterials, atom by atom. Here we will present an overview of very different low-dimensional materials issues, showing how modern electron microscopy can be used to reveal crucial structure-to-properties information.

Abstracts EMAG 2022 Plenary and Invited Talks

(Plenary) High-resolution imaging of human viruses in liquid droplets

Deb Kelly

Pennsylvania State University, USA

Biomedical research improves our understanding of human health and disease through the development of new technologies. High-resolution imaging is one technology that is transforming our view of the nanoworld – permitting us to study cells and molecules in exquisite detail. Structural information of dynamic components, however, reveals only a snapshot of their complex narrative.

Recent advances in the production of materials such as graphene and silicon nitride provide new opportunities for Electron Microscopy (EM) imaging in real-time. Coupled with the fact that interest in liquid-EM has skyrocketed in recent years, scientists can now observe dynamic biological processes at the nanoscale. It is highly desirable to pair high-resolution cryo-EM information with these dynamic observations as many mechanistic events occur at rapid timescales. Improved knowledge of flexible structures can also assist in the design of novel reagents to combat emerging pathogens, such as SARS-CoV-2. Equally important, viewing biological materials in a fluid environment provides a unique glimpse of their performance in the human body.

Using SiN-based environmental chambers we conduct real-time experiments in situ, or “inside”, the EM column. This technology permits us to study the intricate details of viruses and vaccine candidates in a native liquid environment at high resolution (Figure 1). Other recent applications of liquid-EM include real-time recordings of nanoparticle therapies interacting with cancer stem cells and notable changes in tumor suppressor proteins. These results complement our ongoing cryo-EM studies as we strive to analyze molecular events with high spatial and temporal resolution.

Acknowledgements: This work was supported by funding from the National Institutes of Health and the National Cancer Institute [R01CA193578, R01CA227261, and R01CA219700 to D.F.K.].

Figure 1. Determining high-resolution structures of human viruses in liquid droplets. As a complement to cryo-EM methods, structures of human viruses can be determined using rapid data collection procedures in liquid. The Kelly Lab has developed real-time imaging strategies to visualize atomic details of gene-delivery vehicles and vaccine candidates used in the treatment of COVID-19. Design courtesy of Daryl Branford, Director of Science-Art Initiatives at The SciArt Group, Pennsylvania State University.

(Invited) The smaller the better? Small-scale mechanical testing of ceramics and composites

Oriol Gavalda Diaz, Eduardo Saiz, Finn Giuliani

University of Nottingham, UK

New structural materials rely on the nanoscale design of their microstructure to achieve the desired performance. A classic example of this can be found in polymer and ceramic composites used in aerospace, automotive or energy generation, where nanoscale interfaces are customised to achieve the desired strength and toughness. However, understanding the properties of these nanoscale features and their effect to the bulk failure is challenging. In this talk we will be showing the testing (from bulk to micro and nanoscale) that we have developed in the recent years applied to polymer and ceramic composites to better understand their failure in service and allow the design of new improved microstructures.

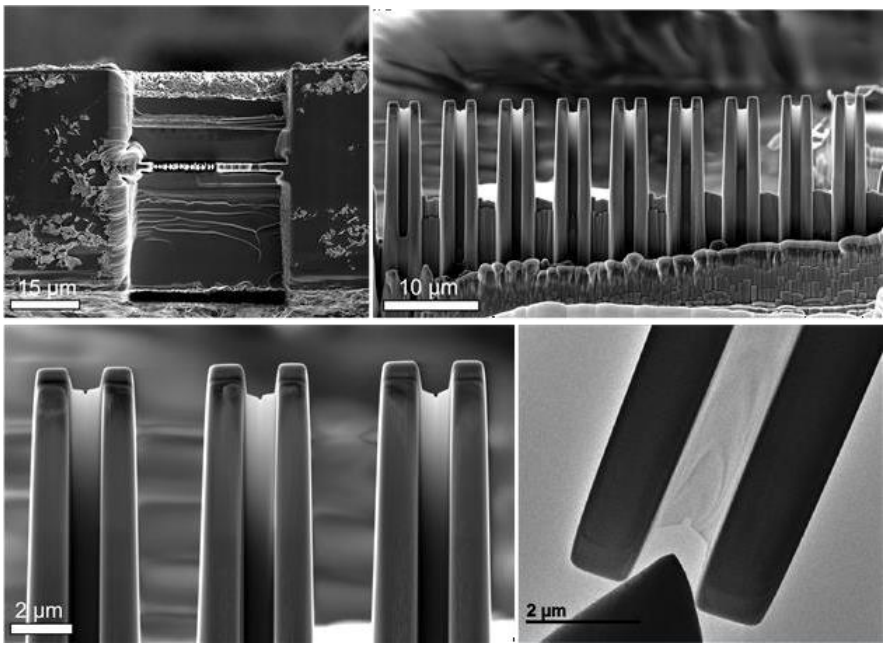

(Invited) Toward quantitative electron tomography of large volumes with preserved detail

Sean Collins

University of Leeds, UK

Materials from metallurgical to biological samples often contain important fine details embedded within a much larger-scale three-dimensional (3D) context, determined by the scale of microstructure or that of a cellular environment. Electron tomography offers a route to unravelling these two imaging aims through reconstruction of volumes from two-dimensional tilt-series data. However, quantitative spectroscopic tomography often imposes severe limitations on the quantity of two-dimensional spectrum image datasets that can be obtained. Moreover, biological and soft matter systems exhibit high rates of beam-induced changes to the sample on electron exposure even on exposure to 10s of electrons per square Ångstrom and under cryogenic cooling, resulting in a low signal-to-noise ratio in dose-fractionated tilt-series data despite image acquisition using electron counting detectors. This presentation will show how compressed sensing electron tomography (CS-ET) approaches using second-order total-variation improve 3D feature visibility while preserving high resolution structural detail in angle- and noise-limited applications.

CS-ET has shown particular success producing high-fidelity reconstructions from nanoparticles as well as in spectroscopic tomography acquisitions [1]. CS-ET relies on known characteristics of physical volumes that enable compression, i.e. a sparse representation of 3D data through the use of mathematical transforms. CS-ET targets recovery of the coefficients of the sparse representation, possible when the sparse transform is incoherent with the data sampling in image acquisition. However, in experimental demonstrations, the optimal choice of parameters to weight the transform to a sparse domain is typically ambiguous. Crucially, the effect of noise or non-linearities in the image intensities requires careful evaluation, but experimental ground truths are often poorly defined. Cryo-electron tomography (cryo-ET) can be combined with subtomogram averaging to recover high resolution reconstructions of macromolecules, either from multiple isolated copies or from within a cellular context. Here, the suitability of second order total variation will be discussed with examples drawn from cryo-ET of hepatitis B capsids, ribosomes, as well as C. crescentus cellular structures [2]. Second order total variation supports the retention of secondary structure details (preserving sub-nanometre resolution) while improving the visibility of features within cellular volumes. In a very different application area, second-order total variation integrated with scanning transmission electron microscopy X-ray energy dispersive spectroscopy for 3D X-ray absorption-corrected tomography will also be discussed.

[1] R. Leary, Z. Saghi, P. A. Midgley, D. J. Holland, Ultramicroscopy (2013), 131, 70-91.
[2] J. Böhning, T. A. M. Bharat, S. M. Collins, Structure (2022), 30, 408-417.

(Invited) Structured illumination ptychography

Andy Maiden

University of Sheffield, UK

Ptychography on the electron microscope has seen rapid progress over the last few years, thanks to new direct detection, ultra-fast, and highly sensitive 4DSTEM detectors. Much of the research in the area focusses on atomic resolution imaging, where ptychography offers unique advantages of high contrast (especially for lighter elements) and insensitivity to lens aberrations. Parallel to this, however, ptychography can also provide high accuracy phase images at medium resolution, around the nanometre level, with a wealth of poten- tial applications in material characterisation and field measurement.

In this talk I will describe recent experiments and results using structured electron beams to implement medium-resolution, large field of view electron ptychography. I will highlight potential advantages and applications of the technique, as well as its limitations. I will also present recent results from X-ray experiments at the Diamond Light Source showing the use of structured illumination in combination with multislice ptychography for extremely large depth of field phase imaging, explaining how this might in future be combined with tomography to image large sample volumes at currently inaccessible resolutions.

(Invited) EELS of low energy magnetic excitations

Budhika Mendis

Durham University, UK

Recent progress in monochromation to sub-10 meV energy resolution has enabled state-of-the-art EELS measurements related to phonon spectroscopy and mapping in the STEM. It is of interest to consider if the

improved energy resolution would benefit detection of other forms of collective excitation, such as, for exam- ple, magnons in magnetic materials. Magnons are thermally excited spin waves that reduce the spontaneous magnetisation, and are the building block of magnonic devices being explored for wave-based computing. Magnons can be detected using spin polarised EELS (SPEELS), which is a surface characterisation technique where the incident electron beam is spin polarised and of low energy (<10 eV). STEM EELS however has a much higher spatial resolution than SPEELS, but magnon detection in a spin unpolarised STEM is yet to be demonstrated.

The scattering cross-section for the interaction of a high energy, spin unpolarised electron beam with a magnon is calculated for a Heissenberg ferromagnet using quantum mechanics. Both conventional plane wave and vortex electron beams are considered. It is shown that in both cases magnon energy losses can take place, although the scattering cross-section is considerably weaker compared to phonons. Furthermore, the winding number of the vortex beam does not affect the interaction, despite the higher orbital angular momentum. Inelastic multislice simulated images at the magnon energy loss show significant delocalisation due to interaction with the long-range dipole magnetic field of individual spins in the solid. However, a localised contribution is also present, which would enable atomic scale resolution magnon imaging at high scattering angles, provided issues with a weak signal can be overcome.

Finally, I will also briefly present results for magnetic energy losses analysed using electrodynamic theory. This theory is useful for large scale, continuum interactions and can potentially be applied to AC magnetic susceptibility measurements in the STEM, EELS energy losses from domain walls and skyrmions etc.

(Invited) Atom-by-atom vibrational spectroscopy in the electron microscope.

Fred Hage

University of Oslo, Norway

Electron energy loss spectroscopy (EELS) in conjunction with aberration corrected scanning transmission electron microscopy (AC-STEM) allows for investigating and correlating structure, chemistry and dielectric response of materials, down to the atomic scale. About 8 years ago [1] it was demonstrated that state-of-the-art electron beam monochromation allows for accessing and analyzing spectral features associated with vibrational modes in STEM-EELS. Exploring this novel landscape, researchers showed that they could detect vibrational modes, including ones involving hydrogen [1], map surface and bulk collective vibrational modes or “phonons” in nanoparticles [2], and more. Common for these studies is that they all reported nanometre spatial resolution.

In vibrational EELS, the achievable spatial resolution is affected by there being two “types” of phonon-scattering at work. For polar materials, so-called “dipole scattering” dominates at small scattering angles and results in a delocalised vibrational loss signal that can be detected in vacuum ~100 nm away from the sample edge. “Impact scattering” on the other hand is highly localized and dominates at larger scattering angles. For polar materials and when using a conventional bright-field STEM-EELS geometry (where the spectrometer collection aperture is centered on the forward scattered beam), dipole scattering dominates and substantially reduces the atomic scale contrast in vibrational STEM-EELS maps [3, 4]. However, if choosing a dark-field STEM-EELS geometry, for which the bright field disc and spectrometer collection aperture do not overlap, the dipole contribution can be suppressed, resulting in atomically resolved phonon loss maps with good contrast, as first shown for hexagonal boron nitride (hBN) [3]. A bright field geometry may still be used for atomically resolved mapping of phonons in hBN, though at the cost lower contrast and interpretation being non-trivial due to probe-channeling [4].

For non-polar materials, a dark-field geometry is not required for practical atomic resolution experiments [5], however, may still be the preferred choice in some cases: for (non-polar) graphene the impact scattering intensity is vanishingly small for small scattering angles [6]. Thus, a dark-field geometry was the experimental methodology of choice when probing single tri-valent silicon dopants in single layer graphene [7] to demonstrate that vibrational STEM-EELS has single atom sensitivity [8].

[1] OL Krivanek et al., Nature 514, 209–212 (2014).
[2] MJ Lagos et al., Nature 543, 529–532 (2017).
[3] FS Hage et al., PRL 122, 016103 (2019).
[4] FS Hage et al., PRB 102, 214111 (2020).
[5] K Venkatraman et al., Nat. Phys. 15, 1237–1241 (2019).
[6] R Senga et al., Nature 573, 247-250 (2019).
[7] FS Hage et al., Science 367, 1124-1127 (2020).
[8] SuperSTEM is the UK Engineering and Physical Sciences Research Council (EPSRC) National Research Facility for Advanced Electron Microscopy.

Improving the sensitivity of off-axis electron holography for studying the in-situ heat treatment of double magnetic tunnel junctions

Trevor Almeida, Alvaro Palomino, Olivier Fruchart, Ioan Lucian Prejbeanu, Bernard Dieny, David Cooper

University of Glasgow, UK

Introduction

Magnetic random-access memory (MRAM) is a non-volatile memory based on the storage of one bit of information by a ferromagnetic memory carrier. Spin-transfer torque (STT) MRAM is viewed as an exciting replacement for embedded FLASH memory and involves the use of a magnetic tunnel junction (MTJ): an MgO tunnel barrier (~ 1.5 nm) sandwiched between a magnetically-pinned reference layer and a switchable storage layer. When the layers are perpendicularly magnetized in parallel and antiparallel states, the significant differences in electrical resistance provides a system of readable / writable '0' or '1' binary information. The bit density of modern STT-MRAM can be increased by reducing the size of the MTJ cell but may lower the thermal stability of the storage layer. A solution to improve both their thermal stability and reduce the critical current required to switch the storage layer is introducing perpendicular shape anisotropy (PSA)[1] and double MTJs (DMTJ)[2]. PSA involves increasing the thickness of the storage layer to larger than its diameter so that its out-of-plane aspect ratio provides further thermal stability. In a DMTJ stack, a secondary MgO tunnel barrier is sandwiched between the storage layer and an additional ferromagnetic thin film above, termed the polarizing layer (Fig. 1a). The polarizing layer can be switched to minimize or maximize the STT of the storage layer during the read and write modes, respectively. Post deposition annealing can be used to further increase the tunnel magnetoresistance and perpendicular magnetic anisotropy of the DMTJs[3], but above certain temperatures these properties can deteriorate. As these devices become smaller and their performance more complex, it is necessary to image their magnetic configurations directly with high sensitivity at nanoscale resolution. The advanced transmission electron microscopy (TEM) technique of off-axis electron holography allows imaging of magnetization within nano-scale materials and can be combined with in-situ heating to investigate the effect of thermal treatment of magnetic nanostructures[4]. Here, we use the summation of electron holograms to image the micromagnetic configuration of ~ 20 nm DMTJs with improved sensitivity to visualize the effect of in-situ annealing.

Methods/Materials

An array of DMTJs nano-pillars was fabricated through sequential e-beam lithography, reactive ion etching and ion beam etching[1]. A simplified DMTJ stack has the following compositions: SiO_2 substrate / synthetic antiferromagnetic layer / Co reference layer / FeCoB ferromagnetic free layer / Co polarizing layer / capping layers / Ta mask. TEM samples were prepared by depositing a protective layer (~ 1 µm) of resin on the array prior to a protective Pt layer being deposited by the focused ion beam (FIB). Cross-sectional TEM lamellae were transferred to Omniprobe copper slots and thinned to ~ 300 nm using conventional FIB methods. The protective resin layer was removed by plasma etching and the remaining Pt layer was broken with the micromanipulator. Scanning TEM (STEM) imaging was performed using a probe-Cs-corrected Thermo Fisher Titan TEM at 200kV, whilst energy dispersive X-ray (EDX) spectroscopy provided chemical analysis. Off-axis electron holograms were acquired under field-free conditions in Lorentz mode on a Gatan OneView 4K camera using a Thermo Fisher Titan TEM equipped with an image-Cs corrector and an electron biprism. The magnetization states of the nano-pillars were visualized through separation of the magnetic contribution to the phase shift from the mean inner potential, achieved by tilting and applying the strong field of the objective lens (< 1.5T) to reverse their magnetism. In-situ heating up to 400°C was performed using a Gatan heating holder under field-free magnetic conditions.

Results and Discussion

Figure 1 presents the morphology, chemical composition and effect of annealing on the magnetism of an individual nano-pillar from the etched Co / FeCoB / Co stack. The schematic of Fig. 1a displays the simplified configuration of a DMTJ cell, comprising the reference, free and polarizing magnetic layers. The STEM image (Fig. 1b) and EDX map (Fig. 1c) displays its morphology (~ 60 nm height, ~ 35 nm largest diameter) and multi-layered composition of Co (20 nm) / MgO (2 nm) / FeCoB (20 nm) / MgO (2 nm) / Co (20 nm). The magnetic phase image (ϕm) of Fig. 1d is reconstructed from an averaged stack of 8 electron holograms and shows that the magnetization lies along the elongated axis DMTJ. The single-pixel line profile taken across its diameter (Fig. 1d, arrowed) is compared to single-pixel and averaged-line (10-pixel width) profiles from a single ϕm image (Fig. 1e), demonstrating a doubling in ϕm signal-to-noise ratio. This is key for imaging subtle variations in the magnetic configuration of such small DMTJ devices. Figs 1f-h illustrates the effect of thermal annealing on the magnetic configuration of the native nano-pillar (Fig. 1f) After initial annealing to 400°C in-situ within the TEM for 30 minutes, the magnetic contours flow in a transverse direction across the central FeCoB layer and deviate away from the long axis in the top Co layer (Fig. 1g). This change in magnetic orientation becomes more pronounced with additional in-situ annealing under the same conditions (Fig. 1h). The higher temperature of 400°C is believed to have chemically altered the multi-layered structure through diffusion and intermixing, which has degraded both the magnetic properties of individual layers and their exchange interaction across their interfaces[5]. Combined with the middle CoFeB layer exhibiting a larger diameter than thickness, which provides a degree of shape anisotropy along a transverse axis of the nano-pillar, all these factors are attributed to degrade the perpendicular anisotropy of the DMTJ.

Conclusions

We have shown that the improved sensitivity of stacking electron holograms can be used to directly image subtle variations in DMTJ nano-pillars caused by in-situ annealing. As smaller and more complex p-STT-MRAM devices are fabricated, this study unlocks practical pathways for direct imaging of the functional magnetic performance of these systems with high spatial resolution and sensitivity.

References

1. N. Perrissin et al., Nanoscale 2018, 10, 12187-12195.
2. A. Chavent, et al., ACS Appl. Electron. Mater. 2021, 3, 2607−2613.
3. J. Chatterjee, et al., Appl. Phys. Lett. 2017, 110, 202401.
4. T. P. Almeida, et al., J. Micros. 2020, 279 (3), 217-221.
5. F. Letellier, et al., J. Appl. Phys. 2014, 116, 203906.

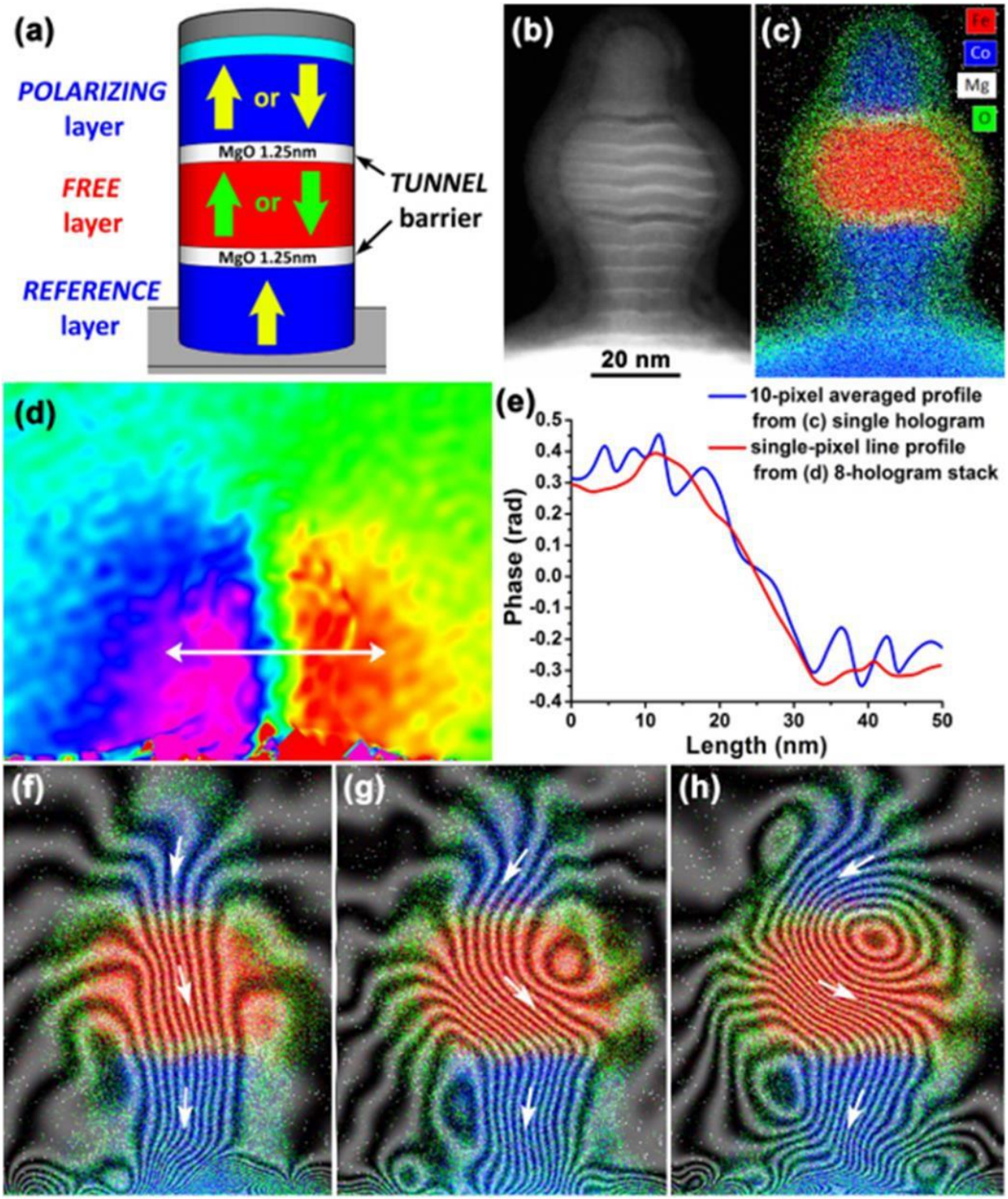

Figure 1. (a) Schematic of a DMTJ cell comprising reference, free and polarizing layers where the arrows denote the expected magnetic easy axis. (b) STEM image of a DMTJ nano-pillar; and (c) the associated EDX chemical map showing the elemental distribution of Fe (red), Co (blue), Mg (white) and O (green). (d) Reconstructed φ_m contribution of the DMTJ averaging an 8-image electron hologram stack. (e) Graph of a single pixel line profile (red) taken across diameter of the nano-pillar in (d) compared to an averaged 10-line profile (blue) from a single φ_m image, demonstrating a significant improvement in φ_m signal-to-noise ratio. (f-h) Combined EDX / magnetic induction maps (f) before; and after (g) first; (h) secondary *in-situ* annealing to 400°C for 30 minutes. The contour spacing is 0.063 rad (cosine × 100 times) and the field direction is indicated with arrows.

From Atom to Nanoparticle. Understanding exsolution through in situ scanning transmission electron microscopy, density functional theory and machine-learning analytics

Eleonora Cali, Melonie Thomas, Ji Wu, Rama Vasudevan, Oriol Gavalda-Diaz, Katharina Marquardt, Eduardo Saiz, Dragos Neagu, Raymond R. Unocic, David Payn

Imperial College London, UK

Nanoparticle exsolution, i.e. metal atoms that, in a reducing environment, diffuse to the surface from sites within a host oxide lattice to form anchored nanoparticles, is considered an exciting alternative to traditional nanoparticle deposition techniques for catalysis and energy applications. The simple material design opportunities offered by this concept, coupled with the resulting increased stability and functional efficiency as exsolved nanoparticles are found partially submerged (or 'socketed') into the surface of the host oxide, results in a range of new application opportunities, such as catalysis, circumventing the major limitations of deposited nanoparticles (agglomeration or coking) which cause loss of catalytic activity. Several studies have suggested that the unique functional properties of exsolved particles are due to the structure and composition of the interface formed between the nanoparticles and the host oxide. However, the holistic mechanism of exsolved nanoparticle nucleation and perovskite structural evolution, is, to date, still unclear. This work presents a fundamental study where we monitor the early stages of nucleation of iridium nanoparticles during exsolution from a stoichiometric Ir-doped $SrTiO_3$ as a model structure. We apply in situ high-resolution high-angle annular dark field scanning transmission electron microscopy (HAADF-STEM) to monitor, in real time, the early stages of nucleation and exsolution of Ir NPs from a stoichiometric Ir-doped $SrTiO_3$ (STO) model structure in ultra-high vacuum (UHV), while heating the sample from room temperature to 1100 °C. This allows us to observe atomic diffusion, nucleation sites, the evolution of the host crystal structure, and the role of evolving host defects in the early stages of nucleation.

We then use Density Functional Theory (DFT) and Molecular Dynamics (MD) simulations to investigate the Ir atomic interaction at the surface during the initial stages of exsolution. The simulations supported our in situ observation of nucleation via Ir atom clustering, furthermore validating the role of surface defects in trapping Ir atoms to initiate the nucleation. In situ EELS studies allowed us to investigate in real-time variations in the composition, chemistry, and structure of the nanoparticles and the host during exsolution. In parallel, we also monitor the evolution of the host perovskite oxide, providing evidence of surface restructuring, and support this through by employing a machine-learning image-analytics approach. This allows us to identify that the evolution of the reconstruction before nucleation contributes to initiate the exsolution mechanism. Finally, we investigated the socket formation, to which the high stability of exsolved nanoparticles is attributed. Although nanoparticle socketing into the host is undoubtedly one of the unique features of exsolution, the mechanistic reason behind its formation is, to date, not well documented and unclear. Through in situ STEM we monitored step-by-step the growth of the sockets around the exsolved particles, which allowed us to elucidate that this socket only occurs once the particles are fully formed at the surface and at relatively high temperatures for our system. We propose that this unique socketing is generated via a similar mechanism to the Vapour-Liquid-Solid (VLS) one, where the exsolving metal nanoparticles catalyze the growth of $SrTiO_3$ pedestals at the surface to lock in the exsolved nanoparticles. The mechanistic insights described in this study correlate the defect formation in the host oxide to the nanoparticle formation at the surface during exsolution, for the first time looking at the process holistically: both atom to nanoparticles nucleation, and perovskite structural evolution at the same scale. This work highlights new opportunities to effectively exploit structural and defect design strategies for the achievement of tailored exsolved NPs, driving the progress in the tailored design of highly advanced systems for catalysis and energy-related applications more broadly.

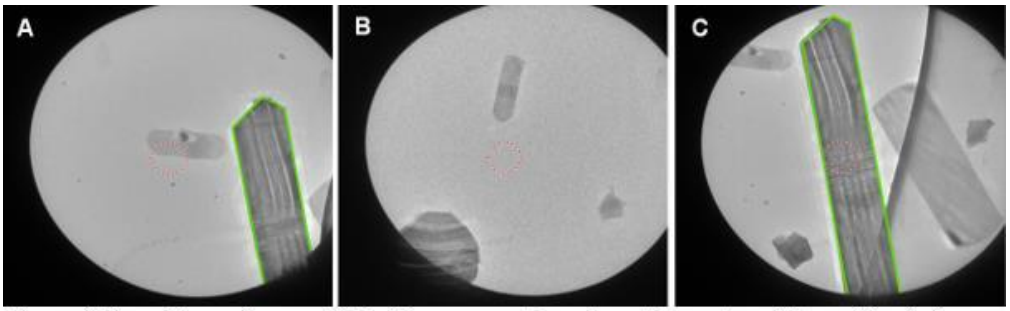

Figure 1. Ronchigram images of MoO_3 nanocrystals, where the centre of the optic axis is marked by a red circle. (A) shows a crystal, outlined in green, oriented off zone. (B) shows the image after tilting, note how the crystal has moved outside the field of view. (C) shows how, after automated stage position correction, the crystal returns to the centre of the image and oriented now on the zone axis.

Direct visualisation of nucleation and synthesis of Ga2Se3 nanostructures from liquid coordination complexes studied by in-situ TEM

Miryam Arredondo, Tamsin O'Reilly, Anne McGrogan, Peter Nockemann, Gosia Swadzba-Kwasny, Miryam Arredondo

Queen's University Belfast, UK

Ionic liquids are molten salts with melting points around ambient temperature, which have attracted attention due to their unusual physico-chemical properties; crucially, due to their strong Coulombic interactions between ions in the liquid which result in high thermal stability and negligible vapour pressure. This makes them uniquely suited for ionothermal syntheses of inorganic materials, in which relatively high temperatures can be implemented without generating high pressures. Due to the negligible volatility, ILs are unique liquids amenable to high-vacuum in-situ studies.

Liquid coordination complexes (LCCs) [1,2] are coordination complexes of metals, designed to have melting temperatures below ambient temperature. LCCs are analogous to ionic liquids and make excellent candidates for studies via in situ transmission electron microscopy (TEM) to reveal dynamic processes (nucleation and growth) with high temporal and spatial resolution [3,4]. However, the main focus of studies on LCCs has been on electrodepositions and Lewis acid catalysis, with no studies reported on semiconductor syntheses, and paucity of knowledge about the actual liquid dynamics that leads to the particle formation.

In this work, LCCs formulated from a gallium salt and a selenium ligand were used as precursors for the synthesis of nanostructured gallium(III) selenide, Ga2Se3, a member of an important family of III-V semiconductors. The presence of Ga-Se bond in the starting material resulted in a very low reaction temperature (160 °C) compared to other methods.

We used in-situ liquid TEM to provide an insight into the dynamics for nano particle formation.

We identified a diversity of coalescence events that lead to be a variety of growth reactions in the liquid. We also observed the formation of large spherical droplet clusters that self-assemble in chains as a function of temperature and eventually coalesce, indicating the kinetics of particle coarsening. Moreover, under elevated temperatures we are able to identify particles with well-defined facets and smaller nanostructures.

This work presents direct imaging on the dynamical processes and particle formation of Ga2Se3, it highlights the potential of LCCs for in-situ TEM studies and discusses the future work needed to further our understanding of growth reactions and nano particle formation in these coordination complexes.

References

[1] Angew Chem Int Ed 52 (2013) 12582-12586
[2] Dalton Trans 46 (2017) 11561-11574
[3] Micron 117 (2019) 16–21
[4] Nanoscale, 2020, 12, 22511–22517

The effect of hydrogen on the mechanical performance of La(Fe,Mn,Si)13 magnetocalorics studied by in situ SEM mechanical testing

Siyang Wang, Oriol Gavalda-Diaz, Ting Luo, Liya Guo, Edmund Lovell, Neil Wilson, Baptiste Gault, Mary Ryan, Finn Giuliani

Imperial College London, UK

Magnetocaloric cooling offers the potential to dramatically improve the efficiency of refrigeration devices and hence cut the significant CO2 emissions associated with domestic and industrial cooling processes. By understanding the mechanisms for mechanical degradation of La(Fe,Mn,Si)13-based magnetocaloric materials during processing and operation, service life of cooling devices can be maximised. Hydrogenation of La(Fe,Mn,Si)13 tunes the Curie Temperature thereby enabling near room temperature refrigeration, which however deteriorate the mechanical performance of the material. To understand this, the mechanical properties of hydrogenated La(Fe,Mn,Si)13 across a range of length scales were studied using macroscale three-point bending tests of polycrystalline specimens and in situ scanning electron microscope (SEM) micropillar compression tests of single crystal specimens with controlled crystal orientations. The impact of hydrogen on the mechanical properties of La(Fe,Mn,Si)13 were quantified. Understanding of the deformation and failure mechanisms is achieved by characterisation with transmission electron microscopy (TEM) and atom probe tomography (APT) to reveal the arrangement of hydrogen atoms in the crystal lattice. APT analysis reveals close arrangement of hydrogen atoms on {222} planes. This has led to an anisotropic weakening effect of hydrogen on single crystal La(Fe,Mn,Si)13; it is significant upon shearing parallel to the {111} crystallographic planes but is negligible when the shear plane is {001}-oriented. As a result, hydrogen deteriorates the strength of La(Fe,Mn,Si)13 through promotion of transgranular fracture in the macroscale.

Scanning Electron Nanobeam Diffraction experiments: from optical set-up to data handling and ML-assisted post-processing – case study for a battery cathode phase

Mohsen Danaie, Andy Bridger, Keith Butler, Thomas Wood, Bill David

Diamond Light Source, UK

The recent advances in direct electron detectors, along with faster read-out systems and supporting computers, has allowed synchronised full-frame electron diffraction signal acquisition triggered by microscope scan coils, the so-called 4D-STEM type of dataset. In Scanning Electron Nanobeam Diffraction (SEND), the convergence semi-angle of the probe is minimised (typically to around 1 mrad) to have a better separation of the diffraction peaks, instead compromising the probe size in real space (2-3 nm probe diameter). This mode of operation has been shown to be optimal for characterising crystallographic defects in large fields of view, especially in specimens with stringent limitations on electron dose. Since small amounts of drift in lower order aberrations, i.e. defocus and two-fold astigmatism, can be tolerated in this mode, it lends itself well to automation with little corrections needed from the operator.

In this contribution, we present the practical aspects of adjusting the microscope optics (in ePSIC's case, a probe and image Cs-corrected microscope), discussing the main challenges and points of future

improvement. Data handling, e.g. saving and compressing, aspects of the experiment, and the calibrations needed to correctly quantify the datasets in reciprocal and real space are also discussed. As a case study, we present data collected on a sodium-ion cathode material, a layered P2 phase with the nominal composition of Na2NiMn2O6, comparing the available workflows in segmenting the dataset based on the diffraction signal. Aiming to automate the workflow as much as possible, we have developed an unsupervised machine learning routine utilising variational auto-encoders to both enhance the signal-to-noise ratio and to classify the real space pixels into crystallographically coherent domains. In the Figure below, section A, an example SEND dataset is shown with pointer in panel A-1 corresponding to the diffraction signal in A-2. Panels A-3 and A-4 show steps in a standard segmentation approach, where a peak identification algorithm in PyXEM library [1] was used to find all the diffraction peaks in the sum pattern and then used to generate a series of virtual dark-field (VDF) images. A real-space pixel-wise search algorithm in the VDF images, resulted in the segmentation shown in A-4. The ML-assisted approach, shown in panel B, the network learns how to best map the variation seen in the experimental data onto a dimensionally reduced latent space (B-2). In doing so, firstly, the present Poisson noise can be separated, boosting the SNR in the patterns (examples provided in B-4) and secondly, by grouping the latent space points with similar features we can perform classification (B-1) with minimal human interaction. By quantifying the robustness of this segmentation, based on slightly varying the initial sampling of the latent space, we can output a confidence map of the final segmentation (B-3). In conclusion, we will compare the performance of the above workflow to the principal component analysis algorithms typically used in the literature.

[1] DOI: 10.5281/zenodo.2649351

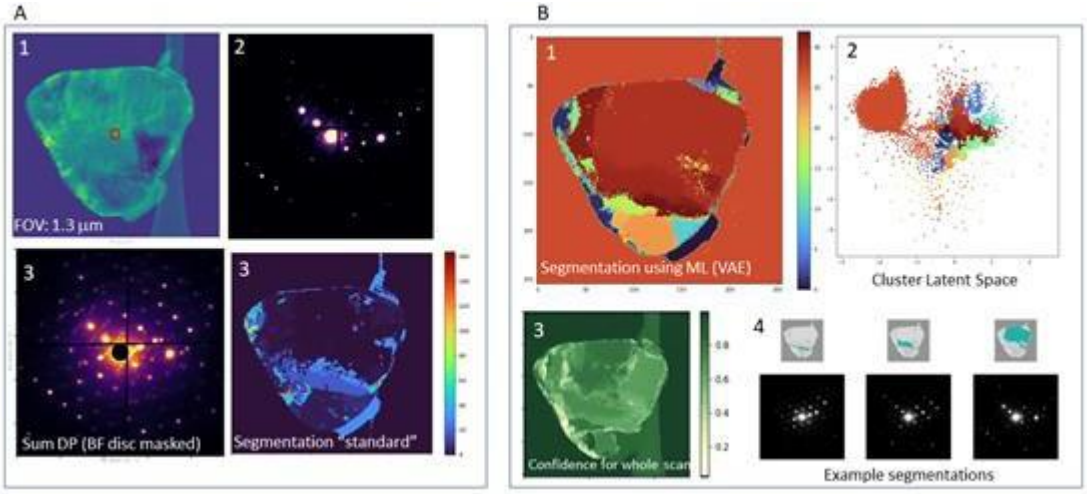

Unsupervised machine learning applied on correlated 4DSTEM/EDS data to investigate the structural ordering of Co2FeSi thin films

Ercin Duran, Irene Azaceta, Adam Kerrigan, Vlado Lazarov, Alexander Eggeman

University of Manchester, UK

Co-based full Heusler alloys, Co_2FeSi (CFS) in particular, have been regarded as promising candidates for spintronics applications because of their full-spin polarization ability and high magnetic moment [1,2]. However, the structural ordering within these materials influences these desired magnetic properties immensely. In this study, the structural ordering of phases within CFS thin films was investigated using correlated EDS and 4DSTEM approaches. Unsupervised machine learning (ML) methods, including decomposition and clustering approaches [3] were utilized to provide insight into the structural and compositional variations within the films. Two known orderings, B2 (Pm-3m) and $L2_1$ (Fm-3m), were

expected from previous XRD measurements, however, probabilistic fuzzy clustering-based ML applied to the combined compositional (EDS) and structural (4DSTEM) information indicated an unexpected additional phase. The attached Figure(a,b) shows clustering outputs of a CFS thin film grown on Si(111). The cluster in Figure(a) indicates the unexpected phase, evident by the highlighted reflection in its diffraction pattern, and the cluster in Figure(b) indicates the B2 phase of this system, evident by the highlighted (002) reflection.

Each cluster output has its own decomposed diffraction pattern and EDS spectrum as well as a membership map which indicates the location of the cluster in the scan. Memberships in the figure show how these phases are complementary in the films. The unexpected phase has a different stacking of {111} lattice planes leading to different stoichiometry to both B2 and $L2_1$ phases, which is supported by the EDS cluster output belonging to this phase. The attached Figure(c) demonstrates a representation of the crystal structure of this unexpected phase in the experimental orientation of [110] (of the cubic sub-lattice), modelled on these structural and compositional findings, along with the simulated diffraction pattern from that structure. DFT calculations based on this model support the stability of this structural ordering in Co-deficient samples and indicate that this minority superstructure could be the reason behind the variations in the magnetocrystalline anisotropy recorded in these thin films.

Correlated signals allow an unprecedented amount of information to be extracted by exploring the covariance of the two orthogonal datasets (EDS and electron diffraction data in this case) and treating it as a single dataset in the ML analysis. This method provides a fast and reliable understanding of the complex microstructure of these materials.

Acknowledgements:

The authors gratefully acknowledge funding from the Royal Society and the Ministry of National Education of Turkey.

References:

[1] Gercsi, Z. et al., Appl. Phys. Lett. 89, 082512 (2006), doi: 10.1063/1.2338025
[2] Zhu, W. et al., J. Magn. Magn. Mater. 479, 179-184 (2019), doi: 10.1016/j.jmmm.2019.01.087
[3] Martineau, et al., Adv. Struct. Chem. Imaging 5, 3 (2019), doi: 10.1186/s40679-019-0063-3

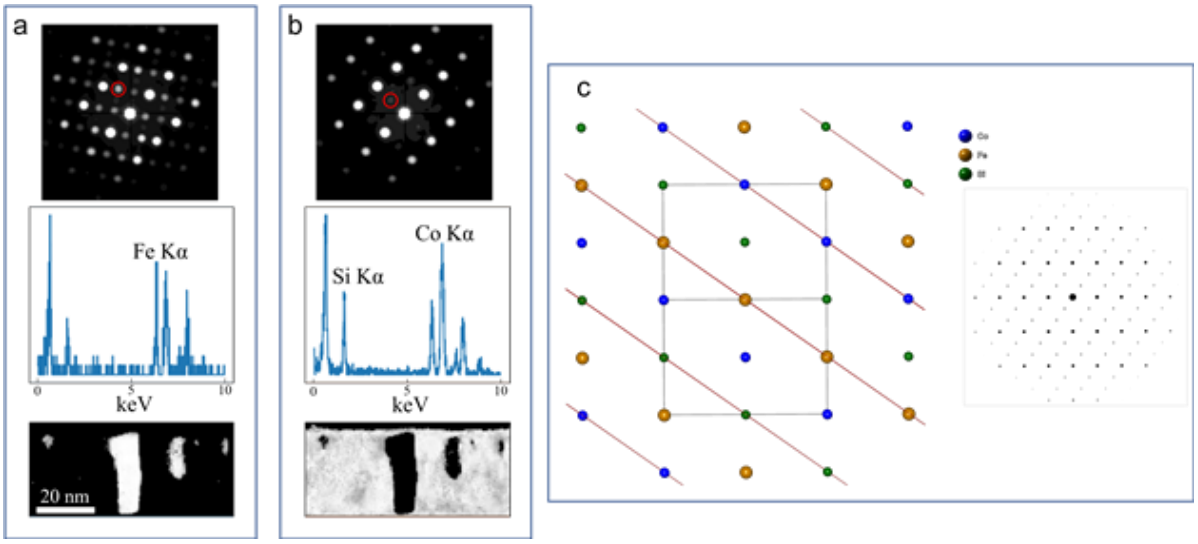

3D-Multidimensional Analysis of Magnetoelectric Multiferroic Topologies via Scanning Transmission Electron Microscopy, Spectroscopy and Atom Probe Tomography

Shelly Conroy, James Douglas, Sinead Griffin, Louise Colfer, Jennifer Halpin, Eoghan O'Connell, Kalani Moore, Ursel Bangert, Lynette Keeney, Baptiste Gault

Imperial College London, UK

Magnetoelectric multiferroic higher order topologies are an emerging solution for future low-power spintronic and quantum devices, due to a combination of their atomic-scale tunable multi-functionality and mobility. In addition to their potential for next-generation interactive technology, topologies with spin to charge coupling are a fertile ground for the exploration and engineering of new states of matter. In our recent report we have shown the presence of vortex topologies present in room temperature magnetoelectric multiferroic Bi6TixFeyMnzO18 thin films by atomic-scale scanning transmission electron microscopy (STEM) polarization mapping.[1,2] We find these chiral polar textures at antiphase boundaries within the thin films. Such topologies related to crystalline defects should be analyzed three-dimensionally to truly understand their formation. In this presentation, we will discuss the use of multidimensional microscopy techniques including Lorentz mode differential phase contrast (DPC) scanning transmission electron microscopy (STEM), atomic resolution integrated DPC STEM, electron spectroscopy, electron diffraction and atom probe tomography (APT).

For Bi6TixFeyMnzO18 the magnetic cation partitioning increases the probability of nearest-neighbor magnetic interactions in the central unit cell layer by up to 90% compared to random distributions over the other available B-sites.[3] Using atomic resolution STEM with corresponding energy dispersive X-ray (EDX) and electron energy loss spectroscopy (EELS) elemental mapping we can determine the location of Fe and Mn within the unit cell. Although electron spectroscopy characterization is also possible for topological defects (Figure 1), using this method we only have a 2D projected view of these 3D microstructural features. As the topologies themselves are the active regions within such material systems, it is vital that we explore the higher order elemental segregation in full real space. We hence used APT's unique 3D characterization capability to move beyond the 2D projection of the elemental segregation knowledge, with an aim to unravel the magnetic cation partitioning of complex 3D vortices and associated crystallographic defect topologies. Theoretical calculations confirm the subunit cell cation site preference and charged topology energetics. We will discuss the opportunities multidimensional characterisation techniques such as STEM, DPC, EELS/EDX and APT can bring to the field multiferroic higher order topology physics.

References:

1. Moore, K., O'Connell, E.N., Griffin, S.M., Downing, C., Colfer, L., Schmidt, M., Nicolosi, V., Bangert, U., Keeney, L., Conroy, M., ACS Appl Mater Interfaces (2022), doi:10.1021/acsami.1c17383
2. O'Connell, E., Moore, K., McFall, E., Hennessy, M., Moynihan, E., Bangert, U., Conroy, M., (2022) doi:10.1017/S1431927622000435
3. Keeney, L., Downing, C., Schmidt, M., Pemble, M.E., Nicolosi, V., Whatmore, R.W., Sci Rep. (2017) doi: 10.1038/s41598-017-01902-1

Acknowledgements:

The authors acknowledge funding from the EPSRC grant EP/V007661/1 that allowed access to the Imperial College London Atom Probe, funding from the EPSRC NAME grant EP/V001914/1, SFI grant that allowed access to the Titan STEM. The work at the Molecular Foundry was supported by the Office of Science, Office of Basic Energy Sciences, of the U.S. Department of Energy, DE-AC02-05CH11231. M.C. acknowledges funding from the Royal Society Tata University Research Fellowship (URF\R1\201318). L.K. acknowledges funding from the Royal Society and SFI University Research Fellowships UF 140263 and URF\R\201008, the Enhancement Award RGF\EA\180206 and SFI Frontiers for the Future Project 19/FFP/6475.

Classification of Fluctuating Gold Clusters using Convolutional Neural Networks

Malcolm Dearg, Henry P Hoddinott, Yubiao Niu, Richard E Palmer, Thomas J A Slater

Cardiff University, UK

The exact atomic structure of nanoparticle surfaces is of great importance in catalysis. Typically, 1-5nm metal particles will adopt decahedral, icosahedral or fcc structures – with glassy structures also common. The structural isomer of a nanoparticle can be measured using high-angle annular dark field (HAADF) scanning transmission electron microscopy (STEM) [1,2] in an aberration-corrected instrument. The isomer identification depends on comparison with a Simulation Atlas [1]. Here we investigate size-selected gold clusters produced by a magnetron sputtering, gas-condensation source [3]. One innovation is video imaging of the fluctuations of a single cluster over time; the second is an automated approach to classifying the structures – e.g., to determine their relative potential energies [1,2].

Machine learning has become popular in electron microscopy [4]. Here we turn this approach to the cluster structure classification problem. We use a convolutional neural network (CNN), a class of machine learning algorithm that can be trained to recognize image features [5]. Specifically, a CNN is trained using HAADF-STEM images of particles (simulated using the plane-wave reciprocal-space interpolated scattering matrix (PRISM) algorithm) to recognize the different shapes and patterns of nanocluster images from HAADF-STEM [6]. The neural network can rapidly determine the proportion of different isomers. The speed improvements afforded by the CNN approach will allow us to process multiple videos of individual clusters, determining the structure in each frame. This concept is demonstrated using the manual classification approach of Fig. 1. Video-rate imaging versus temperature [2] will determine both isomer energies and branching ratios (thus energy barriers) between the different structures.

[1] D. M. Wells, et al., Nanoscale 7 6498 (2015). doi: 10.1039/C4NR05811A
[2] D. M. Foster, R. Ferrando & R. E. Palmer, Nat. Comms. 9 1323 (2018). doi: 10.1038/s41467-018-03794-9
[3] S. Pratontep, et al., Rev Sci. Instr. 76 045103 (2005). doi: 10.1063/1.1869332
[4] J. M. Ede, Mach. Learn.: Sci. Technol. 2 011004 (2021). doi: 10.1088/2632-2153/abd614
[5] A. Dhillon & G. K. Verma, Prog. Artif. Intell. 9 85 (2020). doi: 10.1007/s13748-019-00203-0
[6] L. Rangel DaCosta, et al., Micron 151 103141 (2021). doi: 10.1016/j.micron.2021.103141

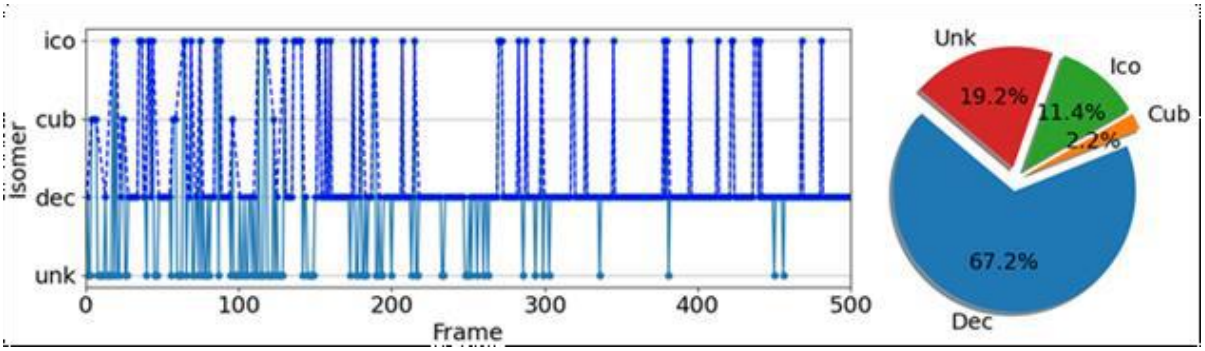

Figure 1. Manual classification results from an HAADF-STEM video of one Au309 cluster on carbon at room temp. Icosahedral (ico), decahedral (dec), cuboctahedral (cub), unknown/amorphous (unk).

Deep neural network pipeline for statistically significant metrics of heterogeneous catalyst systems

Kevin Treder, Chen Huang, Aakash Varambhia, Cameron Bell, Thomas Slater, Manfred Schuster, Doğan Özkaya, Judy Kim, Angus Kirkland

University of Oxford, UK

In the field of heterogeneous catalysis, (Scanning) Transmission Electron Microscopy ((S)TEM) is often used to analyse key characteristics such as size and shape distributions of nanoparticles to understand a system's catalytic performance. Commercialisation of dedicated sample holders, significant technical advances in direct electron detection and introduction of automated imaging routines have extended such analysis towards in situ experimentation in different environments, while large datasets are generated more frequently [1-3]. Those advances limit the applicability of more established manual and semi-automated image analysis methods, as they are often time consuming or require favourable imaging conditions and human intervention. In this context, robust approaches for automated image analysis are required for full analysis and understanding of acquired datasets [3].

Research in electron microscopy (EM) recently showcased machine learning (ML) and deep learning (DL) [4] approaches for large datasets and demonstrated successful application in the physical and life sciences [5]. In the case of nanoparticle systems, however, a number of aspects remain unaddressed as studies focus on topologically uniform support materials with well-discernible contrast between nanoparticles and background. In addition, workable array size of individual images is bound to available GPU resources, which can be a limiting factor for automated and fast data acquisition and processing.

In this work, we present the deep neural network pipeline nNPipe for automated analysis of morphologically diverse catalyst systems. nNPipe passes raw HRTEM images of 2048x2048 pixels through two standalone convolutional neural networks (CNNs) and outputs semantically segmented maps. Both CNNs are trained on large datasets of simulated TEM images to achieve high generalisation and to avoid the introduction of unintentional human bias. The performance of our approach is assessed on experimental HRTEM images of two nanoparticle systems for comparison: Gold nanoparticles on ultrathin amorphous germanium (Au/Ge) as a standard calibration sample and palladium on active carbon (Pd/C) as a realistic, morphologically diverse industrial catalyst. Insights are discussed in light of an automated imaging scenario where statistically significant metrics of thousands of nanoparticles can be extracted at high performance. Finally, we propose a time-efficient retraining scheme to deploy nNPipe on images of other heterogeneous catalyst systems that were acquired with differing imaging techniques, resolution and experimental conditions.

References:

[1] : F. M. Ross, Science (2015), 350, 6267, aaa9886.
[2] : M. L. Taheri, E. A. Stach, I. Arslan, et al., Ultramicroscopy (2016), 170, 86-95.
[3] : S. R. Spurgeon, C. Ophus, L. Jones, et al., Nat. Mater. (2021), 20, 274-279.
[4] : Y. LeCun, Y. Bengio, G. Hinton, Nature (2015), 521, 436-444.
[5] : K. P. Treder, C. Huang, J. S. Kim, et al., Microscopy (2022), 71, i100-i115.

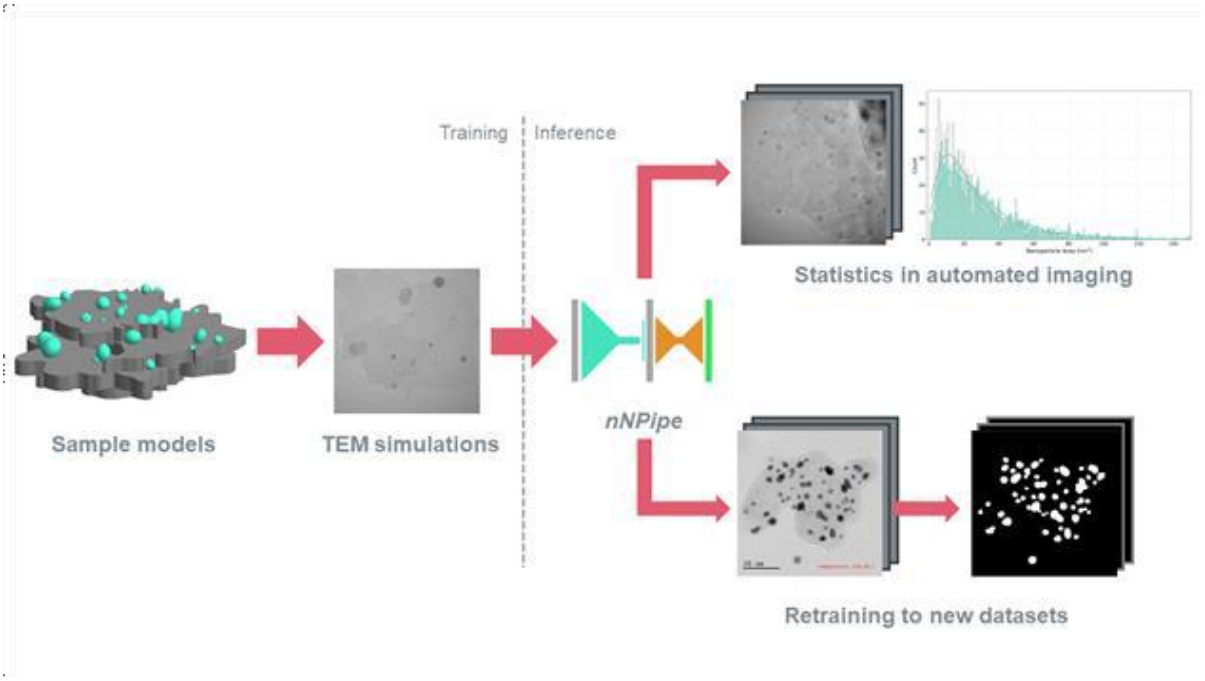

Extracting the crystal orientation information from spectroscopic data for the EMCD experiments

Hasan Ali

Stockholm University, Sweden

EMCD is an electron energy loss spectroscopy (EELS) based technique [1] in the transmission electron microscope which can be used to measure the element specific magnetic moments of the materials at nanometer scale. In a classical EMCD experiment, two or four off-axis EELS spectra are acquired at specific scattering angles in the reciprocal space, with the crystal tilted in two or three beam diffraction condition respectively. The difference of these spectra, after post-processing, gives the EMCD signal. By applying theoretical sum rules to the EMCD signal, ratio of magnetic orbital to spin moments can be calculated.

One of the challenge for the EMCD experiments is the requirement of strict diffraction conditions. It has been previously demonstrated that a crystal mistilt from the perfect two beam condition can significantly influence the EMCD signal [2], causing misleading results. It is not trivial to record the diffraction information from the same region of the sample where EMCD experiment was done, keeping the same experimental conditions. Here, we introduce a way to obtain the crystal misorientation information from a three beam condition directly from the same spectroscopy data recorded for the EMCD experiment, excluding the need to record the diffraction patterns. This simplifies one step of complexity in the EMCD experiments. Moreover, we experimentally verify that carrying out the EMCD experiments in three beam condition is better than the two beam condition and it helps to reduce the effects of small crystal mistilts on the resulting EMCD signal.

[1] Schattschneider, P. et al. Detection of magnetic circular dichroism using a transmission electron microscope. Nature 441, 486–488 (2006).
[2] Ali, H., Rusz, J., Warnatz, T., Hjörvarsson, B. & Leifer, K. Simultaneous mapping of EMCD signals and crystal orientations in a transmission electron microscope. Sci. Rep. 11, 2180 (2021).

Visualising surface chemistry variations across length scales using secondary electron hyperspectral imaging in LV-SEM

James Nohl, Yige Sun, Gareth Hughes, Serena Cussen, Cornelia Rodenburg

University of Sheffield, UK

Summary

The extent of the carbon-binder domain (CBD) coverage on lithium nickel manganese cobalt oxide (NMC) particles in a lithium-ion battery (LIB) cathode film was visualised using secondary electron hyperspectral imaging (SEHI). SEHI provides chemical information on both the nano- and micron scale. This is important as the CBD domain on these length scales impacts the effective transport properties of a NMC cathode. For easy visualisation of the 3D SEHI data volume consisting of 2 spatial and 1 energy dimension, emissions within relevant energy bands were assigned to the channels of an RGB image.

Introduction

Low-voltage scanning electron microscopy (LV-SEM) is useful for imaging beam sensitive and insulating materials [1] [2]. The secondary electron (SE) signal is most commonly used for imaging, as the high signal-to-noise ratio and spatial localisation of emission results in high resolution images with short acquisition times [3]. By collecting SE images series of the same area but each formed by SE with different energy, localised SE spectra can be captured and derived from such SEHI data volumes. A challenge for SEHI – and any hyperspectral imaging – is to visualise the energy dimension of the 3D data volume [4].

Here we apply SEHI to characterise a LIB cathode film (Figure 1), which is a composite of NMC, CBD which consist of PVDF and carbon black (CB). SE spectra including the relevant spectral ranges of interest for NNM and CBD are shown in Figure 1 as identified in [5].

Results and discussion

The SE energy range where NMC material is distinct was used to select SE emission energy ranges to be included in the colour channels of an RGB image by the process described in Figure 2.

The resulting colourised image (Figure 2e) shows red colouring in regions where NMC is present at the particle surfaces, and blue colouring is assigned to regions with spectra typical for CHx surfaces. CHx can be associated with the extent of CBD domain at the surface. This colouring is consistent with the result returned by SE spectral analysis of the NMC associated peak and CHx range shown in Figure 1. However, using colour channels in the way introduced here visualises the distribution of the CBD domain on nano and micron-scales.

References

1. Schatten, Micron, 42(2), 2011, 175-185, doi:10.1016/j.micron.2010.08.008
2. Wuhrer; Moran, 2016 IOP Conf. Ser.: Mater. Sci. Eng. 109 012019, doi:10.1088/1757-899X/109/1/012019
3. Liberman et al., Ultramicroscopy, 218, 2020, 113085, https://doi.org/10.1016/j.ultramic.2020.113085
4. Kim et al., IEEE Transactions on Visualization and Computer Graphics, 16(6), 1441-1448, 2010, doi:10.1109/TVCG.2010.172
5. Nohl et al., Micron, 156, 2022, 103234, doi:10.1016/j.micron.2022.103234

Acknowledgements

The Authors would like to acknowledge funding from: EPSRC; Faraday Institution; Henry Royce Institute; Henry Royce Institute Royce Equipment Access Scheme

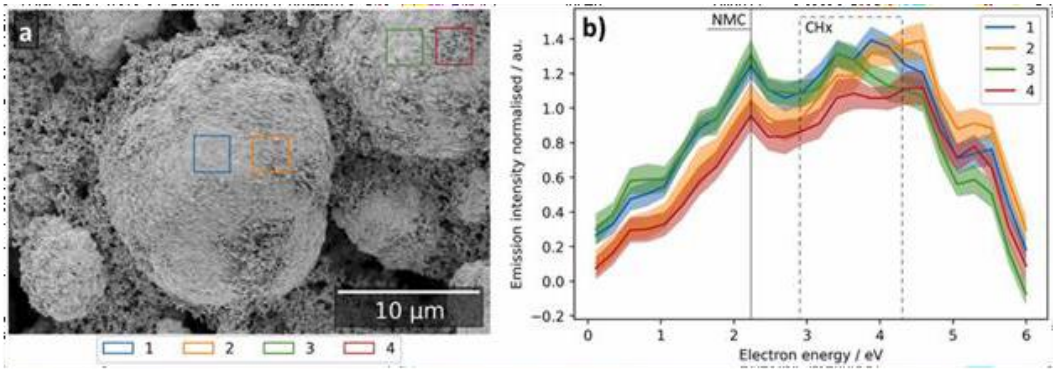

Figure 1 – (a) SE image with regions of interest (ROI) outlined from which SE spectra are derived. (b). Error bars are derived from ± the standard deviation of SE spectra per pixel location in the outlined ROI in (a) Reproduced from [5] under CC BY 4.0 license

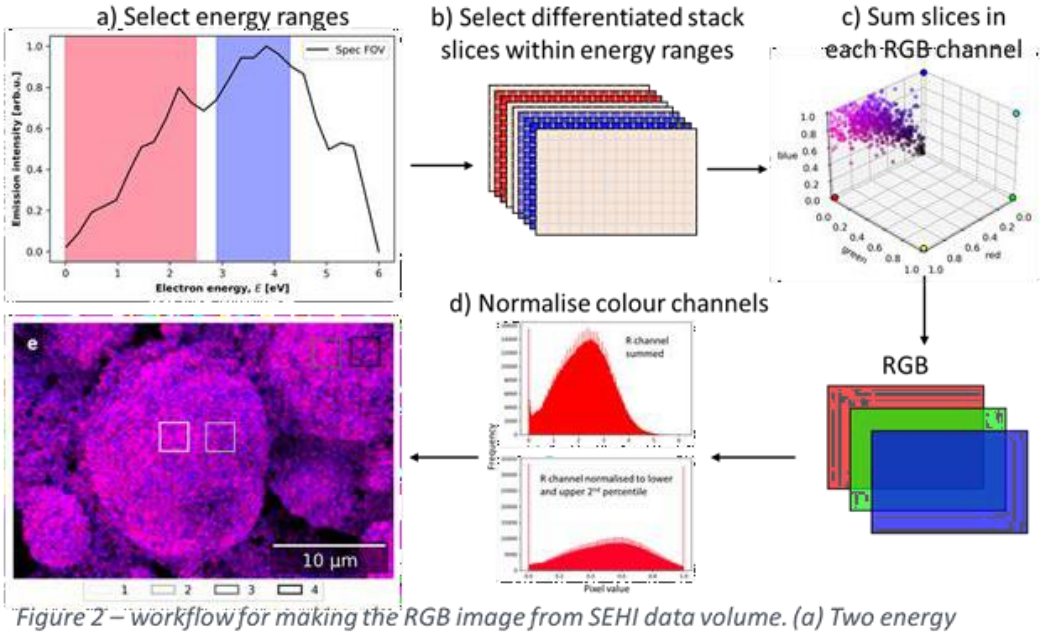

Figure 2 – workflow for making the RGB image from SEHI data volume. (a) Two energy ranges were selected based on regions identified in [5]. (b) The SEHI data volume image slices made up of integrated SE emissions below a cut-off energy were differentiated with respect to the energy to obtain differentiated image slices. (c) The differential slices within the relevant energy range are summed to create one of the RGB colour channels. (d) The colour channel images are normalised per colour channel (e) The colour image with non-zero Red and Blue ranges. Regions of interest from [5] plotted.

Accessing Sub-Angstrom Ptychographic Information in a Scanning Electron Microscope at ≤ 30 kV

Arthur Blackburn, Cristina Cordoba, Matthew Fitzpatrick, Robert McLeod

University of Victoria, Canada

Though electron ptychography was first experimentally demonstrated in a 30 kV scanning electron microscope (SEM) showing 236 pm lattice fringes in gold particles [1], relatively little exploration of ptychography

has been pursued at these relatively low beam energies since. The reasons for this have been primarily technological. Scanning transmission electron microscopes (STEMs) which generally have beam energies ≥ 60 keV offer easily variable camera length, facilitating acquisition of diffraction data for ptychography at variable resolution, in comparison to SEMs. Furthermore, dedicated STEMs and TEMs offer higher resolution imaging, with the possibility of aberration correction. Ptychographic information is complementary to these high-resolution imaging modes. Perhaps most importantly, dedicated TEM instruments are routinely fitted with a pixelated detector for normal imaging modes, which allows some low-speed demonstration of ptychography. However, the technique has only become practical with recent advances in high-speed direct detectors in S/TEM systems. Such detectors have not until very recently become available on SEM instruments. Owing to their commercial and scientific importance, these higher energy instruments have guided the development of advanced high speed direct electron detectors. These detector advances, coupled with computing and algorithm developments, have given rise to the field of 4D-STEM.

Obtaining high-resolution information data, beyond the probe size limit, through ptychography in physically smaller lower beam-energy SEMs nonetheless remains an attractive prospect, by providing low-energy, high-resolution imaging in a convenient and highly accessible instrument. Low-energy imaging reduces electron-beam knock-on damage in some materials, such as transition metal dichalcogenide monolayers and graphene, for example. Fortunately, progress has been made in hybrid direct-electron detector technology to allow robust, efficient and high-speed pixelated detection at 30 keV beam energy and below, as demonstrated in a Dectris Quadro pixelated detector used in this work. This detector was used on a Hitachi SU9000 Cold FEG SEM/STEM, that was customized to include a basic projector lens for camera length control.

Example ptychographic reconstructions taken from gold islands on (nominally) monolayer MoS_2 (Fig. 1 a) and gold particles on amorphous carbon (Fig 1b) using a beam energy of 20 keV and 30 keV respectively, are presented. These reconstructions used a multi-slice algorithm, and here we present the summed phase from all slices. This high-resolution quantitative phase information can, for example, be fitted and compared with models of the system to allow determination of the thickness of the islands / particles. In the case of the MoS_2 sample, analysis yields the relative rotation angles that give rise to Moiré-like effects observed elsewhere through high resolution STEM and TEM. Analyzing the Fast Fourier Transforms (FFTs) of the images (right-hand side of Fig 1a, and Fig 1b), we see features that are present below the 1 Å level. Furthermore, in the case of the Au on MoS_2 reconstruction, we see Moiré related features in the FFT that were expected from modelling [2]. Before this work, such features were only evident in FFTs of high-resolution aberration corrected TEM images of this sample. That such details can be seen in a non-aberration corrected SEM class-instrument using ptychography, leads to exciting possibilities for the use of SEM for high resolution studies of materials that may benefit from low beam-energy imaging.

Reference:

[1] M. J. Humphry, B. Kraus, et al., Nature Comms., Vol.3, (2012), 730.
[2] K. Reidy, G. Varnavides, et al., Nature Comms, 12 (2021), 1290.

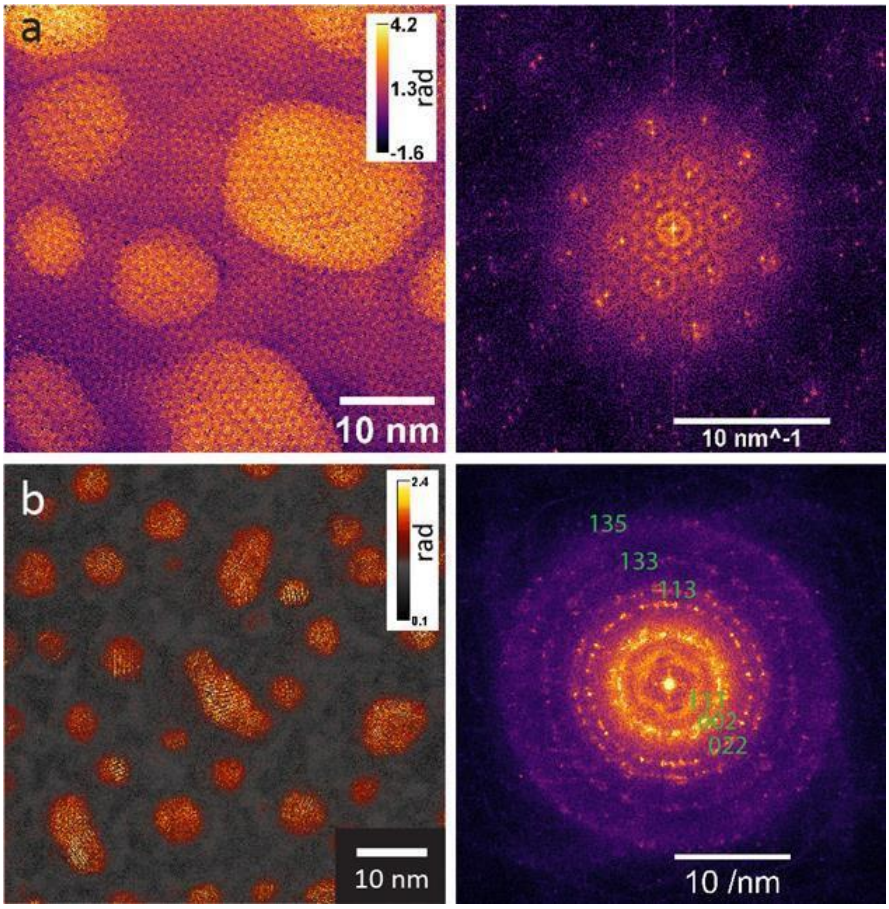

Low Voltage Electron Ptychographic Imaging

Christopher Allen, Mohsen Danaie, Angus Kirkland, Darren Batey

University of Oxford, UK

Recent advances in detector technology [1] have been the catalyst for developments in electron diffraction imaging techniques, the most transformative of which is ptychography [2]. In a ptychographic experiment a far-field diffraction pattern is recorded on a pixelated detector at each electron probe position. Provided certain sampling conditions have been met during acquisition [3] these data sets can be used to reconstruct the complex transmission function of the object being imaged. The resolution of these reconstructions is not limited by the size of the illumination probe, rather by the maximum scattering angle which is recorded on each diffraction pattern. This decoupling of resolution from the optical system of the microscope has the potential to transform electron microscopy, particularly for regimes in which aberration correction is challenging.

Here we demonstrate the ptychographic reconstruction of images from monolayer MoS2 at an accelerating voltage of 30keV on an aberration corrected JEOL ARM300CF instrument. The ADF signal and diffraction pattern are simultaneously recorded at each electron probe position and the complex transmission function of the object reconstructed using the ePIE algorithm [4]. The reconstructed ptychographic images (figure 1b)

show a significant improvement over the resolution achievable using a six-fold astigmatism limited aberration corrector (figure 1a). The power spectrum of the reconstructed phase image (figure 1c) shows information out to at least 1.36 Å and the full width half maximum of atomic sites is measured to be 1.2±0.1 Å (figure 1d).

[1] MacLaren et al. APL Materials 8 (11), 110901 (2020)
[2] Chen et al. Science 372, 6544, 826-831 (2021)
[3] Rodenburg and Maiden. Ptychography. In: Hawkes, P.W. and Spence, J.C.H., (eds.) Springer Handbook of Microscopy. Springer. (2019)
[4] Maiden and Rodenburg, Ultramicroscopy, 109(10),1256-1262. (2009).

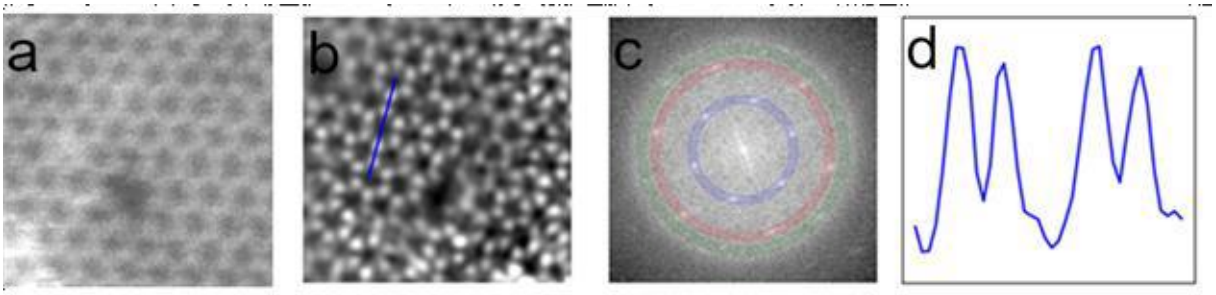

A Correlative Microscopy Technique Development: Exploring 3D Chemistry and Grain Orientation in Ni-W Nanocrystalline alloys

Saurabh Mohan Das, Patrick Harrison, Srikakulapu Kiranbabu, Wolfgang Ludwig, Edgar F. Rauch, Christian H. Liebscher, Michael Herbig

The Max-Planck-Institut für Eisenforschung, Germany

Macroscopic properties such as fracture toughness, corrosion, and the stability of nanocrystalline (NC) alloys are strongly related to grain orientation and grain boundary (GB) segregation phenomena [1]. Grain boundary segregation is highly influenced by the grain boundary character i.e., their five macroscopic degrees of freedom. To establish a relation between grain boundary character and segregation with highest possible spatial and chemical resolution in 3-dimensional space, a correlative transmission electron microscopy (TEM: crystallographic information) and atom probe tomography (APT: chemical information) approach is required [2]. In this correlative method development, 4D-scanning precession electron diffraction (4D-SPED) tomography of a needle-shaped specimen is correlated with APT to obtain grain orientation mapping with high spatial resolution for identify the degrees of freedom of the GBs and their associated solute distribution in three-dimensions. In this technique, a ~1 nm-sized incident beam is precessed by 1° while being scanned over a needle shape Ni-W NC-alloy to realize quasi-kinematical scattering conditions. Nanobeam scanning precession electron diffraction (SPED) patterns are acquired for a ±80° tilt range with 10º tilt increments. The diffraction patterns are recorded using a scintillator coupled CMOS camera (TVIPS TemCam-XF416) for capturing reflections with high signal-to-noise ratio, dynamic range and read-out speed. This generates a 4D dataset which is processed and analyzed using the ASTAR software package and custom written Python codes. The automated crystal orientation mapping (ACOM) algorithm is used to generate an orientation map at each tilt step. The diffraction pattern at each probe position may contain information from overlapping grains along the beam direction and hence a multi-indexing technique is developed to distinguish and index overlapping grains [3]. Subsequently, a virtual dark field (VDF) image of each grain is generated for each tilt step, which are used for tomographic reconstruction of 3D grain shape and orientation map.

Here, we will present the correlation of 3D grain orientation with 3D compositional mapping and discuss the implication of grain boundary segregation effect in Ni-W nanocrystalline alloys.

References:

1. T. Chookajorn, H. A. Murdoch, C.A. Schuh, Science 337, 951-954 (2012).
2. M. Herbig, P. Choi, D. Raabe, Ultramicroscopy 153, 32-39 (2015).
3. A. Valery, E.F. Rauch, L.Clément, F. Lorut, Journal of Microscopy 268, 208-218 (2017).

Visualising beam-activated degradation processes in halide perovskite semiconductors using 4D-STEM nanoprobe diffraction

Jordi Ferrer Orri, Tiarnan Doherty, Duncan Johnstone, Sean Collins, Hugh Simons, Paul Midgley, Caterina Ducati, Samuel Stranks

University of Cambridge, UK

Advances in electron microscopy have recently enabled the study of the structure and properties of lead halide perovskites, promising optoelectronic materials. These techniques use high-energy electrons focused to achieve nanoscale spatial resolution to study the relevant length scales at which carrier trapping inhomogeneities and instabilities exist in optoelectronic performance. However, due to the soft organic-inorganic nature of these materials, they suffer from electron beam degradation, limiting their use. Therefore, understanding the interaction of high-energy electrons in such soft ionic semiconductors is essential for the correct characterization and understanding of these novel energy materials.

Here, we study the interaction of electrons in state-of-the-art triple-cation hybrid halide perovskite films using 4D-STEM electron diffraction (SED). We track the changes in the local crystal structure in-situ as a function of fluence. We quantify the fluence at which we identify perovskite grains with additional reflections corresponding to crystalline degradation phases appear. Concomitant crystallographic changes are observed at the adjacent high-angle grain boundaries, followed by pinhole formation and a tetragonal to cubic phase transition.

Our study explores the radiation limits of halide perovskite films from a crystallographic standpoint and provides a fundamental understanding of the nanoscale degradation of these films. It identifies high-angle grain boundaries as critical for the future improvement of instability, especially for applications vulnerable to high energy radiation such as space photovoltaics. As we tend towards higher exposure techniques, needed for in-situ TEM studies, these findings are crucial for any characterization technique studying the nanoscale of halide perovskites and, more generally, soft semiconductors.

Imaging Structural Defects and Associated Oxygen Positions in Li-rich Li1.2Ni0.13Mn0.54Co0.13O2

Weixin Song, Peter Nellist

University of Oxford, UK

Li-rich Li1.2Ni0.13Mn0.54Co0.13O2 has delivered a high specific capacity over 250 mAh g-1 as a cathode material in Li-ion batteries compared with conventional layered metal oxides (<200 mAh g-1). Such high capacity results from the redox reaction of the lattice O2- ions and transition metals (TMs). Despite the boost in the capacities, Li1.2Ni0.13Mn0.54Co0.13O2 still suffers from voltage hysteresis and degradation in the

voltage and capacity over cycling [1]. Synthesis efforts aim to overcome these issues. The challenge is $Li_{1.2}Ni_{0.13}Mn_{0.54}Co_{0.13}O_2$ has rather inhomogeneous crystalline structures whose role in affecting the materials performance is unclear [2]. The as-prepared $Li_{1.2}Ni_{0.13}Mn_{0.54}Co_{0.13}O_2$ material contains a number of defects, such as stacking faults, and has raised debates on whether the material is a coherent mixture of C2/m Li_2MnO_3 and R-3m $LiTMO_2$ phase or a solid solution with the monoclinic phase [2]. The lack of understandings on the pristine structure of $Li_{1.2}Ni_{0.13}Mn_{0.54}Co_{0.13}O_2$ impedes the approach development for new materials.

In this work, we performed simultaneous annular dark field (ADF) imaging and electron ptychography on pristine $Li_{1.2}Ni_{0.13}Mn_{0.54}Co_{0.13}O_2$ prepared by sol-gel method. Figure 1a shows the ADF image projected along the pseudo [100] zone axis, which rather than showing only monoclinic [100] projection domains, shows three types of monoclinic domains projected along the [100], [110] and [1-10] zone axis, respectively. The domain variants are due to the faulted stacking of the TM layers in c direction. The TM layers composing the three types of domains have an in-plane rotation angle of 120 degree with respect to each other and the resulting stacking faults are referred to as rotation type. In the TM layers, Li^+/Ni^{2+} and Co^{3+}/Mn^{4+} cation ordering in a honeycomb pattern leads to the dumbbell contrast in ADF imaging that arising from the mixing Co/Mn atom columns [1]. The dumbbell contrast is not uniformly seen as shown in Figure 1b, where cation disordering contrast is seen in the transition regions (labelled with white dash) between the [110] and [1-10] projection domains. Such transition regions possibly result from the boundaries of the two types of domains or the in-plane cation disordering. Figure 1c displays several types of TM layers that lead to cation ordering (O), mixing ordering/disordering (O/D) and disordering (D) contrast in ADF imaging. In addition to the rotation-type stacking faults, Figure 1d shows another type resulting from out-of-plane TMs layer shift by a vector of c/2 in the c direction, namely shift type. Both types of stacking faults rely on the imaging of TMs layers whilst lack the understanding of oxygen stacking. To probe the oxygen lattice, we carried out focused-probe electron ptychography to reconstruct the phase image of the material and use the simultaneous aberration-corrected ADF image to point out TMs. Figures 1(e-g) show the simultaneous ADF and ptychographic image and their composite image, respectively, of a rotation-type stacking fault region and Figures 1(h-j) show that of a shift-type stacking fault region. Although TM layers possess a number of rotation-type stacking faults, the oxygen layers are seen in an O3-type stacking, coordinating with the TMs at the octahedral sites. Such TM-O coordination and the more covalent bonding of TM-O than Li-O lead to O layer mismatch in the shift-type stacking faults, indicated by the solid and dash circles in Figure 2f. The imaging on the TMs and O layer stacking shows different structure defects in $Li_{1.2}Ni_{0.13}Mn_{0.54}Co_{0.13}O_2$ that can affect the electrochemical performance [3].

Reference

1. House, R.A., Rees, G.J., Pérez-Osorio, M.A., Marie, J.-J., Boivin, E., Robertson, A.W., Nag, A., Garcia-Fernandez, M., Zhou, K.-J., and Bruce, P.G. (2020). First-cycle voltage hysteresis in Li-rich 3d cath- odes associated with molecular O_2 trapped in the bulk. Nat. Energy 5, 777-785.
2. Shukla, A.K., Ramasse, Q.M., Ophus, C., Kepaptsoglou, D.M., Hage, F.S., Gammer, C., Bowling, C., Gallegos, P.A.H., and Venkatachalam, S. (2018). Effect of composition on the structure of lithium- and manganese-rich transition metal oxides. Energ. Environ. Sci. 11, 830-840.
3. The authors acknowledge John J. Marie and Peter G. Bruce, for providing the materials, and the use of characterization facilities within the David Cockayne Centre for Electron Microscopy, Department of Materials, University of Oxford, and in particular the Faraday Institution (FIRG007, FIRG008), the EPSRC (EP/K040375/1 “South of England Analytical Electron Microscope”) and additional instru- ment provision from the Henry Royce Institute (Grant reference EP/R010145/1).

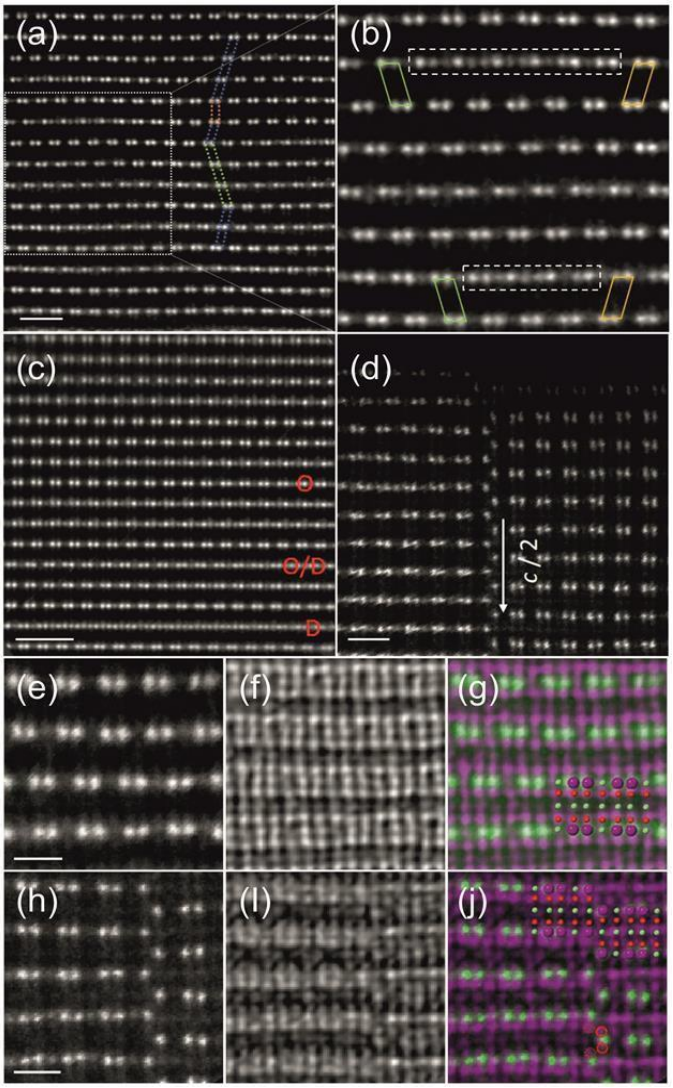

Figure 1 Stacking faults of Li1.2Ni0.13Mn0.54Co0.13O2 from atomic resolution. (a) ADF image along pseudo [100]M zone axis in a rotation-type stacking fault region. The white rectangular region is magnified in (b). The red, green and orange tetragons indicate monoclinic domains projected along [100], [110] and [1-10] zone axis, respectively. (c) ADF image of various types of TMs layers showing cation ordering (O), mixed ordering/disordering (O/D) and disordering (D) contrast. (d) ADF image of shift-type stacking fault structure. Scale bar is 1 nm. (e-j) Imaging of TMs and O layer stacking. (e-g) Rotation-type stacking faults. (h-j) Shift-type stacking faults. (e, h) ADF image. (f, i) Ptychographic image. (g, j) Composite image of the simultaneous ADF and ptychographic image. Superposed image in c and f is the monoclinic crystal models projected along [100] zone axis. Purple sphere is TM, green is Li and red is O. Scale bar is 0.5 nm.

Revelation of electric dipole configurations on the subatomic scale in ferro-electric materials envisaged for quantum device

Ursel Bangert, Michele Conroy, Eoghan O'Connell, Kalani Moore, Alan Harvey,

University of Limerick, Republic of Ireland

Recent advances in electron microscopy enable direct visualization of sites of individual atoms as well as disclosure of their chemical nature, electronic structure and dynamic behaviour. This talk will focus on the

revelation of electric dipole constellations in ferro-electrics. It will also focus on investigations of the atomic constellations of domain walls (DWs) in these ferro-electrics.

Ultra-high resolution (S)TEM investigations have been carried out to study sub-Angstrom structural properties and arrangements of atoms in these ferro-electrics, establishing electric dipole constellations within domains as well as at DWs; the latter constituting 2-D, as well as 3-D, entities. DWs are identified by revealing displacements of atoms in their vicinity, as well as the direction of these displacement, since there is a change in the electric dipole direction at such boundaries. DWs are also identified by polarisation mapping based on strain. We designed the TopoTEM open-source software package to quantify these atomic displacements and thus map the polarisation across DWs and other higher order topologies such as vertex and vortex structures[1]. Also, the structural dynamics of dipoles, i.e., fluctuations of their directions in the vicinity of out-of-phase DW boundaries, leading to the formation of vortices, has been observed[2]. Furthermore, movement of DWs was detected to occur under the influence of electric fields, also in the EM, resulting in the formation of vertex topologies[3]. Low loss EELs measurements were carried out to reveal changes in the bandgap at DWs, to establish and prove whether they are conducting. Possibilities to control the formation and mobility of conducting DWs, with the aim to employ these as electronic switches of nano- and quantum devices, will be explored via EM. The creation of such boundaries is also being attempted in 2-D ferro-electrics, where they constitute 1-D (line) entities. All experimental results are supported by image simulations and modelling.

References

1. E.O'Connell, K. Moore, E. McFall, M. Hennessy, E. Moynihan, U. Bangert, M. Conroy, arXiv preprint arXiv:2110.00112 (2021).
2. K. Moore, E. O'Connell, S. M. Griffin, C. Downing, L. Colfer, M. Schmidt, V. Nicolosi, U. Bangert, L. Keeney, M. Conroy, ACS Appl. Mater. Interfaces (2022).
3. M. Conroy, K. Moore, E. O'Connell, L. Jones, C. Downing, R. Whamore, A. Gruverman, M. Gregg, U. Bangert, Microscopy and Microanalysis (2020) 1-4.

Determining Atomic Structure of Grain Boundaries and Heterostructure Interfaces at Solid-State Electrode/Electrolyte

Connor Murrill

University of York, UK

Improving upon the current generation of lithium-ion batteries requires a holistic understanding of electrochemical and structural/chemical changes due to work-cycles of the electrodes/electrolyte heterostructure. Multiple mechanisms exist for cell degradation, whether this be through structural fatigue in the bulk of the electrodes or via formation of solid electrolyte interfaces (SEIs). With resolutions achievable below 1 Å in aberration corrected transmission electron microscopy (TEM), structural analysis of grains, grain boundaries, as well as interfaces between electrode (LiCoO2, LCO) and electrolyte (Li7La3Zr2O12, LLZO) as well as formed current induced SEIs is possible on atomic scale. This work focuses on atomic structure of LCO and LLZO's grain boundaries, alongside the interface between electrode and electrolyte. The goal will be determining the structural characteristics of the boundaries and interfaces that will allow us to build atomistic models for calculating the electronic properties (including barrier heights etc.) for Li transport/diffusion. The observation of defects and interfacial composition down to atomic resolutions is fundamental to understanding the specific characteristics changing the efficiency of lithium-ion movement through the device. Hence, dynamic analysis

of worked/charge cycled and as prepared devices is the key for understanding the processes that lead to structural degradation and SEIs. Ultimately leading to improved design of solid-state battery devices.

By combining SEM/EDX/EBSD with HRTEM and STEM/EELS we will present structural and chemical analysis of the electrode/electrolyte grain boundaries in sintered systems as well as the interfaces in thin films heterostructures grown by Pulsed Laser Deposition (PLD). EBSD analysis of the sintered LCO-LLZO system has provided band contrast distinguishing individual grains and phase maps across these samples. Multiple grain boundaries existed within both the electrode and electrolyte and crystal orientations of each grain were mapped. Low-magnification bright- and dark-field TEM has allowed grain boundaries and defects in electrode and electrolyte to be analysed, and suitable dislocation and stacking faults analysis to be done in these complex grain boundaries. Fig. 1a, b. Further higher-resolution STEM work has been employed to analyse secondary phases and structure of the defects. The PLD grown heterostructures are less complex in nature, with well-defined gain boundaries within the electrolyte and the electrode. In Fig. 2 is shown a LCO grown film on the Al2O3 substrate. The HRTEM and diffraction analysis shows that film is single phases with unique grain boundaries as shown in Fig.2. Further atomistic imaging of these boundaries is ongoing (Fig. 3), as well as chemical analysis on sub-nm level using STEM-EELS. Finally, we will also present the chemical and structural stability of the LCO/LLZO interface, with focus on comparing these interfaces in as prepared and under bias structures in in-situ conditions.

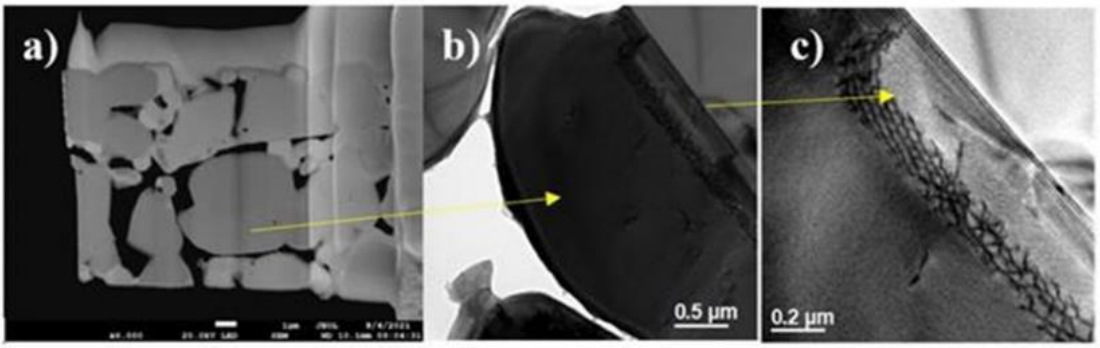

Figure 1: a) SEM of sintered LCO-LLZO system, **b)** and **c)** BF-TEM of dislocation system near an LCO grain boundary.

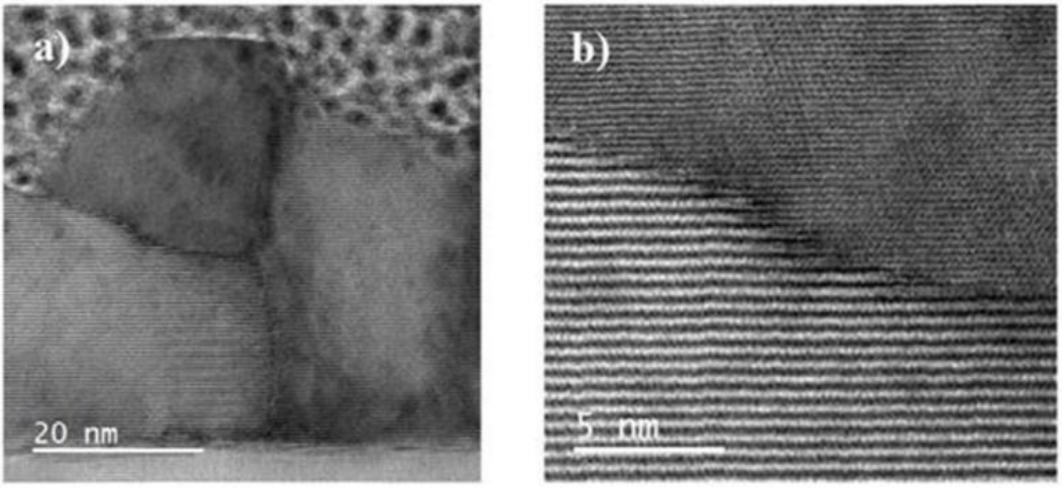

Figure 2: a) HRTEM images of region in the LCO film showing a triple boundary grin. **b)** HTEM of selected region of the LCO showing the different crystal orientation and structure of the grain boundary indicated in **a)**

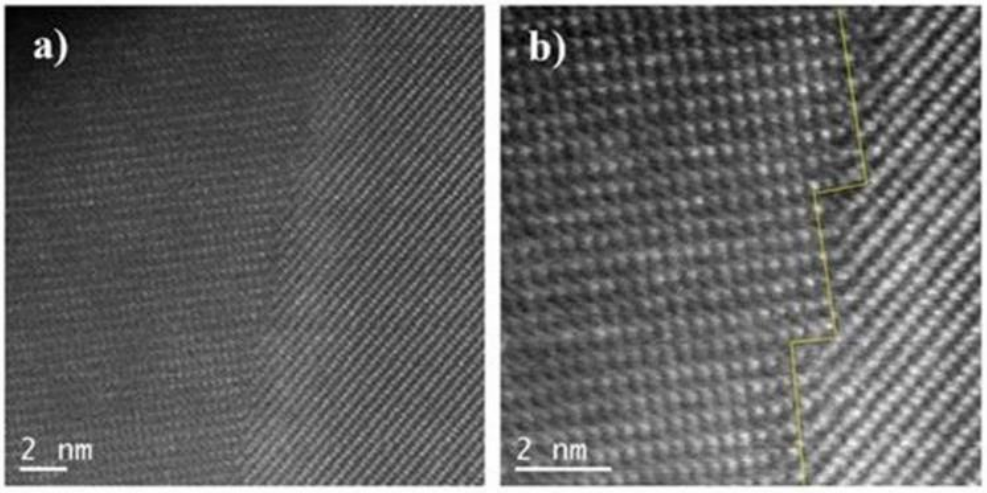

Figure 3: a) HAADF image of interface between LLZO (right grain) and thermal decomposition phase (lanthanum cobalt oxide) (left grain). **b)** Higher magnification of interface displaying a high angle grain boundary containing periodic steps

In search of nothing: characterisation and quantification of vacancy clusters in thermoelectric half-Heusler alloys

Ben Smith, Donald MacLaren, Jan-Willem Bos

University of Glasgow, UK

Thermoelectric (TE) materials have a potential to help reduce fossil fuel-based power generation, in addition to replacing harmful Freon-based refrigerants.(1, 2) A class of structures being studied in relation to their TE properties is half-Heusler alloys, within which the nominal 19-electron half-Heuslers subset have been found to exhibit enhanced TE performance. These materials comprise defective phases including vacancy clusters

that are thought to scatter phonons, decreasing the material's thermal conductivity and improving its TE behaviour.(3) Electron diffraction patterns of 19-electron half-Heuslers show diffuse bands between the fundamental Bragg diffraction spots that have been interpreted as indicating short-range vacancy ordering throughout the alloy. Local clusters such as pairs and triplets, as well as longer-range planar arrangements of vacancies have been proposed and simulated using various electron diffraction simulation packages.(4, 5)

Here, we present an experimental characterisation of diffuse diffractive scattering from V1-xCoSb (x = 0.1 – 0.2) alloys that have effectively been 'doped' with vacancies. Strain effects favour a clustering of vacancies on V sites rather than a random distribution throughout the matrix, yielding characteristic curved bands of diffuse intensity between Bragg diffraction spots. We use multiple scattering geometries to build a three-dimensional picture of the diffuse scattering surfaces in reciprocal space. We complement results with electron diffraction multi-slice simulations(6), in order to optimise the cluster structure and the spatial distribution of clusters throughout the alloy. Of two proposed models, our results are consistent with the short-range ordering of vacancies to form octahedral vacancy clusters, similar to those of a recent study in a related alloy.(7)

We then address the visibility of vacancy clusters using imaging and spectroscopic techniques. STEM simulations are used to assess the viability of detecting vacancy clusters through direct imaging; and found to place stringent limits on sample thickness. Analysis of electron energy loss spectroscopy (EELS), on the other hand, is complicated by overlapping EELS edges and the broad, delayed-onset of the Sb M4,5 edge that would be most suitable for quantitative analysis. As theoretical EELS cross-sections are found to be unreliable, experimental EELS cross-sections were instead determined, leading to more accurate quantification of elements – and their associated vacancies – throughout the alloy matrix. EELS detectability limits for the mapping of vacancies are proposed.

Our work has implications for the detection and analysis of short-range ordering of vacancies in a host of related materials systems.

Bibliography

1. Bell LE. Cooling, Heating, Generating Power, and Recovering Waste Heat with Thermoelectric Systems. Science. 2008;321(5895):1457-61.
2. He J, Tritt TM. Advances in thermoelectric materials research: Looking back and moving forward. Science. 2017;357(6358):9.
3. Jeong H, Kihoi SK, Kahiu JN, Kim H, Ryu J, Lee KH, et al. Origin of low thermal conductivity in Nb1-xTixFe1.02Sb half-Heusler thermoelectric materials. Journal of the European Ceramic Society. 2021;41(7):4175-81.
4. Xia KY, Nan PF, Tan SH, Wang YM, Ge BH, Zhang WQ, et al. Short-range order in defective half-Heusler thermoelectric crystals. Energy & Environmental Science. 2019;12(5):1568-74.

5. Roth N, Zhu TJ, Iversen BB. A simple model for vacancy order and disorder in defective half-Heusler systems. Iucrj. 2020;7:673-80.
6. Lobato I, Van Dyck D. MULTEM: A new multislice program to perform accurate and fast electron diffraction and imaging simulations using Graphics Processing Units with CUDA. Ultramicroscopy. 2015;156:9-17.
7. Gusev AI. Short-range order and diffuse scattering in nonstoichiometric compounds. Physics-Uspekhi. 2006;49(7):693-718.

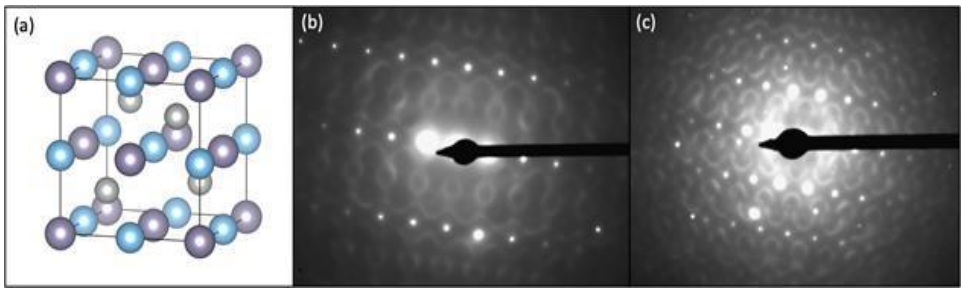

Figure: (a) half-Heusler alloy unit cell. Diffraction patterns of VCoSb in (b) [-201] and (c) [130] orientations showing diffuse intensity between Bragg spots.

Atomic resolution electric field mapping

Ziyi Yuan, Angus Kirkland, Christopher Allen

University of Oxford, UK

Atomic electric field imaging has become increasingly pronounced in the research of nano-electronic devices where the electric field around crystal defects and dopants contributed greatly to the electrical properties. Modern characterization techniques allow sub-Angstrom features to be captured, in which scanning transmission electron microscope (STEM) is one of the well-developed instrument for high special resolution imaging and spectroscopy[1].

Differential phase contrast (DPC) is a phase revealed imaging mode in STEM and allows direct imaging of internal electric and magnetic field in materials[2]. The electrostatic interaction from the materials creates a momentum transfer in the beam electrons and a deflection in the scattered bright field disk. The electric field can be calculated from the intensity distribution in the far-field diffraction pattern. The diffraction pattern at every probe position is recorded by a pixelated detector giving a four-dimensional dataset, and we call this method four-dimensional scanning transmission electron microscopy (4D-STEM)[3]. DPC imaging of nanomaterials is performed at reasonably high electron dose to achieve good signal-to-noise ratio and high accuracy in the electric field, but many two-dimensional nanomaterials, especially those composing of light elements, are beam-sensitive[4]. High electron dose transfers significant energy to the atoms on the investigated area and can cause damage such as crystal vacancies and edge-atom sputtering due to bond-breaking[4, 5]. This work explores the low-dose limit of the electric field measurement from monolayer graphene and monolayer molybdenum disulphide. 4D-STEM simulation was performed to find the limit at which the DPC failed to produce stable electric field images. Simulation considered the Poisson noise of the electron, the major contribution of the noise in low-dose images. A standardised quantitative validation method on noise-induced errors in an electric field image was developed. The noise-induced error is calculated by pixel-wise comparison of electric field vector to a noise-free vector plot.

Experimental 4D-STEM datasets have been acquired at 80keV from graphene and MoS2 samples across a range of electron dose guided by simulation. The lowest electron dose used in the experiment was 16×10^4 e/Å^2 and 2×10^4 e/Å^2 respectively and we successfully reconstructed electric field map from both. Figure 1 shows a low-dose graphene electric field image. In the error quantification of experimental images, the noise-free reference electric field is approximated by cross-correlation averaging over all repeating units in the image. There are three major factors that contribute to the error in imaging the electric field: the electron dose per unit area, the scanning frequency of probe and the minimum interested electric field strength. To achieve a certain accuracy in electric field imaging, a balance of spatial resolution and field resolution need to be considered, since the maximum affordable electron dose is a materials parameter. Experimental measurement showed good agreement to the theriacal calculations.

References

1. Nellist, P.D., Scanning Transmission Electron Microscopy, in Springer Handbook of Microscopy, P.W. Hawkes and J.C.H. Spence, Editors. 2019, Springer International Publishing: Cham. p. 49-99.
2. Lubk, A. and J. Zweck, Differential phase contrast: An integral perspective. Physical Review A, 2015. 91(2): p. 023805.
3. Ophus, C., Four-Dimensional Scanning Transmission Electron Microscopy (4D-STEM): From Scanning Nanodiffraction to Ptychography and Beyond. Microscopy and Microanalysis, 2019. 25(3): p. 563-582.
4. Egerton, R.F., P. Li, and M. Malac, Radiation damage in the TEM and SEM. Micron, 2004. 35(6): p. 399-409.
5. Kretschmer, S., et al., Formation of Defects in Two-Dimensional MoS2 in the Transmission Electron Microscope at Electron Energies below the Knock-on Threshold: The Role of Electronic Excitations. Nano Letters, 2020. 20(4): p. 2865-2870.

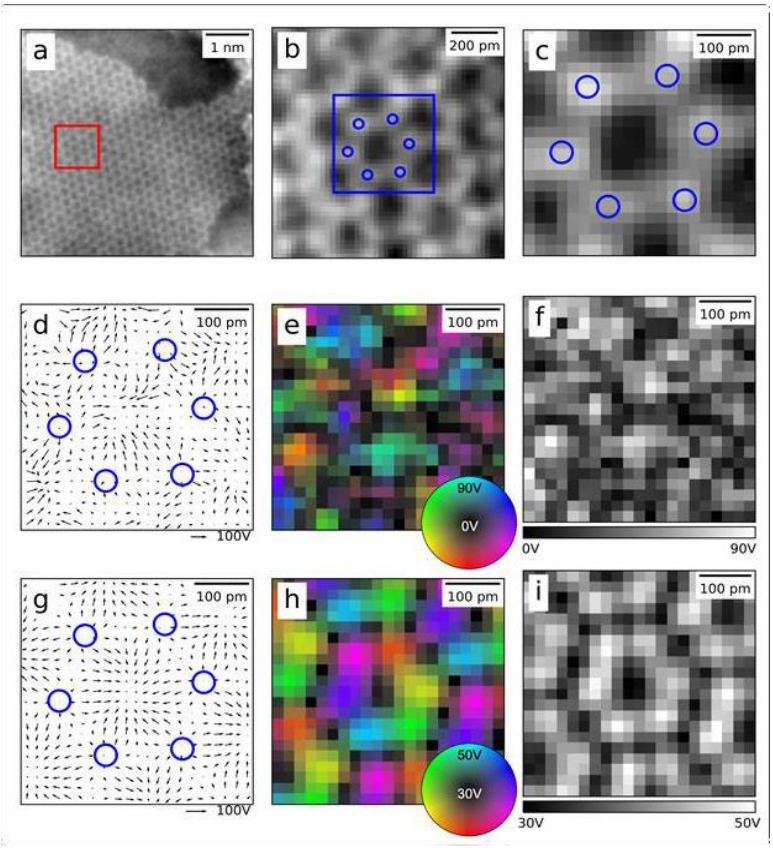

Figure 1: Atomic resolution 4D-STEM experiment of monolayer graphene at dose 16×10^4 eÅ^{-2}. **(a)** Integrated centre-of-mass (iCoM) image reconstructed from the 4D-STEM dataset. **(b)** Zoomed view of the iCoM image. The blue circles indicate carbon atoms. **(c)** A six-carbon ring. **(d)** The electric field vector plot around the carbon ring. **(e)** The electric field vector colour map. **(f)** The electric field strength map. **(g)(h)(i)** Cross-correlation averaging results of (d)(e)(f)

Elucidating the mechanism responsible for swift heavy ion induced crystal rotation in NiO.

Danielle Douglas-Henry, Dr Jacques O'Connell

Trinity College Dublin, Republic of Ireland

Crystal tilts have been observed in certain materials exposed to off-normal swift heavy ion (SHI) irradiation. This phenomenon has been experimentally observed using both X-Ray Diffraction (XRD) and surface shift techniques [1, 2]. Although these techniques allowed for estimations of bulk effects, they limited what could be deduced about the microstructural mechanisms facilitating these observations. Electron microscopy was found crucial in investigating the microstructural changes allowing for such significant rotation.

In this study, single crystal NiO was irradiated with Au ions at 45° with energies of 593 MeV and 940 MeV. Fluences ranged from 3.9×10^{13} to 9.6×10^{14} ions/cm^2. The irradiation was performed at the former ISL lab, Berlin and the FAIR Phase-0 at GSI, Darmstadt (Germany).

A depth dependent investigation of the crystal rotation was performed using electron backscatter diffraction (EBSD). The in-plane rotation across various fluences varied from 5.1°– 51.6°. Scanning transmission electron microscopy (STEM) was utilized to interrogate the microstructural changes facilitating the bulk rotation. No amorphization was observed and the specimen remained crystalline throughout. STEM imaging revealed a dense network of dislocations along the primary slip directions of the material. The dislocations at high fluences are seen to form cells of approximately 30 nm diameter, which resemble mosaic Low Energy Dislocation Structures (LEDS) [3]. A different mechanism of ion hammering is thus considered.

The authors would like to acknowledge Siegfried Klaumünzer for the provision of the NiO specimens used in this study as well as all his valuable discussions.

References

1. I. Zizak, G. Schumacher, N. Darowski, and S. Klaumünzer, "Ion-Beam-Induced Collective Rotation of Nanocrystals," Physical Review Letters, vol. 101, no. 065503, pp. 1–4, 2008, doi: 10.1103/PhysRevLett.101.065503.
2. I. Zizak, N. Darowski, S. Klaumünzer, G. Schumacher, J. W. Gerlach, and W. Assmann, "Grain rotation in nanocrystalline layers under influence of swift heavy ions," Nuclear Instruments and Methods in Physics Research, Section B: Beam Interactions with Materials and Atoms, vol. 267, no. 6, pp. 944–948, 2009, doi: 10.1016/j.nimb.2009.02.018.
3. T. R. Duncan and D. Kuhlmann-Wilsdorf, "Shear-stress field of a simple dislocation cell," Journal of Applied Physics, vol. 39, no. 7, pp. 3043–3045, 1968, doi: 10.1063/1.1656729.

A New Approach for 3D Quantitative STEM Using Defocus Corrected Electron Ptychography

Ali Mostaed, Emanuela Liberti, Chen Huang, Peter Nellist, Angus I. Kirkland

University of Oxford, UK

Electron ptychography is a powerful technique exploited to study the atomic structure of materials including those containing both light and heavy elements. In electron ptychography, first, a series of electron diffraction patterns (i.e. a 4D STEM dataset) are collected by scanning an electron beam (probe) across a specimen. Then, some mathematical algorithms (e.g. SSB, WDD and ePIE) are used to deconvolve the probe and object transfer functions from the 4D STEM dataset. The key assumption in these algorithms is that the probe function is constant for all the probe positions since the aberrations of the microscope's electromagnetic

lenses are almost constant during the very short time of data acquisition. Although the lens aberrations can be assumed to be constant for each probe position in a dataset, the probe function is not unique since the geometry of the specimen at each probe position across the imaging area alter the defocus value of the probe (Figs. 1(a-c)). Thus, we have to use a defocus-corrected probe function for each probe position to calculate the object transfer functions. Here we show that it is possible to calculate the probe's defocus value using electron ptychography. Moreover, we demonstrate that 3D models of nanoparticles can be obtained from 4D-STEM datasets acquired simultaneously with HAADF images. Here, we calculated the number of Pd atoms for each atom column observed in a HAADF image from a Pd nanocube (Fig. 1(d)), and then we measured the height of those columns from their apparent defocus extracted from the WDD ptychographic phase reconstructed from a 4D-STEM dataset acquired simultaneously with the HAADF image. Finally, the 3D model of the Pd nanocube were simply reconstructed as we had the number of atoms in each column as well as the height of those columns (Fig. 1(e-g)). We expect this approach to be applicable to reconstruct not only an accurate ptychographic phase but also a 3D model of any other nanostructure.

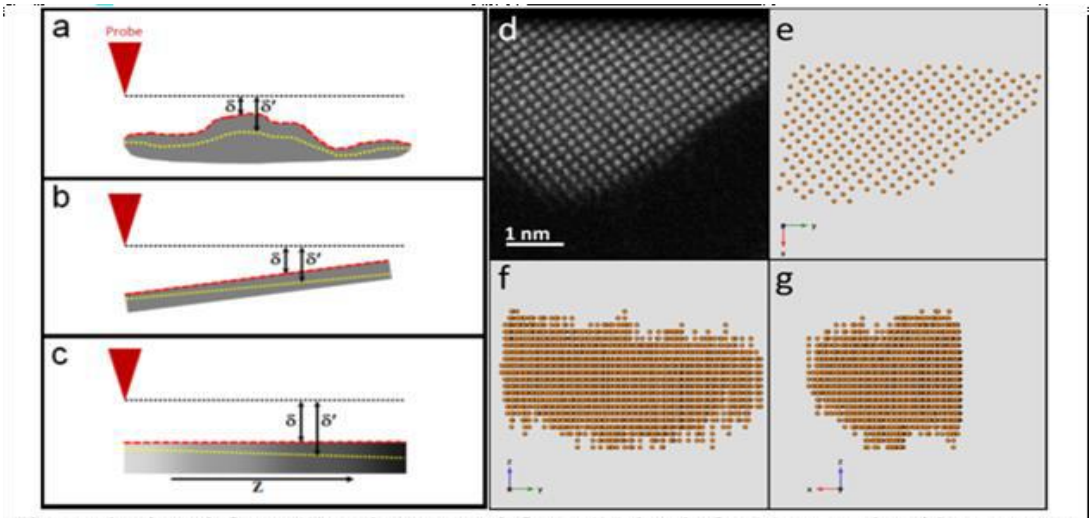

Fig. 1 Absolute defocus (δ) and apparent defocus (δ′) levels for (a) a sample with an uneven surface, (b) tilted sample and (c) sample with compositional variation. (d) ADF image obtained from a Pd nanocube. (e-g) 3D reconstructed model in three different viewing direction for the nanocube shown in (d).

Scanning Electron Diffraction of Pharmaceutical Amorphous Solid Dispersions

Helen Leung, Royston Copley, Duncan Johnstone, Matthew von Lany, Paul Midgley

University of Cambridge, UK

Amorphous Solid Dispersions (ASDs) are a formulation strategy used in the pharmaceutical industry to overcome the poor solubility and therefore low oral bioavailability of some pharmaceutical molecules. The active pharmaceutical ingredient (API) is blended with a water-soluble excipient to create a solid dispersion of the two amorphous substances which has an improved dissolution performance [1]. This consequently increases the absorption of the API in the gastrointestinal tract. Difficulties with ASDs can sometimes arise from the presence of unwanted phase separation and the resulting crystallinity of the API affecting the performance of the drug. The crystallinity can either be residual from the manufacturing process or develop due to the storage conditions of the ASD [2]. Often, a high humidity and temperature are contributory to the latter. However, information about the spatial distribution of this crystallinity and potential crystallisation mechanisms are relatively unknown.

Scanning electron diffraction (SED) is a technique where a convergent electron beam (with a convergence semi-angle of typically 0.5 - 1 mrad) is raster-scanned across a sample area (typically 1 µm x 1 µm). At each probe position, a diffraction pattern is generated, totalling around 105 diffraction patterns per scan [3]. This creates a `4-Dimensional' dataset of spatially resolved diffraction patterns which can be used for powerful post-facto data analysis. This technique can be used to extract a wealth of microstructural information from a sample using a low total electron dose and minimising beam damage. Therefore, SED enhances the microstructural study of organic materials which may have a critical accumulated dose of only several electrons Å-2. Their study via conventional (S)TEM methods has previously been limited by dose problems and beam sensitivity.

In this work, SED was used to investigate the nature of unwanted crystallinity in an ASD of indomethacin (the API) and polyvinylpyrrolidone (PVP, the amorphous polymer excipient). Samples with different ratios of indomethacin to PVP were explored. Diffraction is a powerful tool for the detection of crystallinity and structural changes, making SED an ideal candidate for studying crystallinity in ASDs. Whilst most of the ASD was amorphous as expected, low levels of crystallinity (indicated by the presence of Bragg spots) were detected. Where sufficient Bragg spots were present, diffraction patterns were indexed to confirm the presence of the γ polymorph of indomethacin, its most stable polymorph. Regions of nano-crystallinity found in the sample were undetected using powder x-ray diffraction (PXRD), under which the sample appeared amorphous. Energy dispersive x-ray (EDX) maps were also acquired to confirm the identity of the nanoparticles, using the chlorine in the indomethacin structure as a tag.

These preliminary results highlight the potential of SED to map the microstructure of semi-crystalline solid dispersions. [4]

[1] Ricarte, R.G. et al (2019). Mol. Pharmaceutics, 16, 4089−4103
[2] Chasse, T. et al. (2022) Journal of Pharmaceutical Sciences 00, 1−13
[3] Eggeman, A. S. (2019). Acta Cryst. B75, 475-484
[4] The authors acknowledge funding from EPSRC and GSK for iCASE grant 210193. The authors also thank EPSIC for access to the JEOL ARM microscope.

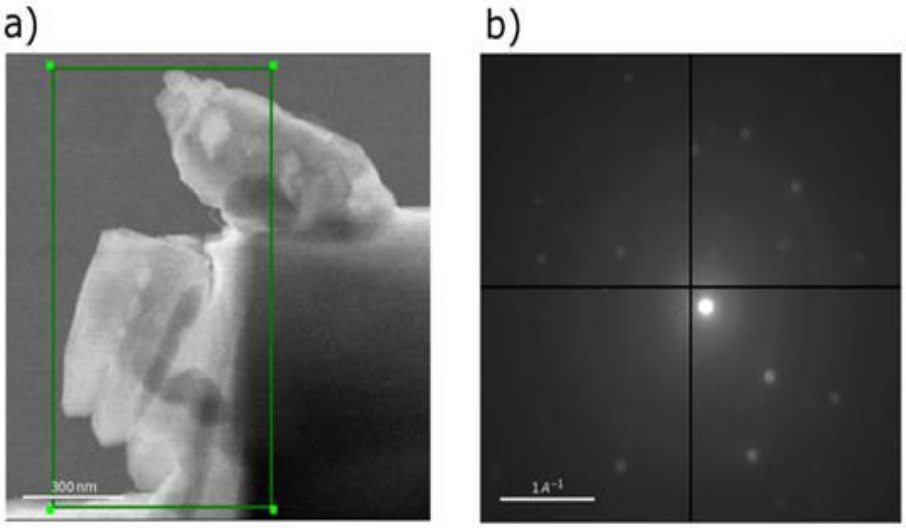

Figure 1: Scanning electron diffraction (SED) of a particle from an indomethacin/ polyvinylpyrrolidone (30wt% : 70wt%) amorphous solid dispersion. The summed diffraction pattern (b) from the area highlighted in real space (a) shows evidence of nano-crystallinity by the presence of Bragg spots. Powder x-ray diffraction results from the same sample show no obvious signs of crystallinity. This demonstrates the unique ability to explore nano-scale structures at a high spatial resolution with SED.

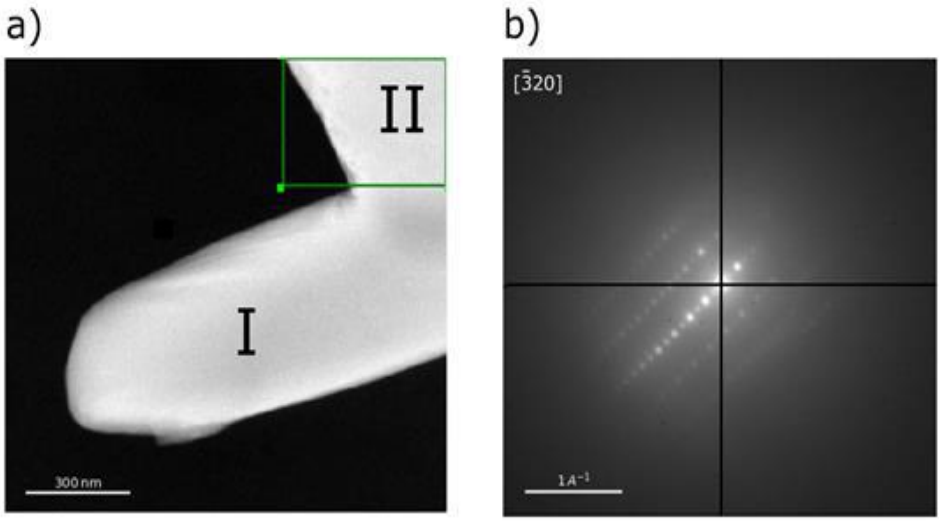

Figure 2: SED of an indomethacin/polyvinylpyrrolidone (70wt% : 30wt%) amorphous solid dispersion. The summed diffraction pattern (b) indicates the area II highlighted in (a) is a single crystallite. It has been indexed to be the γ polymorph. The particle in area I was crystalline but there were not sufficient Bragg spots observed to be able to index it.

Data in Figure 1 and Figure 2 were both taken on JEOL ARM 300F microscope operated at 300kV with a convergence semi-angle of ~ 0.6 mrad. The beam current was 2 pA. Diffraction patterns were collected on a Merlin mediPix3 direct electron detector.

Quantum theory of ultra-low loss aloof beam EELS applied to molecular crystals

Sabrina Wang, Rebecca J. Nicholls

University of Oxford, UK

Electron energy loss spectroscopy (EELS), is a characterisation tool that has recently gained additional capabilities due to advances which have substantially improved the energy resolution down to ~ 5meV [1, 2, 3] and is now able to resolve phonon modes. Scanning transmission electron microscopy (STEM) coupled with EELS, combined with vibrational spectroscopy lead to superior spatial and energy resolution [4], thus providing an complementary technique to common methods like infrared and Raman spectroscopy. In aloof beam EELS, the electron beam passes close to the specimen rather than through it. In this mode, the combination of mitigated knock-on damage as well as the ability to detect phonons opens up a wide range of useful applications, one of them being the characterisation of different drug polymorphs without structural alterations/beam damage due to the differences in their vibrational profiles [5].

Theoretically, there are several methodologies to derive vibrational EELS spectra, from the semi-classical treatment [6] to quantum treatments from the works of Sinha [7], Nicholls et al. [8] and Dwyer et al. [9]. However, the current quantum treatment is not well suited to describe the aloof beam setup. In this work we discuss this limitation, and present a modified version of the quantum impact scattering derivation of the EELS profile for a general molecular crystal in the aloof mode. The main issue that is addressed is how one analytically approximates the continuous charge distribution of the crystal, such that the correct physics is encapsulated in the interaction with the fast electron beam. We show that the dynamic Born effective charges naturally emerge from our derivation, instead of being added ambiguously to account for charge transfer as is carried out in the prevalent practices.

Rez et al. performed an aloof beam EELS experiment on the molecular crystal of β−guanine, with reduced sample degradation due to beam damage. We test and validate our dipole theory using this experimental result. We also compare it's performance against the existing semi-classical [6] and quantum impact scattering theories [8]. We show an improvement in the relative intensity predictions of the energy loss spectrum, shown in figure 1. We then apply it to a molecular crystal with two different polymorphs and show it is possible to distinguish them.

References

[1] Krivanek et al., Math. Phys. Eng. Sci., 367, (2009), 3683–3697.
[2] Krivanek et al., Journal of Physics, 522, (2013).
[3] Dellby et al., Microscopy and Microanalysis, 26, (2020), 1804–1805.
[4] Hage et al., Science advances, 4, (2018).
[5] Crozier, Ultramicroscopy, 180, (2017), 104-114.
[6] Radtke et al., Physical Review letters, 119, (2017).
[7] Sinha, Journal of Physics: Condensed Matter, 13, (2001).
[8] Nicholls et al., Physical Review B, 99, (2019).
[9] Dwyer, Physical Review B, 89, (2014).
[10] Rez et al., Nature Communications, 7, (2016), 1-8.

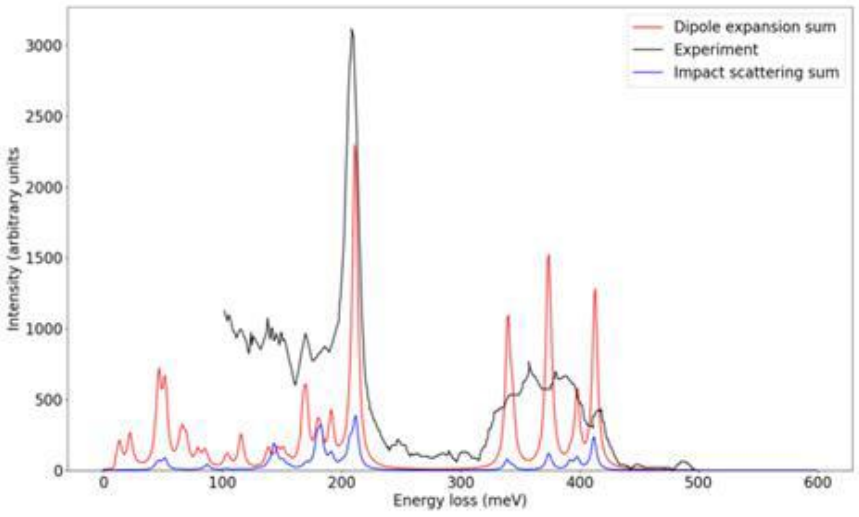

(a)

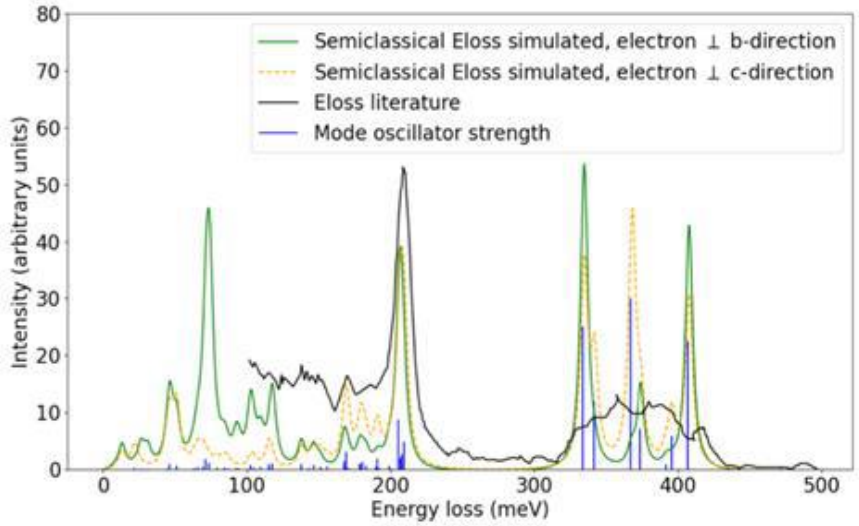

(b)

Figure 1: (a) Comparison between experimental results from literature [10] and the simulated theoretical EELS spectra (b) Comparison between semi-classical theory and experiment. The *b* and *c* directions denote the plane in which the guanine crystals form a 2D sheet, and this is the plane in which the fast electron travels perpendicular to in the experiment performed by Rez *et al.*.

Electron beam induced deposition of functional magnetic nanowires: a correlative EELS study of the link between chemical variations and magnetic properties

John Fullerton, Aurelio Hierro-Rodriguez, Luka Skoric, Claire Donnelly, Amalio Fernandez-pacheco, Donald MacLaren, Dedalo Sanz-Hernandez

University of Glasgow, UK

Cylindrical magnetic nanowires show great promise for a multitude of applications. Thanks to recent advances in nanofabrication, such as focused electron beam induced deposition (FEBID), it is now possible

to move past single nanowires and fabricate complex three-dimensional (3D) interconnected structures [1, 2]. These structures can possess novel and intriguing spintronic properties that can be controlled by altering the geometry of the system, providing a new route to high density, low power computing and sensing devices [3].

The desired magnetic properties of these systems are heavily dependent on the material properties and one of the major hurdles faced when utilising FEBID is fabricating structures with suitably high metallic content. It has been shown that the material properties of FEBID nanostructures depend greatly on several parameters, including: current and dwell times of the electron beam during growth and post annealing procedures [4,5]. It is therefore key to understand how the fabrication process affects the composition and microstructure of FEBID deposits and hence the impact upon the magnetic properties of the system. We optimise the FEBID process through the tuning of growth parameters (Fig. 1a) and outline the protocols required for the deposition of high quality magnetic materials in complex three dimensional shapes. We then present a (S)TEM study of the composition and microstructure of FEBID nanostructures that are fabricated and annealed under a variety of conditions (Fig. 1b). Electron energy loss spectroscopy (EELS) is used to map the distribution of Fe, O and C throughout the FEBID deposits (Fig .1c), revealing a core-shell structure. EELS is also used for an accurate determination of Fe oxidation state in its amorphous environment. We will show how tuning growth conditions and utilising post-fabrication processes can yield suitably pure structures; and we discuss the impact of chemical variations within the nanowires on their magnetic properties. The work is complemented by detailed micromagnetic simulations and XMCD studies that together provide a comprehensive understanding of the link between deposition conditions and eventual spintronic behaviour.

[1] L. Skoric, et.al., Layer-by-layer growth of complex-shaped three-dimensional nanostructures with focused electron beams, Nano Lett., 20, 184 (2020).
[2] D. Sanz-Hernández, et al., Artificial double-helix for geometrical control of magnetic chirality, ASC Nano., 14, 8084 (2020).
[3] A. Fernández-Pacheco, et. al., Three-dimensional nanomagnetism, Nat. Comm., 8, 15756 (2017).
[4] D. Sanz-Hernández, et al., Modelling focused electron beam induced deposition beyond Langmuir adsorption, Beilstein J. Nanotechnol., 8, 2151 (2017).

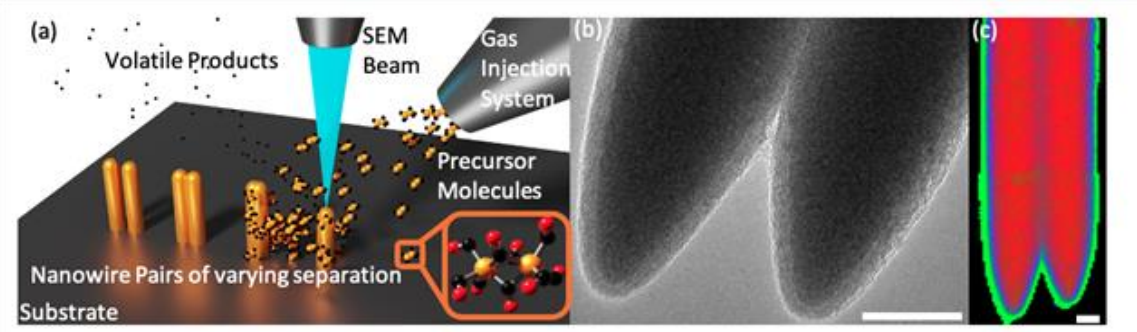

Figure 1: (a) Diagram showing the FEBID process and the precursor molecule that was used: $Fe_2(CO)_9$, Fe – orange, O – red and C – Black. (b) TEM image of the tips of Fe FEBID nanowires, showing a core-shell structure. (c) False colour EELS map of Fe FEBID nanowires, Fe – red, O – blue, C – green. All scale bars 50μm.

ADF/EDS/EELS Characterization of Spontaneous Cathode/Electrolyte Reaction in Air- and Beam-sensitive Solid-state Li-ion Batteries

Ruomu Zhang, Alex Sheader, Weixin Song, Emanuela Liberti, Peter Bruce, Peter Nellist

University of Oxford, UK

Solid-state Li-ion batteries (SSLIBs) have potential to revolutionise the electric-vehicle industry due to both their superior capacity and improved safety relative to conventional liquid cells. However, commercialisation of SSLIBs is at present hindered by the side reaction which occurs at the electrode-electrolyte interface. This reaction leads to voltage hysteresis and capacity fading, and subsequently to degraded battery performance [1].

Gaining insights into the origin of degradation and failure mechanisms at interface in SSLIBs requires the use of high spatial and energy resolution characterisation techniques such as scanning transmission electron microscopy (STEM). In this work, we applied annular

dark field (ADF)/energy dispersive X-ray spectroscopy (EDS)/electron energy loss spectroscopy (EELS) to study the spontaneously formed interface between cathode material LiNi0.6Mn0.2Co0.2O (NMC622) and SSE Argyrodite Li_6PS_5Cl.

However, TEM studies of SSLIBs are complicated due to the extreme air- and electron-beam sensitivity of battery materials. We developed an anaerobic sample transfer protocol to prevent oxygen-related sample degradation. Beam damage on argyrodite was studied from the in-situ diffraction pattern revolution. Critical dose thresholds were calculated by monitoring the diffraction spots intensity decay with time (and therefore increasing electron dose), as shown in Figure 1(f).

By combining this anaerobic sample transfer and knowledge of critical electron dose limits, it was possible to study the argyrodite-NMC622 spontaneous redox side reaction at the interface in its near-native state. STEM EDS and ADF imaging allowed characterisation of chemical elemental distributions and particle morphology respectively. EELS mapping was also used to reveal the extent of side reaction by tracking the Ni L2,3 white line ratio on the NMC622/argyrodite interface. The EELS signal to noise ratio were enhanced from both sample preparation (wet ball-milling) and data acquisition (SmartAlign) [2]. Therefore, we are able to quantify Ni L2,3 white line ratio by performing model fitting (Fig. 2©) in Hyperspy [3] on raw data from single pixel. From the EELS fine structure analysis, we observed a trend of Ni reduction in NMC622 towards the interface with argyrodite due to the spontaneous redox reaction.

With the comprehensive analysis of the microstructure and chemistry of SSE/cathode interphase by using ADF/EDS/EELS in STEM, our work has exciting potential to guide future materials selection and interface design in SSLIBs by correlating the microstructure and composition with electrochemical performance.

References:

1. Tarascon, J.-M. and M. Armand, Materials for sustainable energy: a collection of peer-reviewed research and review articles from Nature Publishing Group, 2011: p. 171-179. doi: 10.1142/9789814317665_0024
2. Jones, L., et al., Advanced Structural and Chemical Imaging, 2015. 1(1): p. 1-16. doi: 10.1186/s40679-015-0008-4
3. Peña, F.d.l., et al., hyperspy/hyperspy: v1.6.5. 2021: Zenodo.
4. The authors acknowledge use of characterization facilities within the David Cockayne Centre for Electron Microscopy, Department of Materials, University of Oxford and in particular the Faraday Institution (FIRG007, FIRG008), the EPSRC (EP/K040375/1 “South of England Analytical Electron Microscope”) and additional instrument provision from the Henry Royce Institute (Grant reference EP/R010145/1).

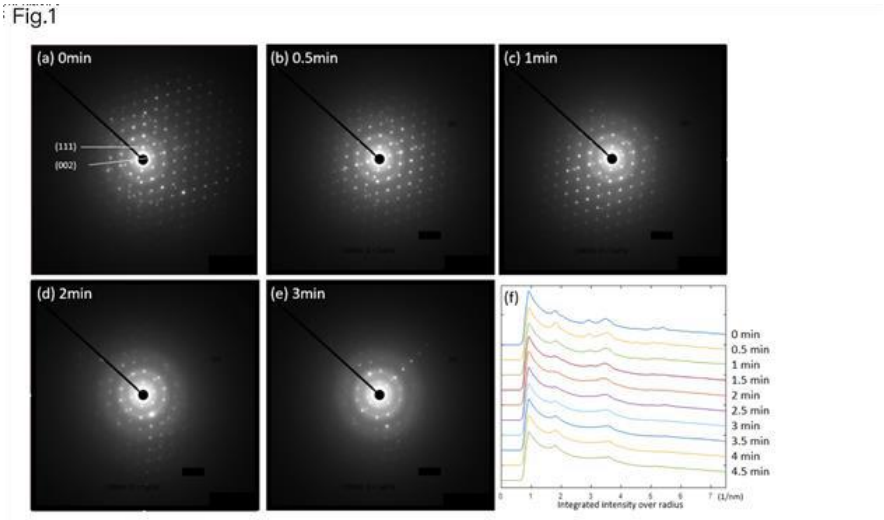

Figure 1: Diffraction pattern of argyrodite at 300kV at (a) t=0min, (b) t=0.5min, (c) t=1min, (d) t=2mi©(e) t=3min; (f) integrated diffraction spots intensity over radius

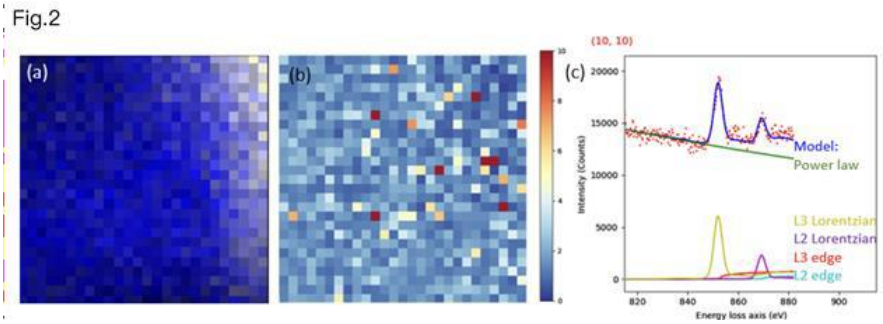

Figure 2: (a) EDS map of S (yellow) in LPSCl and Ni (blue) in NMC622, (b) Ni L2,3 white line ratio map, (c) Model fitting (dark blue) on raw data (red dots), model consists of 5 components.

Improving the Noise Floor and Speed of Your Detector: A Modular Hardware Approach for Under £1000

Jonathan Peters, Tiarnan Mullarkey, Lewys Jones

Trinity College Dublin, Republic of Ireland

Scanning transmission electron microscopy (STEM) has cemented itself as a powerful and pivotal characterization method in the materials scientist's toolkit. Combined with spectroscopy and aberration correction, a wealth of information can be simultaneously acquired. High-angle annular dark field (HAADF) is perhaps the most popular imaging mode of STEM due to its ready interpretability and atomic number contrast. This has given rise to quantitative studies examining chemical and thickness/3D information without the need for time consuming tomographic techniques. Previous studies have shown this to be an effective approach for a range of materials, for example in heterostructure interfaces [1] or catalytic nanoparticles [2]. However, a full and accurate quantification of HAADF images requires an extensive calibration of the STEM and use of simulation. Calibration is required because of the imperfect detection systems and digitization. For example, detector non-uniformity results in individual electron events contributing differently to the image intensity [3]. Similarly, analog to digital conversion results in arbitrary data values in the final image, often with a non-zero dark signal. These effects combine to limit HAADF STEM as a routine quantitative technique.

Whilst newer generations of solid-state electron detectors are improving in areas such as uniformity or adding new capabilities through 4D-STEM [4], these can often be limited in their speed, cost, or collection angles. We recently demonstrated the capability to use existing detectors, including those based on scintillator technology, to perform single electron counting inside the electron microscope [5]. Each electron impinging on a detector results in a voltage peak that, in typical detection modes, is integrated to form the pixel value. Instead, the raw signal data can be processed to detect each peak as one electron. Previous studies used simple intensity thresholding from fast image scans but had poor dynamic range [6], creating an upper limit on dose and specimen atomic number. By differentiating the raw detector signal before applying a threshold, multiple rapid electron events (electron pile-up) can be distinguished to maintain a high detection efficiency (Fig. 1). The result is images with pixel values in units of integer electrons and with a true zero-level background, improving image quantification, and allowing for the summing of large numbers of frames without noise accumulation (Fig. 2). However, our earlier approach required oversampling of data combined with a posteriori processing and manual syncing with the image scan [5].

To provide a more practical electron counting solution, we have developed a modular hardware system to perform digital pulse readout which we call "Digi-pro" (Fig. 3). This can be retrofitted to existing systems or installed on new instruments. The Digi-pro performs all the signal processing in hardware and interfaces with existing scan controllers such as Gatan's Digiscan II/III and point electronic's DISS. The signal of any electron detector can be digitized to electron counts by simply selecting a new signal source in the existing software. To achieve this, we use an off the shelf field programmable gate array (FPGA) single board computer combined with signal conditioning electronics to maximize the dynamic range. The use of FPGAs provides the necessary speed for signal processing and hardware syncing, but also retains flexibility to customize and expand capability should it be needed. All of this can be achieved with components that cost under £1000 in total. Our hardware therefore provides a modular, accessible and sustainable approach to extend the capabilities and lifetime of any microscope.

[1] S. Van Aert, J. Verbeeck, R. Erni, S. Bals, M. Luysberg, D. Van Dyck, G. Van Tendeloo, Quantitative atomic resolution mapping using high-angle annular dark field scanning transmission electron microscopy, Ultramicroscopy. 109 (2009) 1236–1244.
[2] A. De Wael, A. De Backer, L. Jones, A. Varambhia, P.D. Nellist, S. Van Aert, Measuring Dynamic Structural Changes of Nanoparticles at the Atomic Scale Using Scanning Transmission Electron Microscopy, Phys. Rev. Lett. 124 (2020) 106105.
[3] K.E. MacArthur, L.B. Jones, P.D. Nellist, How flat is your detector? Non-uniform annular detector sensitivity in STEM quantification, J. Phys. Conf. Ser. 522 (2014) 012018.
[4] S. Seifer, L. Houben, M. Elbaum, Flexible STEM with Simultaneous Phase and Depth Contrast, Microsc. Microanal. (2021) 1–12.
[5] T. Mullarkey, C. Downing, L. Jones, Development of a Practicable Digital Pulse Read-Out for Dark-Field STEM, Microsc. Microanal. 27 (2021) 99–108.
[6] A. Mittelberger, C. Kramberger, J.C. Meyer, Software electron counting for low-dose scanning transmission electron microscopy, Ultramicroscopy. 188 (2018) 1–7.
[7] The authors would like to acknowledge the Centre for Research on Adaptive Nanostructures and Nanodevices (CRANN) and the Advanced Materials and BioEngineering Research (AMBER) Network for financial and infrastructural support for this work. L.J. is supported by SFI award number URF/RI/191637. J.J.P.P. and L.J. acknowledge SFI grant 19/FFP/6813, T.M. acknowledges the SFI-EPSRC CDT-ACM (grants 18/EPSRC-CDT-3581 and EP/S023259/1).

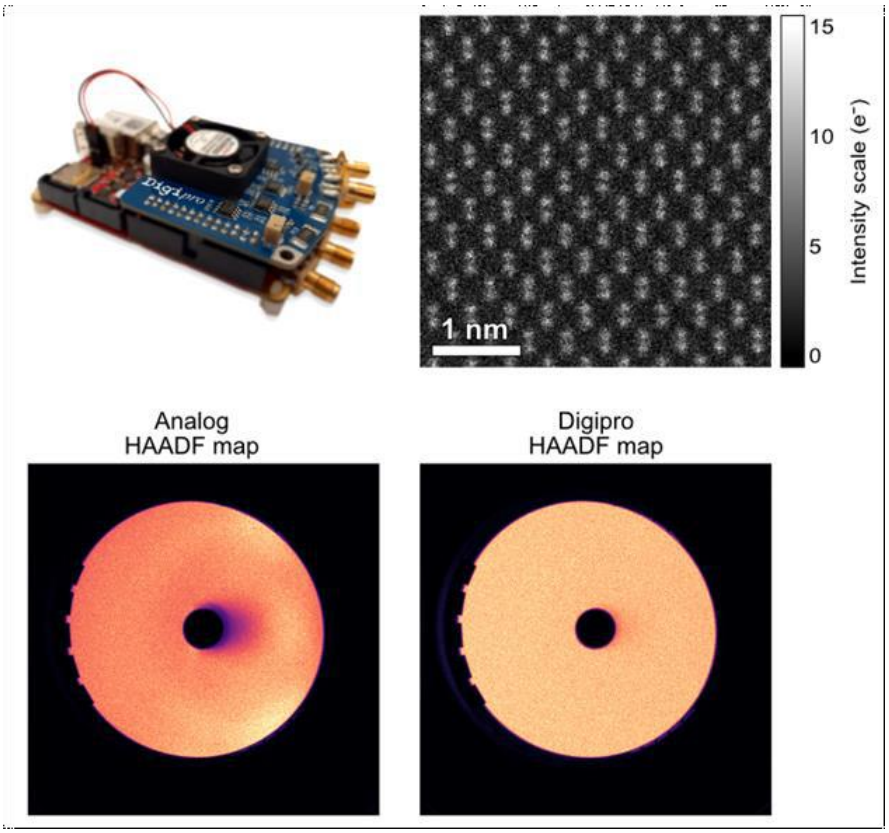

The Use of Advanced Electron Microscopy for the Characterisation and Structure-Property Correlation of BaMnO3 for the Oxygen Reduction Reaction

Lucia Hughes, Ahin Roy, Clive Downing, Michelle Browne, Ainur Zhussupbekova, Valeria Nicolosi

Trinity College Dublin, Republic of Ireland

With the past and future development of 21st century economy and technology heavily reliant on the supply of energy, there is an urgent need for low-cost sustainable energy sources.[1,2] Therefore, researchers and scientists face the challenge of designing electrochemical technologies that can perform both safely, and at rates and costs comparable to that of well-developed fossil-fuel technologies prevalent in today's society.

Metal oxides represent one of the most common, diverse and richest class of materials in terms of their electronic, structural, chemical and physical properties.[3-5] As a result, they prove indispensable in the design and development of electrochemical devices. However, the optimisation of such devices requires a thorough understanding across all length scales of the required materials, in addition to the physical processes that occur. Electron microscopy and related spectroscopic techniques offer the opportunity to investigate materials on different length scales, thus bridging the gap between material properties and their structure, and subsequently aiding in the fine tuning of material properties for device performance. With this in mind, we combine the use of advanced electron microscopy techniques with spectroscopic analyses to reveal the atomic scale chemical and crystallographic structure of barium manganese oxide ($BaMnO_3$), a perovskite oxide system.

$BaMnO_3$ rods are synthesised via a low temperature, low pressure hydroxide composite-mediated method. X-ray diffraction (XRD), selected area electron diffraction (SAED) and high resolution transmission electron microscopy (HRTEM) harmoniously reveal the 2H-hexagonal crystal structure of the rods, with space group

$P6_3/mmc$ and lattice parameters a = b = 5.6991 and c = 4.8148 Å. Here the 2H indicates the presence of continuous chains of face-sharing MnO_6 octahedra along the c-axis. which can be directly imaged using aberration corrected scanning transmission electron microscopy (STEM). Not only does this imaging modality reveal the single crystalline nature of the bulk of the rods, but also the presence of an amorphous layer at their surface.

Due to the structural abnormality of the rod surface, electron energy loss spectroscopy (EELS) is used to probe its chemical nature. The Mn L-edge and O K-edge in the EEL spectra act in unison to discover the existence of reduced Mn states within the amorphous surface layer of the rods. X-ray photoelectron spectroscopy (XPS) further confirms this statement, and identifies the presence of both Mn(III) and Mn(IV) states. Consequently, the rods show electrocatalytic activity for the oxygen reduction reaction (ORR), which is considered a key bottleneck reaction in the performance of electrochemical devices, such as fuel cells and metal-air batteries, due to its slow kinetics.[6-8] Modification of the as-synthesied powder by annealing in air results in oxidation of the rod surface, a decrease in the number of Mn(III) states and subsequent lowering of the ORR activity. As a result, the ORR activity is attributed to the presence of Mn(III) states at the surface of the rods, and thus an eg orbital occupancy of 1, which allows for a greater interaction between the adsorbed oxygen and catalytic substrate.[9]

References

[1] Energy Information Administration, International Energy Outlook 2019, US Departments of Energy report, Washington DC, 2019.
[2] Energy Information Administration, Annual Energy Outlook 2021, US Departments of Energy report, Washington DC, 2021.
[3] M. S. Chavali and M. P. Nikolova, SN Applied Sciences, 2019, 1, 607.
[4] J. A. Rodríguez and M. Fernández-García, Synthesis, properties and applications of oxide nanomaterials, John Wiley and Sons, 2007.
[5] C. Noguera, Physics and Chemistry at Oxide Surfaces, Cambridge Press, Cambridge, 1996.
[6] P. Chandran, A. Ghosh and S. Ramaprabhu, Scientific Reports, 2018, 8, 3591.
[7] X. Ren, Q. Lv, L. Liu, B. Liu, Y. Wang, A. Liu and G. Wu, Sustainable Energy & Fuels, 2020, 4, 15-30.
[8] A. Ostadhossein, J. Guo, F. Simeski and M. Ihme, Communications Chemistry, 2019, 2, 95.
[9] X. Long, P. Yu, N. Zhang, C. Li, X. Feng, G. Ren, S. Zheng, J. Fu, F. Cheng, X. Liu, Nanomaterials 2019, 9, 577.

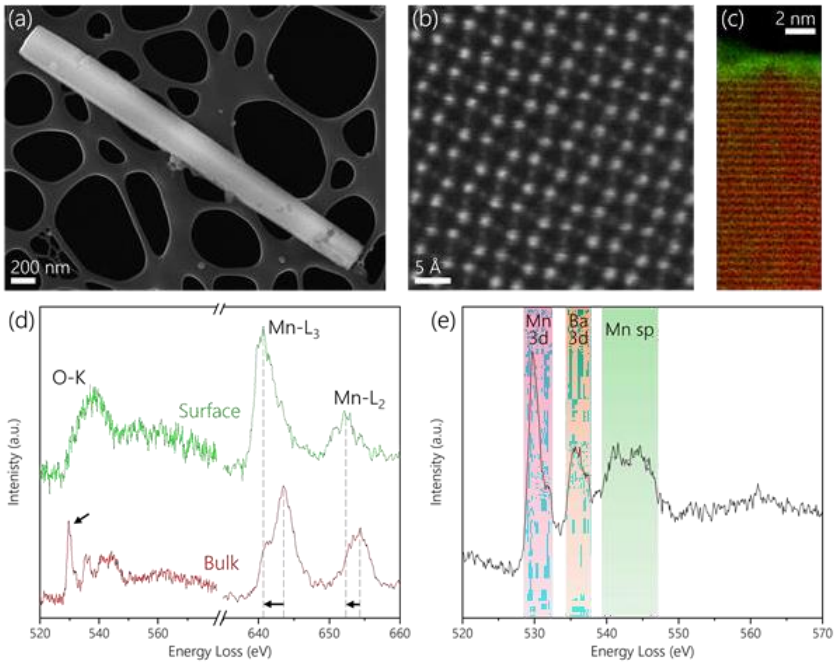

Figure 1: Advanced characterisation of $BaMnO_3$ rods synthesised via low-cost and scalable methods. (a) SEM micrograph and (b) HAADF STEM image displaying the $BaMnO_3$ rod-like microstructure and 2H-hexagonal atomic structure, respectively. (c) EEL spectrum image with Mn(IV) states and Mn reduced states mapped in red and green, respectively. Corresponding O-K edge and Mn-L edge EEL spectra from the bulk and surface of the rod are shown in (d). (e) A closer look at the O-K edge, displaying the origin of the near edge structure features.

Atomic Resolution Investigation of Ultra-Low Energy Ion-Implanted Monolayer TMDs Using Scanning Transmission Electron Microscopy

Michael Hennessy, Eoin Moynihan, Eoghan O'Connell, Stefan Rost, Manuel Auge, Minh Bui, Beata Kardynal, Hans Hofsäss, Ursel Bangert

University of Limerick, Republic of Ireland

The modification of monolayer-thick transition metal dichalcogenides (TMDs) on the atomic scale is a crucial step towards the development of nano-photonic devices with new functionalities [1]. Monolayer TMDs can be incorporated into electrically driven devices, which in turn can be coupled to optical microcavities or photonic circuits [2]. Ultra-low energy ion implantation [3] allows for highly pure, clean and selective substitutional incorporation of dopants [4] and is compatible with standard semiconductor processing. Additionally, post-growth doping of TMDs offers an expanded selection of possible dopants compared to the popular method of doping via CVD growth [5].

Here, we present results of ultra-low energy (10-25 eV) ion implantation of monolayer TMDs, modified using the ADONIS mass-selected ion beam deposition system at the University of Göttingen [6]. Transition metal (Cr) and chalcogen (S, Se) dopants are introduced into the MoS2 and MoSe2 crystal lattice. Atomic resolution high angle annular dark field (HAADF) scanning transmission electron microscopy (STEM), together with core-loss electron energy loss spectroscopy (EELS) analysis, is used to identify the sites of individual dopants in the host lattice and examine the atomic structure of the defects and dopants in the monolayers on the sub-atomic scale. Low loss EELS is used in conjunction with low temperature photoluminescence to study excitonic behaviour at the implantation sites.

Analysis of experimental HAADF STEM data is carried out using the TEMUL Toolkit Python library [7], based on Atomap [8], to determine the percentage of ions that cause substitutional implantation, create adatoms, and create vacancies. We introduce the Model Refiner class from the TEMUL Toolkit Python package, which automatically identifies and fully characterises each atomic site in the experimental HAADF STEM image. We report that accurate atom statistics can be obtained from non-ideal STEM imaging conditions through post-processing and avoidance of contaminated areas when extracting atom sites. Furthermore, by simulating images based on the atomic arrangements determined via the software package, and by comparing these and achieving agreement with the experimental images, the individual atom positions of the dopants can be revealed with sub-Angstrom accuracy.

This work constitutes a proof-of-principle study concerning the possibility and procedure of incorporating non-classical single photon emitting diodes into monolayer TMDs [9]. The development of such devices has far-reaching implications for quantum science and technology, with applications in the fields of quantum cryptography and quantum metrology [10].

The authors gratefully acknowledge funding from Volkswagenstiftung (grant no. A123203).

References:

[1] K. Mak, C. Lee, J. Hone, J. Shan, and T. Heinz, Phys. Rev. Lett. 105, 136805 (2010).
[2] K. F. Mak and J. Shan, Nat. Photonics 10, 216 (2016).
[3] V. P. Pham and G. Y. Yeom, Adv. Mater. 28, 9024 (2016).
[4] J. W. Mayer, 1973 Int. Electron Devices Meet. 3 (1973).
[5] A. Azcatl, X. Qin, A. Prakash, C. Zhang, L. Cheng, Q. Wang, N. Lu, M. J. Kim, J. Kim, K. Cho, R. Addou, C. L. Hinkle, J. Appenzeller, and R. M. Wallace, ArXiv In Press, 1 (2016).
[6] M. Uhrmacher and H. Hofsäss, Nucl. Instruments Methods Phys. Res. Sect. B Beam Interact. with Mater. Atoms 240, 48 (2005).
[7] E. O'Connell, M. Hennessy, and E. Moynihan, (2021).
[8] M. Nord, P. E. Vullum, I. Maclaren, T. Tybell, and R. Holmestad, Adv. Struct. Chem. Imaging 3, 9 (2017).
[9] S. V. P. M. D. Eisaman, J. Fan, A. Migdall, Acta Med. Okayama 67, 259 (2013).
[10] M. Toth and I. Aharonovich, Annu. Rev. Phys. Chem. 70, 123 (2019).

Advanced TEM and STEM/EELS study of Zr and Nb doped Titanium dioxide Nanoparticles

Fayzah Talbi, Leonardo Lari, Demie Kepaptsoglou, Vlado Lazarov

University of York, UK

Titanium dioxide (TiO2) is an attractive material for optoelectronic applications due to its low cost, abundance, and high photoelectric characteristics. Up to date, it is most commonly used as an Electron Transport Layer (ETL) in solar cells [1]. ETLs should have an appropriate band alignment, high stability, and relatively high conductivity in order to obtain a good device Power Conversion Efficiency. However, main deficiency of TiO2 are poor electron mobility, and high electron trap states. Those are strongly influenced by the microstructure including grain boundaries and point defects in TiO2. Hence, understanding the correlation between structure and functionality of TiO2 NPs and thin films is critical for device applications.

Here, we present a microstructural and chemical study for pure and Zr and Nb doped TiO2 NPs using in-situ environmental TEM, SEM and EDX as well as STEM/EELS. In-situ annealing shows distinctive facets formation as a function of annealing temperature, grain boundaries formation within and between the NPs, as

well as presence or absence of point defects depending of the background environment, i.e. reductive or oxidising. Furthermore by employing a low energy EELS, we show that band gap is sensitive to both doping and thermal treatment of TiO2. Those changes were correlated to change in absorption properties of the TiO2 NPs.

[1] Liu, Z. Huang, S. Wei, L. Zheng, L. Xiao, Q. Gong, Nano-structured electron transporting materials for perovskite solar cells, Nanoscale 8 (2016) 6209e6221

The User Adjustable Pole-piece – A TEM Heart Transplant

Lewys Jones, Patrick McBean, Pat Murphy, Ryusuke Sagawa

Trinity College Dublin, Republic of Ireland

The transmission electron microscope (TEM) is a powerful characterisation instrument for both physical and life sciences. However, it represents a significant investment of often several million dollars followed by the running costs, cooling/energy bills, support staff salaries, and maintenance contracts for perhaps a further 15 years [1]. Many consider the objective lens pole-piece to be the heart of the TEM, with the pole-piece gap specification being crucial in dictating the capabilities and performance of the instrument [2]. While a smaller gap results in reduced spherical and chromatic aberrations, and improved resolution [3], a larger gap offers wider flexibility for sample-tilting, tomography, in-situ experiments, or energy-dispersive x-ray spectroscopy (EDX) collection efficiency. As the former is typically preferred by the physical science community, but the latter by the analytical/life-science communities, the result is that two (or more) columns are often needed, or alternatively, a single intermediate gap may be commissioned but compromises must be made. As an alternative approach, we propose a User Adjustable Pole-piece (UAP) with a pole gap that can be adjusted by the microscopist to suit a variety of experiments, reducing wasteful duplication [4]. To be of practical use, the proposed UAP must be; adjustable while under high vacuum, mechanically stable with ultra-precise alignment about the optic axis, and be realignable to a good tuning without a specialist engineer present. In this presentation we will elaborate on our progress in the design and manufacture of the UAP. We will present our preliminary results from multi-physics modelling simulations which confirm that the larger pole gaps yield better tilt/access for experiments, while the smaller gaps yield reduced aberrations. Furthermore, these simulations allowed us to evaluate geometric predictions for EDX collection solid-angles [5] and the attainable tilt-ranges of these customised holders [6].

References:

[1] G. Owen, “Purchasing an electron microscope? – Considerations and scientific strategies to help in the decision making process,” Wiley Analytical Sciences, 2018.
[2] K. Tsuno and D. A. Jefferson, Ultramicroscopy, vol. 72, no. 1–2, 1998.
[3] “JEM-2200FS Field Emission Electron Microscope Specification” www.jeol.co.jp/en/products/detail/JEM-2200FS.html (accessed Oct. 14, 2021).
[4] P. McBean, D. O’Mahony, and L. Jones, in European Microscopy Congress Proceedings, 2020, p. 322.
[5] N. J. Zaluzec, Microsc. Microanal., vol. 20, no. 4, pp. 1318–1326, 2014.
[6] We acknowledge funding from Science Foundation Ireland (URF/RI/191637), the AMBER Centre (17/RC-PhD/3477), & Enterprise Ireland (CF-2021-1769-A). We also acknowledge JEOL Tokyo for fruitful discussions and insights.

Revealing mechano-chemical interactions on the surface of polypropylene surgical mesh using Secondary Electron HyperSpectral Imaging

Nicholas Farr, Sabiniano Roman, Jan Schäfer, Antje Quade, Shelia MacNeil, Corneila Rodenburg

University of Sheffield, UK

Summary:

Is there a spectroscopy method that can reveal the multiscale effects of mechanochemical interactions on the surface of biomaterials spanning several length scales? Such a technique would be a breakthrough for medical device characterisation and could be employed as pre-test to clinical deployment. Biomaterials introduced into the body are subject to dynamic, mechanical and chemical stimuli but these are rarely studied prior to device implantation. Here we demonstrate SE Hyperspectral Imaging (SEHI) has the ability to identify and map chemical alternations on the surface of polypropylene (PP) surgical mesh post laboratory based dynamic distention and chemical induced oxidation [1].

Introduction:

Thousands of women have had PP mesh inserted into their pelvic cavity to relieve stress urinary incontinence and pelvic organ prolapse but PP meshes have caused inflammation, pain, contraction and in many cases, erosion of the material through the patients' tissues. The exact reasons for the mesh failure are still hotly debated.

Materials are rarely deployed in static environments, rather in clinical use they are exposed to diverse and varying stresses within dynamic environments. Recent advances in mechanochemistry have offered previously unobtainable opportunities in the production and screening of materials [2]. To date this field of research has been constrained by the inability of current characterisation techniques to provide essential localised multiscale chemically mapped information. Established averaging methods for the estimation chemical alternations post dynamic testing do not provide information of a materials spatial distributions. For this reason, novel surface chemical spectroscopy and imaging methods on nano- and micro-scale levels are needed. Furthermore, a biomaterials surface properties are defined by its underlying chemical and structural relationships whose local variations determine cell growth propensity. Here we show that SEHI, a technique applied within a Scanning Electron Microscope (SEM), can provide the necessary spectral information and can also be exploited to produce chemically sensitive surface mapping. To show this we used SEHI to analyse PP mesh after oxidative stress combined with mechanical distention.

Methods/Materials:

PP mesh (Gynemesh® (Johnson & Johnson) was subjected to both mechanical distension and hydrogen peroxide. SEHI was performed as described previously [1] using a FEI Nova Nano 450 SEM.

Results and Discussion:

Figure 1A shows the Secondary Electron (SE) spectra of Gynemesh after 5%, 25% and 50% dynamic distention compared to that of control non-treated materials. For all conditions differences in intensities within the 1.4–2.3 eV range are noticeable. These point to differences in surface molecular order/crystallinity. Figure 2B presents the SE spectra of Gynemesh after 25% dynamic distention when combined with 3% H2O2 treatment or dH2O, respectively. 3 % H2O2 treatment during mechanical testing mimics the attack of neutrophils which can occur post implantation and resulted in further marked differences in molecular order but also surface functional group variations due to surface oxidation. This was confirmed by X-ray photoelectron spectroscopy (XPS) data (Fig 1C). XPS data show an increase in O/C ratio on the surface of Gynemesh as a result of mechanical distention. To visualise the variations in oxidation on different length scales SEHI maps were generated (Fig.1D). SEHI pseudo-colouring presented in Fig. 1D of cross sectioned Gynemesh after

25% mechanical distention with 3% H2O2 treatment shows surface as well as bulk material oxidation after treatment. Demonstrating SEHI can map mechano-chemical interactions of PP mesh as a result of oxidative mechanical distention.

Conclusion:

SEHI showed polymer oxidation and crack formation in PP long before any gross material failure could be demonstrated by any other techniques. This “early warning “system should rapidly help identify materials which will not cope well with distension and immune attack.

References:

[1] Farr et al. 2021. RSC Adv., 2021, 11, 34710
[2] O'Neill, R.; Boulatov, R. 2021. Nature Rev. Chem., 5, 148-167
[3] Authors thank EPSRC funding (EP/V012126/1), (EP/N008065/1) and (EP/T517835/1).

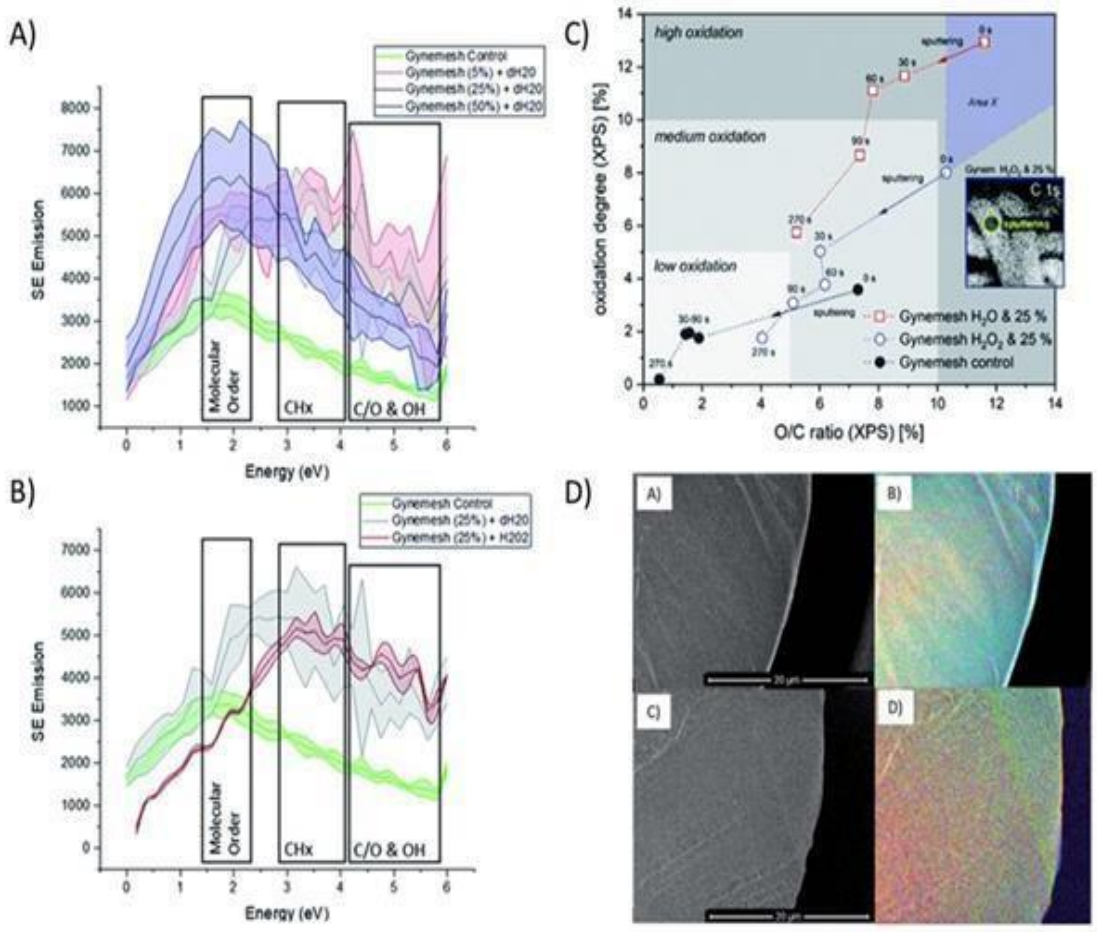

Figure 1: Figure reproduced under creative commons license (CC-BY) from [1]. Secondary electron spectra for Gynemesh (n=4) (A) after dynamic distention at varying degrees and (B), after treatment combining 25% dynamic distention with H2O2 or dH20. C) Oxidation of Gynemesh samples characterized by means of XPS depth profiling (sputter time in seconds (s)), three levels of oxidation are indicated by step of 5% change, area X indicates potentially higher oxidation of the samples before the analysis, inset: XPS image of C 1s for Gynemesh after 25% mechanical distention with 3% H2O2 treatment. D) SEHI images generated from SEHI colouring of cross sectioned Gynemesh after 25% mechanical distention with 3%H2O2 treatment (A) and (B) and Gynemesh – no treatment (C) and (D). Red regions symbolise high molecular order, green regions symbolize CHx, and blue region indicate (CO, COO, OH) oxidation products.

Optimization of (cryo-)FIB-SEM protocols to study interactions between Airborne Pollution Particles and Nasal Epithelial Cells

Victoria Garcia Giner, Alexandra Porter

Imperial College London, UK

High levels of airborne particles found in cities, PM 2.5 (<2.5µm), which include carbonaceous particles, as well as, redox-active metals, such as Cr, Fe or Ti, are associated with inflammatory responses and respiratory diseases. Identifying the effect of this PM composition/size with cell damage will help understand why pollution can be so damaging to respiratory system cells . This is a multiscale problem that requires correlation between PM composition and intracellular location to alterations in cell metabolism and organelle structure at the cellular level. Here an optimal workflow is devised to make this correlation.

To address this question complementary scanning electron imaging (SEM) and energy-dispersive X-ray spectroscopy (EDS) techniques under cryogenic conditions were first used to analyse the cellular uptake, and the intracellular destination and composition of PM 2.5 (from roadside and London Underground locations), in cultured human nasal epithelial cells. Cryo-SEM imaging reduced alterations to the chemical composition of the PM and cell morphology caused by conventional electron microscopy sample preparation protocols. The optimised protocol involved the sublimation of the ice layer covering the cell monolayer which revealed pollution PM agglomerates associated with the cells (Figure 1). PM agglomerates associated with the plasma membrane were composed of several metals including Al, Fe, Ti, Si, etc. - and carbonaceous particles. To study the intracellular presence of PM, Ga+ beam cross-sectional milling (Ga-FIB-SEM) of the cryogenic samples was attempted and showed particles were internalised. However, the volume removal capabilities of the beam were insufficient to cross-section through entire cells and draw meaningful conclusions of the localisation of PM after internalisation.

Plasma-FIB-SEM was subsequently used to visualize larger cellular cross-sections of embedded cell monolayers exposed to underground pollution, using a FEI Helios Hydra DualBeam PFIB-SEM. O beams were most suitable for resin milling. Large, high-quality cross-sections (> 90 µm width and >12µm depth) of cells were milled rapidly for posterior EDS compositional analysis and the structure of cell organelles and pollution PM were observed. However, it was very difficult to find co-localised PM and cell organelles due to the orientation that the cell monolayers were embedded in (the layer being exposed to the beam not showing any morphological reference). This was overcome using a cryogenic cell culture sample, where the cell morphology and PM are exposed after sublimation.

In parallel, other soft X-ray tomography (cryo-SXT) with structured illumination microscopy (cryo-SIM) (B24 Beamline, DLS) was employed to generate whole-cell structural and metabolically relevant information about the cells exposed to PM. Our preliminary data indicates significant mitochondrial alterations associated with PM co-localisation inside the cells.

Introducing these 3D imaging capabilities at the start of the workflow, could allow for a more holistic understanding of the variability of cell damage by PM and which sizes and chemistries are responsible for causing more intracellular damage. We will discuss how optimisation of cryo-FIB-SEM techniques could be used subsequently in specific areas for higher resolution imaging and complementary compositional analysis, as well as for lamella preparation for high-resolution cryo-TEM, where oxidation states and composition of damaging PM can be attained. In future, the development of this multidimensional workflow will bring together imaging of whole-cell structure and metabolism with chemical analysis of the PM to identify which chemistries are most damaging to intracellular cell organelles and their mechanisms of toxicity. This novel approach will offer new insights into how to mitigate the health effects of pollution PM.

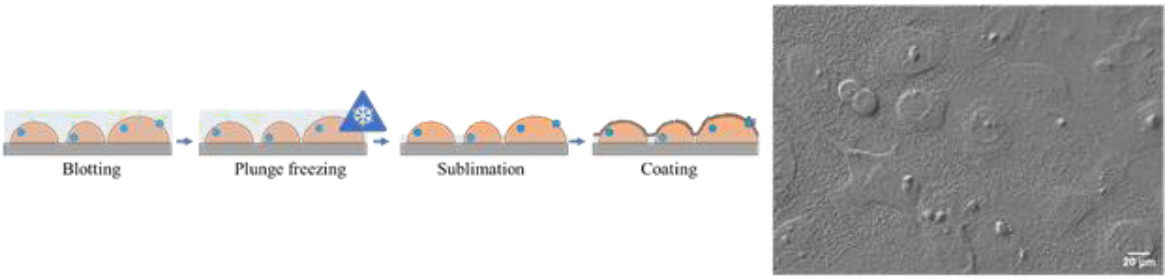

Figure 1. From left to right. Sample preparation workflow for cryo-SEM imaging of cell monolayers. Cryo-SEM imaging of nasal epithelial cells exposed to PM2.5 roadside pollution (Zeiss Auriga Cross beam, SE, 2kV) Exposure of cell monolayer after sublimation of the ice layer, pollution agglomerates can be observed on the surface of the cells (scale bar 20 µm).

Cryogenic Electron Ptychographic Single Particle Analysis (Cryo-EPty SPA)

Peng Wang, Xudong Pei, Liqi Zhou, Chen Huang, Mark Boyce, Judy Kim, Emanuela Liberti, Takeo Sasaki, Peijun Zhang, Peter Nellist, David Stuart, Angus Kirkland

University of Warwick, UK

Cryo-electron microscopy (cryo-EM) is a powerful method for the high-resolution three-dimensional structural characterization of a wide range of biological samples in a close-to-native, frozen-hydrated state [1]. Due to the extreme radiation sensitivity of vitrified biological samples [2], images of these have low signal-to-noise ratios [3] and low contrast [4,5]. Cryo-EM single particle analysis (SPA) relies on the use of conventional phase-contrast images recorded at high defocus to improve information transfer at low spatial frequencies. However, defocusing the image corrupts the information transfer at higher spatial frequencies [6].

Cryo-electron ptychography (Cryo-EPty) [7] as shown in Fig. 1a is an alternative technique based on scanning ptychographic diffractive imaging [8]. Ptychography uses a defocused probe to scan over a specimen with highly overlapping probe positions. In physical science, this approach has shown great potential in applications such as super-resolution imaging [9,10], high-contrast light-element detection [11], low dose imaging [12] and three-dimensional imaging [13,14]. Moreover, as ptychography utilizes the full diffraction pattern, it is dose-efficient particularly when data is recorded using direct electron detectors, which record high signal-to-noise at low electron dose. This has recently been demonstrated for micrometer wide phase reconstruction of an unstained virus-infected cell at a dose of 27 e/Å2 [7].

Here, we show a new 3D SPA technique based upon cryogenic ptychography (cryo-EPty SPA) and experimentally demonstrate that cryo-EPty SPA under cryogenic conditions can restore 3D information from a single sample. Experimental cryo-EPty SPA datasets (Fig. 1 b) were acquired in a scanning diffraction configuration as shown schematically in Fig. 1 a, in which a defocused probe is scanned over a cryo-sample. Using the ePIE algorithm [8], the ptychographic phase of rotavirus double-layered particles (DLPs) with 76.5 nm in diameter were reconstructed at a dose of 22.7 e/A2. The particle-picking procedures that have been developed for cryo-EM SPA can be directly applied to the phase, giving a positionally coordinated stack of particle phases, as shown in Fig. 1b. We will show that using the SPA pipeline, a 3D density map of rotavirus DLPs (Fig. 1 c) can be reconstructed with 300 particles from the stack of particle phases [7]. We expect that cryo-EPty combined with SPA has great potential to yield high-resolution 3D reconstructions of biological samples[16].

References:

[1] R Henderson et al., Journal of Molecular Biology 213 (1990), p. 899.
[2] KA Taylor et al., Science 186 (1974), 1036.
[3] R Henderson, Quarterly Reviews of Biophysics 28 (2009), p. 171.
[4] R Danev et al., Ultramicroscopy 88 (2001), p. 243.
[5] R Danev et al., Proceedings of the National Academy of Sciences 111 (2014), p. 15635.
[6] K H. Downing et al., Ultramicroscopy 108 (2008), p. 921.
[7] L Zhou, et al., Nature Communications 11 (2020), p. 2773.
[8] JM Rodenburg, Advances in Imaging and Electron Physics 150 (2008), p. 87.
[9] PD Nellist et al., Nature 374 (1995), p. 630.
[10] Y Jiang et al., Nature 559 (2018), p. 343.
[11] P Wang et al., Scientific Reports 7 (2017), p. 2857.
[12] J Song et al., Scientific Reports 9 (2019), p. 3919.
[13] AM Maiden et al., J. Opt. Soc. Am. A 29 (2012), p. 1606.
[14] S Gao et al., Nature Communications 8 (2017), p. 163.
[15] AM Maiden et al., Ultramicroscopy 109 (2009), p. 1256.
[16] The authors acknowledge funding from the University of Warwick Research Development Fund (RDF) 2021-22 Science Development Award

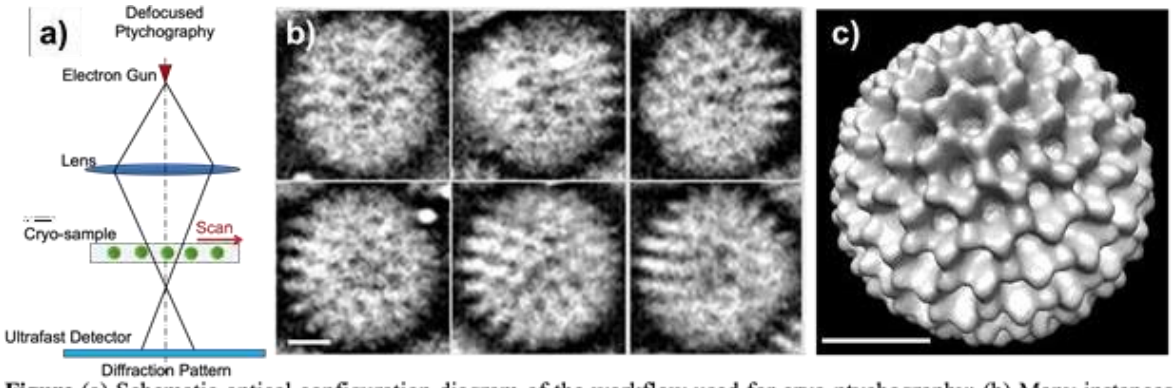

Figure (a) Schematic optical configuration diagram of the workflow used for cryo-ptychography; (b) Many instances of the viral particles for single particle analysis can be extracted from reconstructed ptychographic phases, scale bars: 20 nm. c) 3D map corresponding to the particle instances, scale bars: 25 nm

Poster Abstracts

Fast Ptychographic Reconstruction for Sparse Binary Ptychography data

Emma Hedley, Björn Eckert, Heike Soltau, Peter D. Nellist

University of Oxford, UK

Hardware developments in fast-pixelated detectors for 4D-STEM have significantly advance din recent years [1]. The high sensitivity and fast readout-speed of modern pixelated detectors means that low dose 4D STEM scans be acquired as faster rates, resulting in a lower cumulative dose. Combined with the high dose efficiency 4D STEM techniques such as ptychography this has opened new areas of materials science to 4D STEM imaging.

In particular a strong focus has developed on dose efficient method of imaging highly beam sensitive materi- als including, battery materials, zeolites and biological samples[2] [3] [4] . O'Leary et al have demonstrated that despite very low bit-depth in sparse binary CBED patterns which have as few as 30 electron interaction events each that high quality reconstructions could be obtained by single side band reconstruction [3].

The slowest step in the ptychographic reconstruction process usually the Fourier Transform of the square modulus of 4-dimensional dataset which is recorded by the detector. This can be very fast in the case of sparse binary data, especially when the number of electrons detected in very low since the speed of the Fourier Transform scales linearly with the number of events being recorded. Ultimately, we aim to demonstrate that this will speed up the ptychographic reconstruction using the widely used single side band method.

The JEOL 4D Canvas used here is a charge integrating detector with a high sensitivity, therefore, to reduce the data to a binary list of electron detection events with a pre-set threshold level for the integrated signal to be registered as an electron detection event. Instead of storing the entire pixel array – which is very large and in the case of sparse data contains mainly 0's -we transform the dataset into an event-stream of 4D-coordinates where electrons are detected. An example of a low dose image (a) and relevant 4D-STEM diffraction pattern (b) with a summary of the initial lines of the 4D-hitlist (c) is shown in Figure 1. This will decrease the memory required for data storage and processing and increase the throughput of datasets in the ptychographic reconstruction step.

In this presentation we will demonstrate the memory and time improvement potential in this workflow for low dose ptychographic reconstruction. We will demonstrate the advantages of this method for processing data from highly beam sensitive materials such as cathodes for Li-ion batteries. We will harness this low dose capability of ptychography and demonstrate the improved workflow to understand structural changes in cathodes materials which result in performance degradation [5].

References

1. H. Ryll et al., J. Instrum. 11 (2016).
2. J.G. Lozano, G.T. Martinez, L. Jin, P.D. Nellist, P.G. Bruce, Nano Lett. 18 (2018) 6850–6855.
3. C.M. O'Leary et al , Appl. Phys. Lett. 116 (2020).
4. L. Zhou, et al. Nat. Commun. 11 (2020) 1–9 .
5. The authors acknowledge use of characterization facilities within the David Cockayne Centre for Electron Microscopy, Department of Materials, University of Oxford and in particular the Faraday Institution (FIRG007, FIRG008), the EPSRC (EP/K040375/1 "South of England Analytical Electron Microscope") and additional instrument provision from the Henry Royce Institute (Grant reference EP/R010145/1).

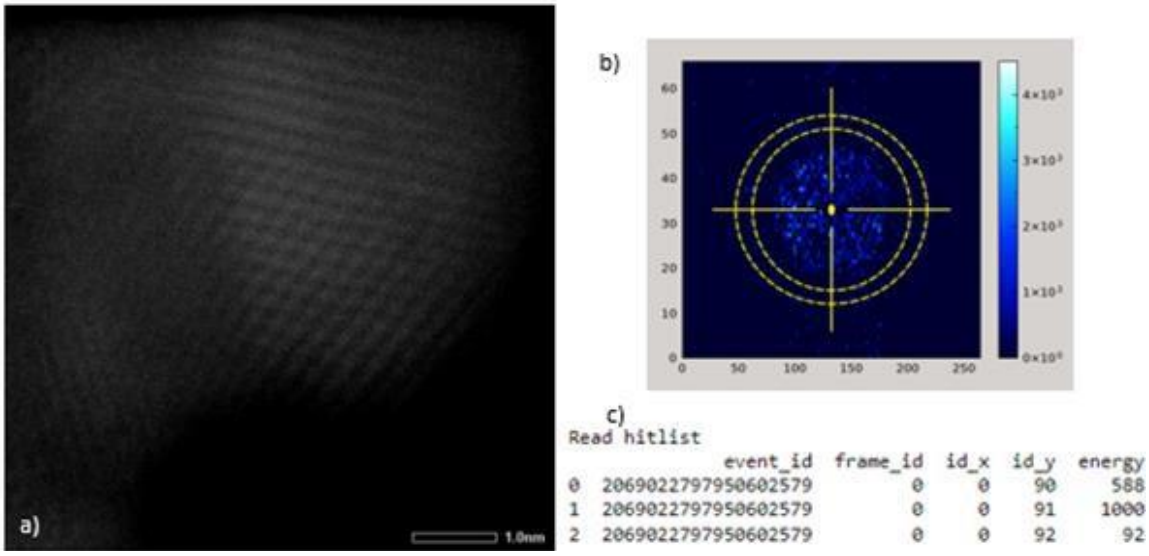

Figure 1. a) Low dose ADF image of Au nanoparticle. b) Individual diffraction pattern acquired on JEOL 4D Canvas equipped with a pnCCD® (S)TEM Camera® System. c) Short edit of 4D-hitlist of electron interaction events.

Electron microscopy of crystalline and amorphous phases in model leaf waxes

Emily Wynne, Neil George, Adam Keates, Rachael Shinebaum, Helen Blade, Andy Brown, Sean Collins

University of Leeds, UK

Wax layers on leaves play a controlling role in essential biological processes including transpiration. Identifying and understanding the structure of leaf waxes at a scale of 1-100s of nanometres holds the key to understanding how water and active agrochemical ingredients interacts with plant crops. Natural leaf waxes have a complex composition and structure; the intracuticular wax (IW) layer structure is believed to resemble a "bricks and mortar" model, with highly ordered crystalline domains separated by an amorphous matrix or highly disordered regions between ordered lamellae [1]. The IW layer consists mainly of very long chain aliphatics, with various terminal functional group interactions contributing to disorder between stacks of ordered long chain. The Schefflera elegantissima plant contains only four major long chain hydrocarbon species. Therefore, simplified replica leaf waxes can be formed from a subset of the major constituent long chain hydrocarbons [2]. Analytical techniques like X-ray diffraction and selected area electron diffraction fail to achieve the required spatial resolution to visualise their domain microstructures [3]. Scanning electron diffraction (SED) is a technique that can offer a spatial resolution of ~5 nm and low-dose SED can achieve the spatial resolution required to visualise the domain microstructures of these beam sensitive materials.

This poster presents work on chain orientation control of carbon alkyl chains in a single-phase wax prepared by two different TEM grid preparation methods and initial results on low-dose SED of the paraffins. Drop-casting sample preparation confirms the orthorhombic [001] orientation of the carbon chains, with an epitaxial orientation method confirming the [100] orientation for a Pbcm unit cell typical of long chain paraffins at room temperature. Measures of the critical fluence of these model waxes will also be discussed, including an outline of the low electron dose techniques that are required. Initial SED analyses show domain structure, with an average size of 230 nm, with some tilting of the crystal structure between domains as well as spatial variations in anisotropic diffuse scattering within alternate domains (likely due to chain displacements along the c-axis and perpendicular to the long axis of the domains). From this, a simple structural model of a pure

phase alkane material will be presented showing regions of higher disorder dispersed within regions of more order in agreement with the proposed brick and mortar model. Further work for more complex binary, ternary and quaternary mixtures at compositions relevant to leaf wax compositions will be investigated.

References

[1] M. Riederer, Annual Plant Reviews, Volume 23, Biology of the Plant Cuticle | Wiley, 2007.
[2] I. Basson and E. C. Reynhardt, Chem. Phys. Lett., 1992, 198, 367–372.
[3] D. L. Dorset, Acta Crystallogr. Sect. B, 1995, 51, 1021–1028.

Influence of Plasmon-excitation Electrons on Ptychography Phase Imaging

Zhiyuan Ding, Angus I Kirkland, Peter D Nellist

University of Oxford, UK

Electron ptychography is a phase retrieval method in transmission electron microscopes (TEM) in which the phase of exit wavefunction is reconstructed from electron diffraction patterns [1]. It is used for a wide range of specimens for atomic-scale imaging, including sensitive battery materials [2] and biological structures [3]. As a method of coherent imaging, contrast of electron ptychography is based on coherence of electron beam. However, inelastic scattering that happens in the interaction between beam and specimen introduces an energy distribution of the exit beam. With increased thickness of the sample, the proportion of inelastic scattered electrons (most of which are plasmon-excited electrons) increases. In this work, we investigate the influence of inelastic electrons, especially plasmon-excited electrons on ptychographic reconstruction.

To explore the influence of inelastic scattered electrons, in an aberration-corrected TEM at 200kV, 4D-STEM datasets with and without energy filter were recorded at different defocus conditions on a sample of gold nanoparticles and carbon film. The convergence angle of the electron beam is 22 mrad. Then ptychography reconstructions were carried out on recorded 4D-STEM datasets using the ePIE algorithm [4].

The reconstruction results shows that phase contrast images for atomic-scale resolution are stable whether or not the inelastic scattered electrons are filtered. This result is in line with the prediction based on characteristic scattering angle for inelastic scattering. For this experiment, the characteristic scatter angle of plasmon-exited electrons (energy loss: 20 eV) is 0.005 mrad. However, the pixel size of 4D-STEM detector used in the experiment is 0.25 mrad, which is far bigger than the characteristic scatter angle. This means that statistically, most electrons will still be detected by the same pixel whether or not they are inelastic scattered along with the image-forming elastic scattering. Therefore, the normalized intensity distribution of recorded diffraction patterns with or without energy filter are almost the same.

However, if a smaller pixel size is used, i.e. a larger camera length, for a beam with a smaller convergence angle, the situation is different. For example, if a convergence angle of 1~2 mrad is used for large field-of-view ptychographic imaging [3], the pixel size on detector may be comparable to characteristic scatter angle under a similar experimental condition. In this situation, the influence of inelastic scattered electrons on electron ptychography should not be ignored.

Reference

1. Nellist, P., McCallum, B. & Rodenburg, J. M. Resolution beyond the'information limit'in transmission electron microscopy. Nature 374, 630-632 (1995).

2. Lozano, J. G., Martinez, G. T., Jin, L., Nellist, P. D. & Bruce, P. G. Low-dose aberration-free imaging of Li-rich cathode materials at various states of charge using electron ptychography. Nano letters 18, 6850-6855 (2018).
3. Zhou, L. et al. Low-dose phase retrieval of biological specimens using cryo-electron ptychography. Nature communications 11, 1-9 (2020).
4. Maiden, A. M. & Rodenburg, J. M. An improved ptychographical phase retrieval algorithm for diffractive imaging. Ultramicroscopy 109, 1256-1262 (2009).

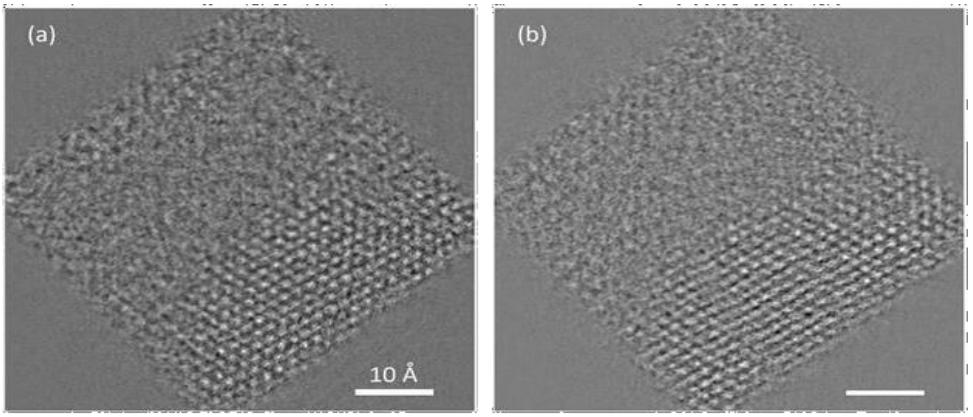

Figure 1 | Ptychographic phase reconstructions (a) without energy filter, i.e. elastic and inelastic scattered electrons are both recorded, and (b) with energy filter, i.e. only elastic scattered electrons are recorded. Defocus value is -14 nm.

Using Low-Dose Scanning Electron Diffraction Microscopy to Observe Hydration/Dehydration of Theophylline

Natalia Koniuch, Sean Collins, Mark S'ari, Martha Ilett, Zabeada Aslam, Helen Blade, Leslie Hughes, Nicole Hondow, Rik Drummond-Brydson, Andy Brown

University of Leeds, UK

Identifying and understanding phase transformations of organic drug compounds when exposed to water during processing or storage, is of great importance to the pharmaceutical industry. Hydrated forms of active pharmaceutical ingredients can alter the dissolution profile of a drug but limiting hydration requires identification and understanding of reaction pathways so that improved processing, formulation, and storage can be developed. In this experimental work, we propose a novel way to observe structural changes of a model channel hydrate, theophylline, at the single particle level by transmission electron microscopy, particularly scanning electron diffraction (SED).

Anhydrous theophylline form II rapidly transforms to the monohydrated form (M) when placed in contact with water at ambient temperature or during storage in high humidity conditions. Dehydration of form M is however a two-step process, with the first step being the formation of a metastable intermediate (T*) before formation of the anhydrous and stable form II. Paiva et al. (1) studied the structure of T* by low-frequency vibrational spectroscopy and propose that T* has a highly disordered form of the monohydrate structure with the water molecules removed. A slow rate of transformation to form II will result in a build-up of T* that has serious consequences on product performance. The transformation of M to T* has not been fully characterised, in part, because standard solid-state analytical techniques have a limit of sensitivity to the presence of trace amounts of phases such as T*. TEM/SED present the opportunity to address this characterisation gap.

We have already demonstrated phase identification by TEM electron diffraction and phase contrast imaging on single particles of theophylline form II and M using a Titan3 Themis 300 equipped with a Gatan OneView camera (2). The critical fluence for loss of crystallinity of theophylline form II at 300 keV is measured to be 36 ± 8 e-/Å2. Electron transparent monohydrate phases were generated on TEM grids by (a) hydration of form II crystals in 93% RH and (b) recrystallisation from a solution in nitromethane with water activity of 0.8. Moreover, we produced highly faulted particles of partially hydrated form II plates by full water immersion.

To enhance our understanding of these phase transformations we have performed low-dose SED imaging at an electron fluence of ~ 5 e-/Å2 using Merlin/Medipix direct electron detector at ePSIC. Initial observation of a form II theophylline sample left in direct contact with water reveals areas where form M crystallised on the surface of form II plates and tilting of small regions of form II plates away from the initial orientation which might be a precursor for M formation. In addition, we analyse dehydration of form M crystals by in-situ vacuum drying of particles cryo-transferred into the TEM. The average SED pattern of these partially transformed crystals shows a 'halo' around some diffraction spots indicating the presence of structural distortion due to dehydration which may be indication of T* formation. Furthermore, the virtual dark field images reconstructed from a particle analysed after 35 and then 110 min in vacuum, confirms that the structural changes start at the edges of the crystal. Thus, low-dose SED imaging can provide a better understanding of phase transformations of channel hydrates and this understanding may be used to improve solubility in drug formulations.

Reference:

(1) E M Paiva et al, Mol Pharm 18 (2021), 3578-3587.
(2) N Koniuch et al, MMC2021, 10.22443/rms.mmc2021.255.

In-situ environmental TEM study of the oxidation and reduction of Ni/NiO

Arej Eid, Ahmed Althumali, Adam Kerrigan, Leonardo Lari, Vlado Lazarov

University of York, UK

Metallic nanoparticles and their oxide have been used significantly in the field of catalysis and these nanoparticles show high selectivity and activity. Many catalytic reactions require the oxidation and reduction of metal/metal oxide as an initial step. Moreover, these reactions of the catalysts with the surrounding environment (gases and temperatures) involve structural changes and phase transformation. Therefore, understanding the reaction mechanisms of oxidation and reduction requires tracking the dynamic interaction of the material under realistic conditions at the atomic scale.

Environmental TEM (ETEM) has a capability for in-situ studies of gas-solid reactions by allowing gases in the sample area. In this work, we employed aberration-corrected ETEM to investigate the dynamic of metal/oxide interface interaction during oxidation and reduction processes on the example of Ni and NiO nanoparticles. These nanoparticles have attracted significant research attention as catalysts due to their low cost and wide applications that include: CO oxidation, oxygen evolution, photocatalytic reaction, and water-gas shift reaction [1],[2].

The in-situ experiments for the oxidation and reduction of NiO/Ni were conducted under different gases (H2, O2, a mixture of CO2 and H2O vapor), pressure of 1 Pa, and controlled temperature ranging from room temperature to 900 oC. We will present the structural changes including atomic ordering/disordering, defects formation, nanoparticles facets development as well as oxide formation and metal/oxide interface atomic structure, obtained by HRTEM and electron diffraction.

Reference:

1. Alnarabiji, M. S., Tantawi, O., Ramli, A., Zabidi, N. A. M., Ghanem, O. B., & Abdullah, B. (2019). Comprehensive review of structured binary Ni-NiO catalyst: Synthesis, characterization and applications. Renewable and Sustainable Energy Reviews, 114, 109326.
2. Xia, S., Dai, T., Meng, Y., Zhou, X., Pan, G., Zhang, X., & Ni, Z. (2020). A low-temperature water–gas shift reaction catalyzed by hybrid NiO@ NiCr-layered double hydroxides: catalytic property, kinetics and mechanism investigation. Physical Chemistry Chemical Physics, 22(22), 12630-12643.

Observing calcium sulfate crystallisation and phase transformation using in situ transmission electron microscopy techniques

Martha Ilett, H. M. Freeman, Z. Aslam, J. M. Galloway, D. P. Klebl, S. P. Muench, I. J. McPherson, O. Cespedes, Y-Y. Kim, F. C. Meldrum, S. R. Yeandel, C. L. Freeman, J. H. Harding, R. M. Drummond-Brydson

University of Leeds, UK

Understanding the nucleation, growth and phase transformations of calcium sulfate crystals is key to improving a number of industrial processes and understanding its formation in the natural environment. However there remains ongoing discussion and research regarding the true mechanism of formation of calcium sulfate from aqueous solution and this is in part due to the differing methods of sample preparation and characterisation techniques employed in these studies [1-3]. Mineral phases often change on drying or by the addition of solvents and whilst in situ techniques can eliminate these problems they in turn can induce changes to the samples. Consequently, in this study we combine and correlate advanced in situ techniques to further our understanding of calcium sulfate crystallisation pathways and better understand the impact and effect of sample preparation and characterisation techniques on studying these crystallisation processes.

We used a combined analytical approach of liquid cell transmission electron microscopy (LC TEM), cryogenic-TEM (cryo-TEM) and Raman spectroscopy to observe: (1) the phase transformation of bassanite to gypsum via hydration with an undersaturated calcium sulfate solution and, (2) the early stages of the mechanism of formation of gypsum crystals from equimolar aqueous solutions of 100 mM $CaCl_2$ and Na_2SO_4. A dual flow Hummingbird Scientific LC TEM holder was used and TEM data collected using an FEI Titan3 Themis G2 S/TEM operated at 300 kV with an FEI super-X energy dispersive X-ray (EDX) system and a Gatan OneView CCD. For correlative cryo-TEM studies either an FEI Vitrobot© was used to prepare plunge frozen samples or a home built spray plunge freezing set up was used for time resolved cryo-TEM which allowed rapid freezing after <20 s mixing [4].

Our results highlight the complexities of microscopy-based studies of reactions in solution where discrepancies in the reaction kinetics of the bassanite phase transformation to gypsum between LC TEM, cryo-TEM and Raman spectroscopy were evident. Notably the confined region within the LC microfluidic environment (~2 nL) slowed down the reaction kinetics by an order of magnitude in comparison to the less confined cryo-TEM analysis. Furthermore, electron beam induced radiolysis of the aqueous solvent in LCTEM increased the reaction kinetics due to the decrease in pH which promotes bassanite dissolution. From our combined EM approach we conclude that ca 300 nm bassanite nanorods transform to gypsum predominantly via a dissolution and reprecipitation pathway.

Further preliminary studies looking at gypsum crystallisation from solution again illustrate the need to study these processes in situ, where comparisons with conventional dry TEM analysis have shown substantial differences. On studying gypsum formation after mixing $CaCl_2$ and Na_2SO_4 solutions, intermediary bassanite aggregates were only observed when samples were dehydrated and prepared either by vacuum filtering onto

a TEM grid or quenching in ethanol. Comparative studies using cryo-TEM did not indicate any bassanite intermediates with only gypsum crystals observed.

Ultimately this work adds to the growing discussion surrounding gypsum formation and highlights the importance of using multiple in situ techniques in a correlative approach when studying dynamic crystallisation processes in order to extract and understand true mechanistic pathways.

Reference:

1. Stawski, T. M.; van Driessche, A. E. S.; Ossorio, M.; Rodriguez-Blanco, J. D.; Besselink, R.; Benning, L. G., Formation of calcium sulfate through the aggregation of sub-3 nanometre primary species. Nature Communications 2016, 7.
2. Van Driessche, A. E. S.; Benning, L. G.; Rodriguez-Blanco, J. D.; Ossorio, M.; Bots, P.; Garcia-Ruiz, J. M., The Role and Implications of Bassanite as a Stable Precursor Phase to Gypsum Precipitation. Science 2012, 336 (6077), 69-72.
3. Wang, Y. W.; Kim, Y. Y.; Christenson, H. K.; Meldrum, F. C., A new precipitation pathway for calcium sulfate dihydrate (gypsum) via amorphous and hemihydrate intermediates. Chemical Communications 2012, 48 (4), 504-506.
4. D. Kontziampasis, D. P. Klebl, M. G. Iadanza, C. A. Scarff, F. Kopf, F. Sobott, D. C. F. Monteiro, M. Trebbin, S. P. Muench and H. D. White, A cryo-EM grid preparation device for time-resolved structural studies. IUCrJ 2019, 6 (Pt 6), 1024-1031.

Structural and electronic study of Cu doped NiO

Ahmad Althumali, Adam Kerrigan, Leonardo Lari, Vlado Lazarov

University of York, UK

Nickel oxide (NiO) is a wide band gap p-type oxide semiconductor with good optical transparency and high chemical stability. This properties has been exploited for applications in photovoltaics and light emitting diodes as a hole transporting layer. Doping NiO with other metal elements such as Cu is an effective way to adjust its grain size, crystallinity, transmittance and conductivity, which can enhance its applications in devices.

In this work we have studied the role of Cu concentration on microstructure of NiO films grown by molecular beam epitaxy (MBE) as a function of doping concentrations, between 3% and 42 at.%. The in-situ Reflection High-Energy Electron Diffraction (RHEED) analysis of Ni1-xCux thin films show presence of diffraction spots along modulated RHEED streaks for low doping concentration and distinctive transmission spots (indicative of 3D island growth) for higher Cu doping. The X-Ray diffraction results show that the structure of the $Ni_{1-x}Cu_xO$ thin films remains cubic with (001) as preferred growth orientation, though crystallinity of NiO films degrades, e.g. polycrystalline film structure develops, when Cu content exceeds 10 at.%. The further AFM films surface imaging reveals that surface morphology greatly increase with increase of Cu concentrations.

Finally, we will present in-situ dynamical study of Ni1-xCux thin films oxidation process utilising environmental AC-TEM and correlate the structure and properties with thin Cu-doped NiO films prepared by MBE.

Mapping oxygen columns in magnetite crystals using differential phase contrast STEM imaging

Xuyang Zhou, Baptiste Gault, Dierk Raabe, Gerhard Dehm, Christian H. Liebscher

Max-planck-institut Fuer Eisenforschung Gmbh, Germany

Differential phase contrast (DPC) imaging in the scanning transmission electron microscope (STEM) is an emerging technique to observe light elements with low atomic number and to determine the local charge density of crystalline materials at atomic resolution [1, 2]. DPC images reconstructed from four-dimensional (4D) STEM data have extended the application to reveal information about electrical fields and with this indirectly information on local atomic bonding at sub-Ångstrom resolution [3]. In this talk, we will present our calibration of the electron microscope pixel array detector (EMPAD) using polycrystalline Au samples and compare our DPC measurements on $SrTiO_3$ (STO) single-crystalline samples to results published in literature [2, 3]. Furthermore, we have applied the DPC technique to map oxygen columns and charge density maps in magnetite (Fe_3O_4) crystals and at the interface between magnetite and iron. The talk will also discuss data processing methods to increase the signal-to-noise ratio and steps to correct scanning artifacts. Direct experimental observations of charge transfer between neighboring atoms at magnetite-iron interfaces will provide novel insights into our fundamental understanding of iron corrosion and the contribution of the interface structure in catalytic processes.

References:

1. N. Shibata, S.D. Findlay, Y. Kohno, H. Sawada, Y. Kondo, Y. Ikuhara, Nature Physics 8(8), 611-615 (2012).
2. K. Müller, F.F. Krause, A. Béché, M. Schowalter, V. Galioit, S. Löffler, J. Verbeeck, J. Zweck, P. Schattschneider, A. Rosenauer, Nat. Commun. 5(1), 5653 (2014).
3. W.P. Gao, C. Addiego, H. Wang, X.X. Yan, Y.S. Hou, D.X. Ji, C. Heikes, Y. Zhang, L.Z. Li, H.X. Huyan, T. Blum, T. Aoki, Y.F. Nie, D.G. Schlom, R.Q. Wu, X.Q. Pan, Nature 575(7783), 480-484 (2019).

Automated sample alignment in the transmission electron microscope

Zaeem Najeeb, Timothy Poon, Thomas Slater, Christopher Allen

Imperial College London, UK

When imaging beam-sensitive samples, such as perovskites, MOFs and supramolecular crystals, prolonged exposure to the electron beam can lead to the sample's crystal structure breaking down [1-3]. In particular, knock-on damage and radiolysis can be major contributors to structural changes at high and low accelerating voltages, respectively [4]. Therefore, all processes which require illumination of the sample should be completed while minimising electron fluence. However, obtaining high-resolution STEM images of single crystals typically requires the sample to be oriented onto a major zone axis. This is achieved using the Kikuchi diffraction patterns as a roadmap to orient the sample, where the bands form from diffuse inelastic scattering of electrons in the sample and connect major zone axes. Due to the patterns varying for different crystal systems, finding the correct zone axis can be difficult in some cases. One specific challenge is that large tilts may be required, which can quickly make the user lose track of their position and hinder their ability to find which zone axis corresponds to the desired orientation. Moreover, predicting the correct stage correction after a tilt requires parameters unique to a specific sample holder and microscope combination.

This work aims to create scripts in Digital Micrograph to automate the process of sample orientation to a specific zone axis [5]. The scripts allow a user to reorient the sample stage on a double-tilt holder given an image containing Kikuchi bands. This is done by either manually clicking on a zone axis within an image or via using line detection algorithms in Python to find a specific zone axis. This has been tested on a JEOL ARM300CF where the tilts were first measured from the distance a zone axis travelled on the camera. The stage shifts were then calculated by modelling a tilt to be about a centre point, correcting for shift errors such as backlash using scaling parameters unique to a sample holder and microscope combination. These unique parameters can be rapidly determined using provided helper scripts. Lastly, the possible zone axis will be simulated and displayed to aid the user in determining the symmetry of the zone axis.

Reference

[1] Song, K., et al. Advanced Energy Materials. 10(26), 1904006, (2020).
[2] Liu, L., et al. Communications Chemistry. 3(1), 1-14, (2020).
[3] Olenyuk, B., et al. Nature. 398(6730), 796-799, (1999).
[4] Egerton, R. F. Microscopy research and technique, 75(11), 1550-1556, (2012).
[5] Mitchell, D. R. G., & Schaffer, B. Ultramicroscopy. 103(4), 319-332, (2005).

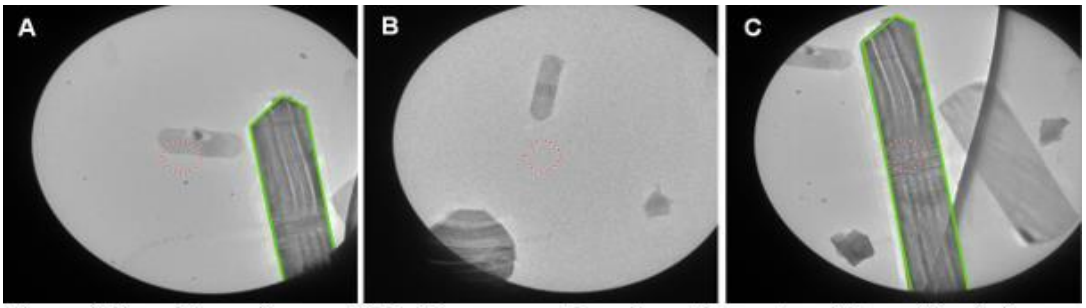

Figure 1. Ronchigram images of MoO_3 nanocrystals, where the centre of the optic axis is marked by a red circle. (A) shows a crystal, outlined in green, oriented off zone. (B) shows the image after tilting, note how the crystal has moved outside the field of view. (C) shows how, after automated stage position correction, the crystal returns to the centre of the image and oriented now on the zone axis.

Spin-scattering function of confined magnons in magnetic interfaces.

Júlio Do Nascimento, Vlado K. Lazarov

University of York, UK

Efficient electron beam monochromators have opened new possibilities for experimental techniques available to scanning transmission electron microscopy (STEM)[1]. Recent developments allowed for the measurement of vibrational spectra, in the form of collective vibrations of the lattice also known as phonons[2]. Such phonon modes occupy an energy range from zero to tens or a few hundreds of meV in solid-state materials. Qualitatively the same energy range is also occupied by energy losses due to excitations in the spin-lattice of the system. These quantised excitations are known as magnons.

Although it is well known that, compared to the Coulomb interaction, the magnons interaction with the electrons is 3 or 4 orders of magnitude weaker, in some particular situations detecting such perturbations to the magnetic ordering by TEM can be feasible [3, 4].

In our work, using the theory developed by Beairsto et. al [5], we calculate the spin scattering function for surface and interfacial magnons as a proxy for the detection of magnons in STEM experiments. We focus on

the role of surfaces and interface confinement of magnons, with a focus on surface and interface anisotropies and how that affects the scattering amplitudes. We finally discuss how the spin scattering function relates to the EELS signal in STEM conditions.

References

1. O.L. Krivanek, N. Dellby, J.A. Hachtel, J.-C. Idrobo, M.T. Hotz, B. Plotkin-Swing, N.J.Bacon, A.L. Bleloch, G.J. Corbin, M.V. Hoffman, C.E. Meyer, and T.C. Lovejoy. Progress in ultrahigh energy resolution eels. Ultramicroscopy, 203:60–67, 2019.
2. Ondrej L. Krivanek, Tracy C. Lovejoy, Niklas Dellby, Toshihiro Aoki, R. W. Carpenter, Peter Rez, Emmanuel Soignard, Jiangtao Zhu, Philip E. Batson, Maureen J. Lagos, Ray F. Egerton, and Peter A. Crozier. Vibrational spectroscopy in the electron microscope. Nature, 514(7521):209–212, Oct 2014.
3. Keenan Lyon, Anders Bergman, Paul Zeiger, Demie Kepaptsoglou, Quentin M. Ramasse, Juan Carlos Idrobo, and J ́an Rusz. Theory of magnon diffuse scattering in scanning transmission electron microscopy. Phys. Rev. B, 104:214418, Dec 2021.
4. J. C. Loudon. Antiferromagnetism in NiO observed by transmission electron diffraction. Phys. Rev. Lett., 109:267204, Dec 2012.
5. Seamus Beairsto, Maximilien Cazayous, Randy S. Fishman, and Rogério de Sousa. Confined magnons. Phys. Rev. B, 104:134415, Oct 2021.

Exploring the Cryogenic Phase Changes within 2D MoTe2 via TEM, 4DSTEM and Electron Spectroscopy Techniques

Samad Abdus, Michele Conroy, Ursel Bangert

University of Limerick, Republic of Ireland

Research in the field of atomically thin 2D materials has grown remarkably since the discovery and isolation of graphene, the 2010 Nobel Prize 2D material, due to its structural flexibility and tunable electronic properties[1] [2]. Graphene has been one of the most well-researched 2D materials, but being a quasi-metal limits its applications in electronic devices [3][4]. This has fueled research into two-dimensional transition metal dichalcogenides (2D TMDs) which can exhibit more than one phase with distinct structures and physical properties such as the metallic distorted octahedral (1T') phase and the semiconducting trigonal prismatic hexagonal (2H) phase [5]. Among them, MoTe2 is a topological Weyl semimetal (TWS) and is the most promising TMD material for phase engineering at the atomic level [6]. Since TWSs are highly conducting at low frequencies, they challenge the classical idea of polarization and metallicity, this phenomenon has gathered a lot of attention in the ferroelectric community [7]. The possibility of controllable TMDs phase engineering has attracted tremendous attention due to its appeal in both fundamental physics and potential applications beyond graphene [8].

MoTe2 has a smaller phase energy difference ($\Delta E < 50$ meV) between the 1T′ and the 2H phase which can make phase transitions possible compared to other TMDs such as MoS2 ($\Delta E > 0.8$ eV) [9]. Recently, MoTe2 phase changes have been achieved by strain engineering [10], controlled chemical vapor deposition (CVD) [11], electrostatic doping[12] and laser irradiation [13]. The underlying mechanisms of these phase changes has been proposed to be heating, Te defects, and strain effects [9][14][15]. However, a microscopic understanding at the atomic level is still lacking and more experimental evidence is required to further explore the phase change phenomenon.

Transmission electron microscopy (TEM) characterization of 1T'MoTe2 shows a clear change in the phase structures between room and cryogenic temperatures, which is an important feature, since the electronic properties of 2D materials are highly dependent on their precise structural arrangement and chemical composition[16]. This temperature-driven study focuses on atomic-scale observations of local phase transitions in MoTe2 in cryogenic environments by using in-situ cryogenic TEM and 4D Scanning Transmission electron microscopy (4DSTEM) for strain mapping while monitoring electronic band structure and chemical composition changes via monochromated high-resolution electron energy loss spectroscopy (EELS).

In this poster presentation, we will detail the benefits of using low-temperature atomic resolution electron microscopy and spectroscopy to explore the exotic phase changes of topological semimetals.

References:

1. M. H. Kang, D. Lee, J. Sung, J. Kim, B. H. Kim, and J. Park, "Structure and chemistry of 2D materials," in Comprehensive Nanoscience and Nanotechnology, vol. 1–5, Elsevier, 2019, pp. 55–90.
2. A. K. Geim, "Graphene: Status and Prospects," Science (80-.)., vol. 324, no. 5934, pp. 1530–1534, 2009.
3. R. Vargas-Bernal, "Graphene against Other Two-Dimensional Materials: A Comparative Study on the Basis of Electronic Applications," in Two-dimensional Materials, P. K. Nayak, Ed. Rijeka: IntechOpen, 2016.
4. G. R. Bhimanapati et al., "Recent Advances in Two-Dimensional Materials beyond Graphene," ACS Nano, vol. 9, no. 12, pp. 11509–11539, Dec. 2015.
5. D. Mackenzie, "Reuse of N95 Masks," Engineering, Apr. 2020.
6. Y. Tan et al., "Controllable 2H-to-1T′ phase transition in few-layer MoTe2," Nanoscale, vol. 10, no. 42, pp. 19964–19971, 2018.
7. F.-T. Huang et al., "Polar and phase domain walls with conducting interfacial states in a Weyl semimetal MoTe2," Nat. Commun., vol. 10, no. 1, p. 4211, 2019.
8. Y.-C. Lin, D. O. Dumcenco, Y.-S. Huang, and K. Suenaga, "Atomic Mechanism of the Semiconducting-to-Metallic Phase Transition in Single-Layered MoS2," Nat. Nanotechnol., vol. 9, p. 391, 2014.
9. K.-A. N. Duerloo, Y. Li, and E. J. Reed, "Structural phase transitions in two-dimensional Mo- and W-dichalcogenide monolayers," Nat. Commun., vol. 5, no. 1, p. 4214, 2014.
10. S. Song, D. H. Keum, S. Cho, D. Perello, Y. Kim, and Y. H. Lee, "Room Temperature Semiconductor–Metal Transition of MoTe2 Thin Films Engineered by Strain," Nano Lett., vol. 16, no. 1, pp. 188–193, Jan. 2016.
11. T. A. Empante et al., "Chemical Vapor Deposition Growth of Few-Layer MoTe2 in the 2H, 1T′, and 1T Phases: Tunable Properties of MoTe2 Films," ACS Nano, vol. 11, no. 1, pp. 900–905, Jan. 2017.
12. Y. Wang et al., "Structural phase transition in monolayer MoTe2 driven by electrostatic doping," Nature, vol. 550, no. 7677, pp. 487–491, 2017.
13. C. Suyeon et al., "Phase patterning for ohmic homojunction contact in MoTe2," Science (80-.)., vol. 349, no. 6248, pp. 625–628, Aug. 2015.
14. S. Yuan et al., "Room-temperature ferroelectricity in MoTe2 down to the atomic monolayer limit," Nat. Commun., vol. 10, no. 1, p. 1775, 2019.
15. M. B. Vellinga, R. de Jonge, and C. Haas, "Semiconductor to metal transition in MoTe2," J. Solid State Chem., vol. 2, no. 2, pp. 299–302, 1970.
16. M. C. Michael J. Zachman,Jacob Madsen,Xiang Zhang,Pulickel M. Ajayan,Toma Susi, "4D-STEM: Interferometric 4D-STEM for Lattice Distortion and Interlayer Spacing Measurements of Bilayer and Trilayer 2D Materials (Small 28/2021)," Wiley-VCH GmbH, vol. 2170142, no. 17, 2021.
17. S. Fang et al., "Atomic electrostatic maps of 1D channels in 2D semiconductors using 4D scanning transmission electron microscopy," Nat. Commun., vol. 10, no. 1, p. 1127, 2019.

18. All authors acknowledge Science Foundation Ireland funding for access to the Titan TEM at the University of Limerick. M.C. acknowledges funding from the Royal Society Tata University Research Fellowship (URF\R1\201318).

Native state structural and chemical characterisation of Pickering emulsions

Dario Luis Fernandez Ainaga,

University of Leeds, UK

Soft matter and nanoparticles dispersed aqueous samples present unique imaging challenges in the electron microscope: the requirement for vacuum appropriate dry samples leads to the loss of structure that would be present in the native aqueous state. Cryogenic freezing of the sample before imaging is an established sample preparation technique used extensively in biology, allowing for the preservation of the sample structure. This technique can be applied to soft hybrid inorganic-organic materials such as Pickering emulsions to enable representative 2D imaging and electron tomography. The focus of this study is to explore a range of characterisation techniques in cryo-TEM for the analysis of Pickering emulsions in 2D and 3D, along with elemental analysis using STEM-EDX and EELS.

After blotting and plunge-freezing 3.5 µl of a Pickering emulsion comprised of hexadecane in water droplets stabilised by ~5 nm platinum nanoparticles, the sample was imaged in cryo-TEM and then cryo-HAADF-STEM to allow for higher magnification imaging without damaging the vitreous ice. Electron tomography of the emulsions droplets was performed in cryo-HAADF STEM using a ±60° tilt range, permitting 3D visualisation of the sample structure. With electron tomography, the position of the stabilising nanoparticles could be visualised in 3D space, and confirmed that the structure of the droplets is maintained when the sample is cryogenically frozen. Further STEM-EDX and EELS elemental analysis confirmed the presence of the oil phase within the emulsion droplets.

Beam-induced damage to the vitreous ice (and consequent damage to the sample structure) remains a major obstacle for the imaging of cryogenically frozen samples, limiting the characterisation techniques that can be used and imaging magnification. Cryo-HAADF STEM-EELS was found to be useful for imaging and elemental analysis at higher magnifications while minimising the damage to the amorphous ice leading to the development of an initial protocol for imaging and elemental analysis of Pickering emulsion droplets. Further work needs to be done to improve the electron tomography results using Pickering emulsions with nanoparticles larger than 10nm, attempting to obtain more accurate positions of the nanoparticles on the oil-water interface.

Compressive Scanning Transmission Electron Microscopy

Daniel Nicholls, Alex Robinson, Jack Wells, Amirafshar Moshtaghpour, Mounib Bahri, Angus Kirkland, Nigel Browning

University of Liverpool, UK

Scanning Transmission Electron Microscopy (STEM) offers high-resolution images that are used to quantify the nanoscale atomic structure and composition of materials and biological specimens. In many cases, however, the resolution is limited by the electron beam damage, since in traditional STEM, a focused electron

beam scans every location of the sample in a raster fashion. In this study, we propose a scanning method based on the theory of Compressive Sensing (CS) and subsampling the electron probe locations using a line hop sampling scheme that significantly reduces the electron beam damage. We experimentally validate the feasibility of the proposed method by acquiring real CS-STEM data, and recovering images using a Bayesian dictionary learning approach. We support the proposed method by applying a series of masks to fully-sampled STEM data to simulate the expectation of real CS-STEM. Finally, we perform the real data experimental series using a constrained-dose budget to limit the impact of electron dose upon the results, by ensuring that the total electron count remains constant for each image.

Stability-limited Subsampled Scanning in Scanning Transmission Electron Microscopy

Daniel Nicholls, Alex Robinson, Jack Wells, Amir Moshtaghpour, Angus Kirkland, Nigel Browning

University of Liverpool, UK

Probe subsampling has been shown to reduce the electron dose-rate required to form high resolution images when performing compressive sensing (CS) scanning transmission electron microscopy (STEM) (Kovarik et al. 2016). By acquiring only a portion of the image, via manipulation of the electron beam probe scanning architecture, incomplete images can be formed and an inpainting algorithm can be used to inpaint the missing information (Stevens et al. 2014). This allows images to be acquired faster, and with less beam-induced damage.

Probe subsampling is typically performed using some control software, and an external scan generator connected to the electromagnetic scan coils. In some implementations, subsampling can be performed inherently based on the design of the microscope and the integration of the appropriate control software, such as with the JEOL-IDES system. The quality of the inpainted images is limited by two factors; the inpainting algorithm, and the sampling pattern.

Our investigations on artificially subsampled images (complete images which have had pixels selectively removed) show that the design of the sampling pattern affects the quality of the reconstruction in a drastic way. The sampling pattern, however, is limited by the stability of the scanning system; the ability of the scanning coils to move the beam to a location and for the beam to remain still at that location. The time taken for these to happen is referred to as the settling time, and is proportional to the distance between the starting location and the target location of the beam - the larger the displacement the larger the settling time. As the ratio of the settling time to the dwell time increases, streaking can be observed in images, and this is especially evident when performing fast scanning (Buban et al. 2010).

This ultimately limits the types of sampling patterns that can be used when performing probe subsampling; any sampling pattern which utilises large movements of the probe will have a large settling time to dwell time ratio, and as such will suffer a loss in quality due to this. This includes a large grouping of sampling patterns that are of interest with regards to the inpainting algorithms; random-like sampling patterns. This leaves the microscopist at an impasse; whether they should prioritise what is best for the inpainting algorithm, or what is best for the scanning system.

To contribute to this, a number of scanning solutions is presented in an attempt to minimise streaking (by minimising the settling time) during subsampling whilst also producing images which current inpainting algorithms can handle efficiently.

Fast frame-rates from STEM interlacing: Two frames for the price of one?

Jonathan Peters, Tiarnan Mullarkey, Dr James Gott, Prof. Lewys Jones

Trinity College Dublin, Republic of Ireland

Scanning transmission electron microscopy (STEM) has become a ubiquitous and powerful technique in materials science, however there is a constant compromise between signal to noise (SNR), beam dose and imaging speed. To achieve a sufficient SNR, beam-current can be increased, aggravating the imaging of beam-sensitive specimens such as biological tissues or two-dimensional materials. Alternatively, pixel dwell time can be increased, reducing image frame-rates for in-situ events and risking increased effects from scan distortions. In recent years attention have been given to sparse sampling methods, combined with compressed sensing, to reconstruct full images while only illuminating part of the specimen. These approaches, such as using spiral scans, often require purchasing new hardware, struggle with inaccuracies in the scanning system, are not real-time, and cannot be combined with existing non-rigid image corrections. Here we discuss the use of STEM interlacing as an approach to reduce beam dose and achieve higher frame-rates using existing conventional scan generators. We compare a range of deinterlacing algorithms with varying complexity, from simple line doubling to advanced in-painting algorithms, to optimise reconstruction quality and computation speed. We further show that, when combined with non-rigid alignment, our approaches can improve strain precision by more than 30% for the same electron dose. Our interlacing approach allows for greater flexibility in imaging dose sensitive materials, increased framerates for in-situ measurements, increased strain precision and can be performed, while needing no new hardware.

Experimental Optimization and Data Analysis of In-Situ Electron Energy Loss Spectroscopy

Eoin Moynihan, Temilade Adegoke, Kevin Ryan, Ursel Bangert, Michele Conroy

University of Limerick, Republic of Ireland

Through the development of transmission electron microscopy (TEM) techniques it is possible to observe changes in materials at the atomic level. Developments in aberration correctors pushed the spatial resolution of TEM and scanning TEM (STEM) to the sub-Angstrom regime. [1] Monochromators have allowed electron energy loss spectroscopy (EELS) in the TEM to progress to tens of meV energy resolution. [2,3] Direct electron detectors make fast frame-rate high speed imaging possible and has pushed forward the development of in-situ electron microscopy. [4] New hardware can drive electron microscopy forward, but we can also move forward by combining techniques, assessing their procedures, and developing a deeper understanding for the physics and geometry of the system.

This research combines the techniques of EELS and liquid in-situ electron microscopy, optimizing the experimental parameters and data analysis approach. EELS has been successfully used in in-situ microscopy before but there are clear challenges and issues to overcome. [5] A major challenge is the opposing criteria for the two techniques. Most liquid in-situ holders require a SiN membrane to encapsulate the cell where the liquid flows, resulting in a relatively thick sample. However, in EELS experiments it is often easier to use thin samples to avoid the complicated analysis involved with multiple scattering events. We investigated the effects of collection semi-angle on EELS acquisition and how much useful signal can be discarded due to high angle scattering. Data analysis techniques like fourier deconvolution, multiple linear least squares fitting, normalisation, and principle component analysis each have their own considerations as well.

EELS in the liquid cell also has issues with the liquid itself. Interactions between the electron beam and the liquid inside the cell require smaller beam currents and consequently poorer signal to noise ratio in the EELS

spectra. It is possible to work around this by purging the cell with dry nitrogen to remove the solvents while keeping the cell environment inert. [6] We were able to conduct EELS before and after a charge/discharge cycle, while using STEM imaging to capture live changes inside the cell during cycling. The procedures for experiments and analysis we developed, along with the raw and processed data we intend to make publicly available, should offer a useful training tool for the in-situ community.

Reference:

1. H. Müller, S. Uhlemann, P. Hartel, and M. Haider, Microsc. Microanal. 12, 442 (2006). doi: 10.1017/S1431927606060600
2. P. C. Tiemeijer, M. H. F. Overwijk, and A. F. de Jong, Microsc. Microanal. 6, 170 (2000). doi: 10.1017/S1431927600033341
3. O. L. Krivanek, T. C. Lovejoy, N. Dellby, and R. W. Carpenter, Microscopy 62, 3 (2013). doi: 10.1093/JMICRO/DFS089
4. M. L. Taheri, E. A. Stach, I. Arslan, P. A. Crozier, B. C. Kabius, T. LaGrange, A. M. Minor, S. Takeda, M. Tanase, J. B. Wagner, and R. Sharma, Ultramicroscopy 170, 86 (2016). doi: 10.1016/J.ULTRAMIC.2016.08.007
5. M. E. Holtz, Y. Yu, J. Gao, H. D. Abruña, and D. A. Muller, Microsc. Microanal. 19, 1027 (2013). doi: 10.1017/S1431927613001505
6. R. Serra Maia, E. Detsi, J. Corsi, M. Wang, J. Pikul, and E. Stach, Microsc. Microanal 27, 2021 (2022). doi: 10.1017/S1431927621003925
7. E.M. acknowledges funding from Irish Research Council Enterprise Scheme (EPSPG/2017/311) in conjunction with the Ernst Ruska-Centre, Forschungszentrum Jülich. M.C. acknowledges funding from the Royal Society Tata University Research Fellowship (URF\R1\201318). SFI grant 16/US/3344 allowed access to the Titan STEM for these experiments.

A preliminary investigation into plasmons in topological insulator Bi2Se3 using electron energy loss spectroscopy

Mairi McCauley, Timothy Moorsom, Craig Knox, Matthew Rogers, Philippa Sherpley, Oscar Cespedes, Bryan Hickey, Satoshi Sasaki, Donald MacLaren

University of Glasgow, UK

Topological insulators such as Bi2Se3 are of interest in plasmonics because of their topological surface states. The presence of these surface states is independent of the thickness of the topological insulator, as they are formed due to spin-orbit coupling in the bulk, which leads to a Dirac cone-like band structure[1–3]. The electrons within these surface states, described as Dirac fermions, are confined to the 2D surface and show supressed scattering. The resulting Dirac plasmonic excitations could provide a means of low-loss transport in plasmonic devices for THz computing, if the topological behaviour can be controlled.

Here we present a preliminary investigation into plasmons within multilayer Bi2Se3 using electron energy loss spectroscopy (EELS). As the plasmonic behaviour is strongly influenced by the presence of defects, we first outline the optimised substrate preparation and thin film growth protocols. TEM and STEM images are analysed to assess epitaxial strain and the nature of the substrate (silicon/sapphire)-TI interface, which would be expected to influence the plasmonic behaviour. Multi-slice STEM simulations are used to aid interpretation of the images.

We then turn to spectrum imaging of the low-loss, plasmonic excitations throughout the film. Volume plasmons at 7.2 eV and 17.3 eV were observed to be consistent with previous studies and we monitor shifts in

the plasmon energy and evidence of coupling to surface states. It is interesting to note that the volume plasmons are excited most when the electron probe is positioned within the van der Waals gaps, as indicated in figure 1d. At this energy, Bi atoms appear darkest in the spectrum image and the Se columns are more clearly distinguished than in the HAADF image. Despite the delocalised nature of plasmonic excitations, the spatial variations in plasmon intensity allow for clear identification of the layers in the spectrum image. The enhanced plasmon signal in the van der Waals gap is proposed to be similar to 'aloof mode' EELS [4], in which plasmonic signals are often seen to be enhanced when the electron probe is placed alongside a specimen and undergoes less scattering from atomic cores. Finally, we address the Dirac nature of the plasmons by outlining a momentum-resolved mapping [5,6] of the dispersion.

Reference:

[1] M Bianchi et al, 2010, Nature Communications, 1
[2] J E Moore, 2010, Nature, 464, 194–8
[3] F Ortmann et al, 2015, Topological Insulators (Wiley)
[4] P A Crozier, 2017, Ultramicroscopy, 180, 104–14
[5] F S Hage et al, 2013, Physical Review B - Condensed Matter and Materials Physics, 88
[6] S C Liou et al, 2013, Physical Review B - Condensed Matter and Materials Physics, 87

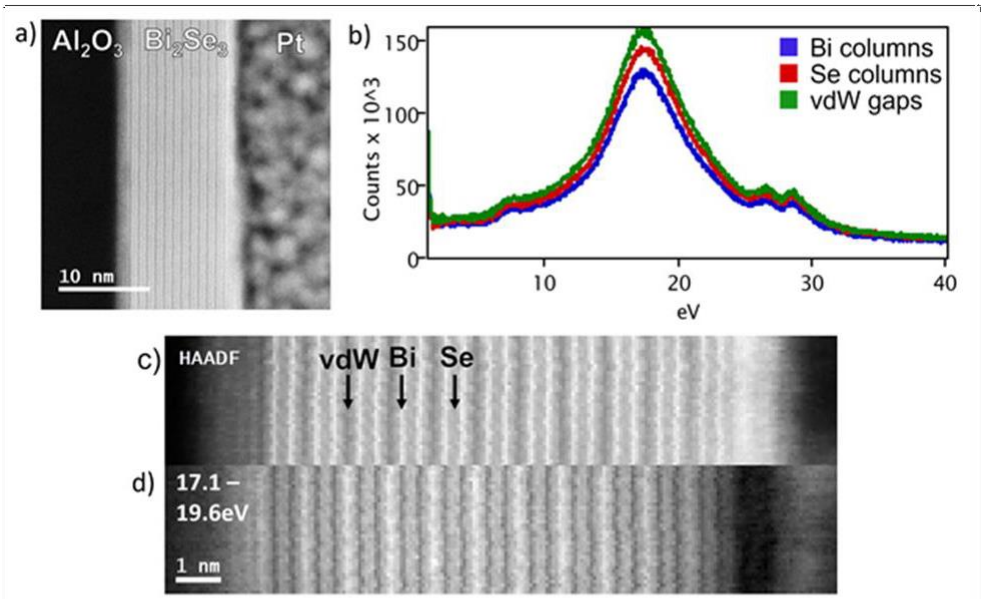

Figure 1: a) HAADF STEM image of multilayer Bi_2Se_3 sample, b) low-loss EELS spectra taken vertically at each region of the sample, c) HAADF STEM image of Bi_2Se_3 with regions indicated, d) EELS spectrum at 17.1 eV to 19.6 eV over the large volume plasmon region.

Atomic Study of Structural Changes of LiNiO2 Charged at High Voltage in Lithium Ion Batteries

Jun Chen, Robert House, Weixin Song, Paul Adamson, Peter Bruce

University of Oxford, UK

The demand of high-energy lithium-ion batteries boosts the interest in increasing Ni content in cathodes and/or raising charge cutoff voltage. The Co-free LiNiO2 (LNO) has the advantage of lower production cost, high discharge capacity and high energy density compared to traditional LiCoO2, whilst the underlying mechanisms of their capacity loss and degradation when highly charged are not fully understood. The issues

along with high charged states include surface O2 evolution and structural degradation. Finding pathways to unlock extra capacity is contingent upon an exact understanding of their structural behaviours. Several decades of effort worldwide have been devoted to developing characterization techniques across multiscale to study the mechanisms involved LNO charge storage but the knowledge still lacks regarding the nanoscale evolution. Here, we use the atomic-resolution annular dark-field scanning transmission electron microscopy (ADF-STEM) combined with electron energy loss spectroscopy (EELS) to directly examine intrigue structural and chemical change mechanisms during the LNO electrochemical process. We have directly visualised the surface densification, void formation at the bulk, stacking fault evolution of LNO over charging to high cut-off voltage. We also provide detailed EELS spectroscopy analysis of Ni oxidation changes at different charged states, comparing the trends at different distances to the surface. This offers atomic-level insights of structural behaviours and degradation mechanisms of highly charge LNO in lithium-ion batteries.

4D-STEM study of phospholipid microbubble microstructure

Bing Han, Alexander Eggeman, Sarah Cartmell, Patrick Dong Min Chang, Naomi Matsuura

University of Manchester, UK

Drug delivery systems, especially nontoxic degradable delivery agents have been investigated for the last decade in terms of agent imaging and directly lesions targeting delivery. Microbubbles are an emerging contrast agent (diagnostics) and targeted drug delivery carriers with stronger ultrasound back-scatter echo compared with tissue[1]. Phospholipid molecules are used to stabilise the interface between micron scale gas bubbles in an aqueous medium. The resulting cavity can then be filled with a drug or other biological agent. The wall structure has not been resolved using light microscopy, suggesting it is smaller than the resolution limit for these systems. However, the TEM observation of such systems was limited by the electron dose and data recording speed. As with many organic materials there aren't enough delocalized extra-nuclear electrons moving around to repair ionization damage or to remove local heat build-up, making them extremely energy sensitive systems[2]. The direct observation and study has been performed using an ultra-fast electron detector that allows extremely low electron dose, which helps to improve the microbubble stability.

Samples of microbubbles produced by the Matsuura group were coated with silica nanoparticle produced by a simplified Stober method[3] to further improve their stability when deposited on a TEM grid. 4D-STEM experiments were performed on a Talos F200X (operated at 200kV) with a Merlin diffraction camera. The virtual bright field(VBF) images (Figure 1a)) suggest a wall thickness of 30nm, given the size of the lipid molecules used this suggests a monolayer rather than the head-to-head or tail-to-tail bilayer structures as which are more commonly seen[4].

Furthermore, a pronounced beam deflection/streaking (c.f. Fig 1b) and c))), was observed when the beam traversed the bubble wall. For example, for two serial points (indicated by the red and blue positions in Fig 1 a), there is a clear streaking of the beam intensity in a direction parallel to the bubble radius (or normal to the wall surface) as seen in the line trace through the direct beam shown in Fig. 1 d) In this case, the cause of the beam deflection between scanning points was suggested to be the difference in the atomic inner potential. This difference arises from the large change in the thickness gradient for the spherical shell of material. Therefore, a geometric model (Fig. 1e)) was then developed to fit the deflection values with the thickness gradient. The streaking was then calibrated with the amorphous carbon ring (present in the diffraction patterns. to give the angular deflection values tabulated in Fig. 1f). These deflections are being compared to values published for controlled deflections from a micro-capacitor[5] to allow the wall density to be calcu-

lated and so provide further insight into the lipid arrangement present. The direct observation of microbub- bles under TEM provides a key initial step to further study their microstructure and also help to establish a protocol to analysis beam sensitive materials.

Reference:

1. Lindner J R. Microbubbles in medical imaging: current applications and future directions[J]. Nature reviews Drug discovery, 2004, 3(6): 527-533.
2. S. Inagaki, N. Goto, and K. Yoshikawa. Antibonding delocalization: Geminal Interaction of σ-bonds and Angle Strain. J. Am. Chem. Soc. 1991, 113, 7144-7146.
3. Eggeman A S, Petford-Long A K, Dobson P J, et al. Synthesis and characterisation of silica encapsulated cobalt nanoparticles and nanoparticle chains[J]. Journal of magnetism and magnetic materials, 2006, 301(2): 336-342.
4. Divecha N, Irvine R F. Phospholipid signaling[J]. Cell, 1995, 80(2): 269-278.
5. Wu M, Spiecker E. Correlative micro-diffraction and differential phase contrast study of mean inner potential and subtle beam-specimen interaction[J]. Ultramicroscopy, 2017, 176: 233-245.

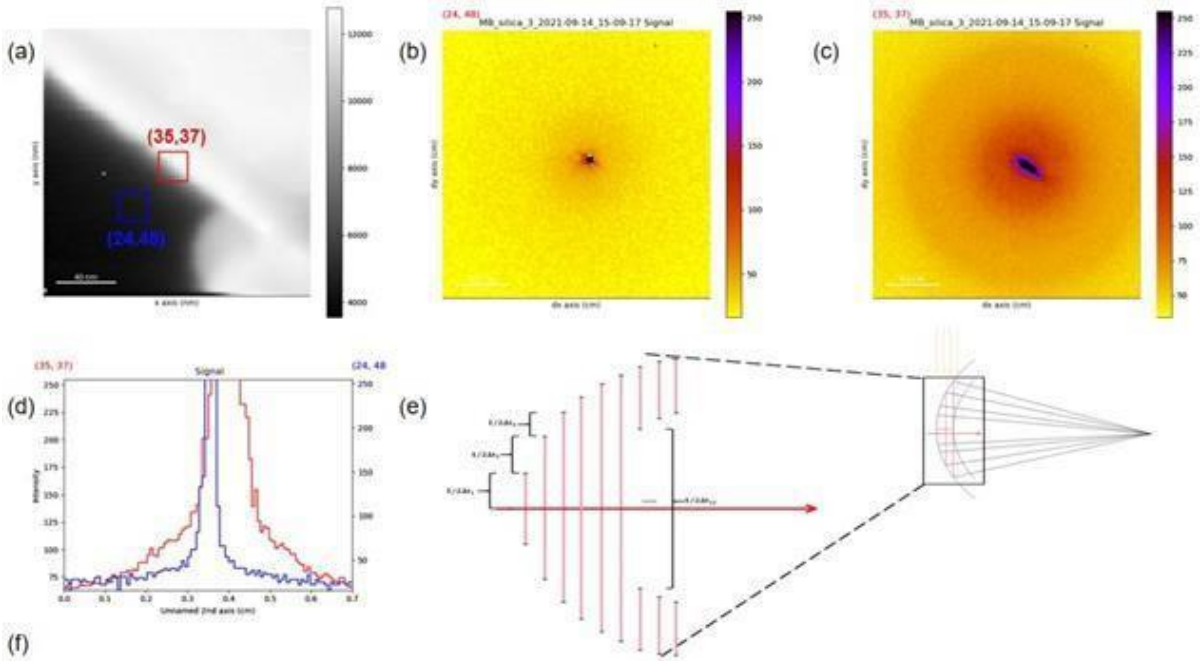

Point	(25,47)	(26,46)	(27,45)	(28,44)	(29,43)	(30,42)	(31,41)	(32,40)	(33,39)	(34,38)	(35,37)	(36,36)	(37,35)	(38,34)	(39,33)	(40,32)	(41,31)	(42,30)	(43,29)	(44,28)	(45,27)	(46,26)	(47,25)	(48,24)
ΔDeflection(cm)	None	–	–	–	0.6	1	1.6	1.6	1.9	2.2	2.8	2.5	2.4	2.4	1.8	1.6	1.5	1.5	1.4	1	0.7	-0.7	0	0
Δθ(μrad)	None	–	–	–	34.37	57.28	91.65	91.65	108.83	126.02	160.39	143.20	137.48	137.48	103.1	91.65	85.92	85.92	80.20	57.28	40.10	-40.1	0	0
Δt(nm)	0	0	0	0	0	0	0	0	0	0	20.5	16	13	10.5	10	9.5	9	8.5	8	7.5	7	-48.4	-20	-15.2

Figure 1. (a) Virtual image of a portion of microbubble wall produced from 4D-STEM data, the two scanning points in vacuum (blue) and on microbubble layer (red) have diffraction patterns shown in (b) and (c) respectively (d) Line trace across the patterns showing deflection/streaking of the direct beam. (e) Schematic of the geometric model with the change of thickness gradient. (f) Table of the incident beam deflection variation with corresponding deflection angle variation and scanned microbubble thickness variation.

Understanding Wet Impregnation Synthesis for Sustainable Hydrogenation Catalysts via In-situ TEM Observation

Rongsheng Cai, Lifeng Xiao, Sankar Meenakshisundaram, Sarah Haigh, James Paterson

University of Manchester, UK

Wet impregnation method is the most common way to synthesize commercial heterogeneous catalysts, especially on oxide supports. However, many questions remain about the mechanism of the catalyst formation process and how this depends on interactions between metal to metal and metal to support. Recently it was found that the addition of excess Cl- ions to the metal precursors dramatically influence the particle size, distribution and composition of PdAu nanoparticles supported on titania1, a good catalyst system for aerobic oxidation of alcohols and hydrogenation/hydrogenolysis of bioderived feedstock, although the mechanism remains unknown. Therefore, understanding this behaviour could open the door to new multi-metallic nanoparticle materials, with control of size, shape and composition, providing the industrial catalysts needed to address the current energy emergency. Scanning transmission electron microscopy (STEM) imaging was employed to investigate the size and elemental distribution of wet impregnated PdAu catalysts synthesized with different salt concentrations and reduced for different times (0-12 hrs). We found that for the samples synthesized with HCl as the promoter, the particle size decreases with the reduction time whereas for the samples synthesized without promoters, the particle size does not change significantly. Combined the in-situ STEM experiments with theoretical calculations on metal to metal and metal to support interactions, the role that the excess Cl- ions play in the nanoparticle growth was investigated. This suggests the addition of excess HCl to the precursors can slow down the diffusion of the metal ions on the support during the reduction, due to a strong interaction with HCl modified TiO2. Therefore, newly formed smaller particles shift the particle size distribution.

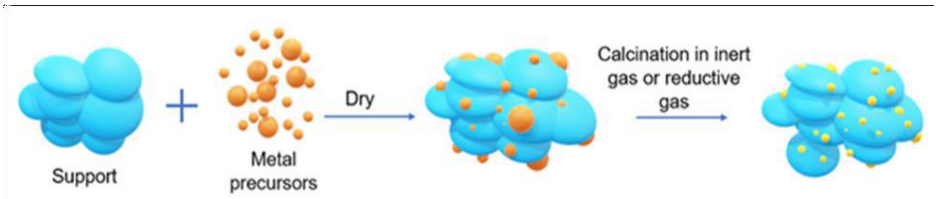

Fig. Schematic diagram of wet impregnation process

3D reconstruction and correlative multidimensional characterisation of graphene nanocomposites

Yuhan Li, Milo Shaffer

Imperial College London, UK

Carbon nanocomposites have attracted significant research interest in recent years as an efficient way of exploiting the full potential of carbon nanomaterials in various applications. To understand the structural characteristics of carbon nanocomposites, microscopic imaging techniques have been routinely applied. However, the conventional two-dimensional surface and subsurface imaging are not representative of the hierarchical nature of nanocomposites, which have an essential influence on the final properties. Serial sectioning techniques provide the possibility to probe beyond two-dimensions across multiple length scales. In this study, a 3D characterisation method combing serial sectioning and scanning electron microscopy (SEM) is established for carbon nanocomposites. The successful 3D reconstruction of volumetric structures is demonstrated in graphene nanocomposites. Crucial steps including obtaining stack images with optimal image

quality, image pre-processing and alignment are first resolved in the developed workflow. Correlative characterisation combing optical and scanning electron microscopy is realised by preserving serial sections on indium tin oxide (ITO) deposited glass slides, multimodal repetitive imaging, and landmark-based correlative registration. The significance of correlative characterisation is illustrated in three representative graphene nanocomposite systems with different graphene lateral sizes (sub-micrometre to tens of micrometre). Multimodal characterisation reveals the real volumetric multiscale structures with rich information on the dispersion, distribution, orientation, and organisation of nanoparticles. The methodology provided here is transferrable to other nanocomposite systems, which will enhance understanding towards the hierarchical structure of nanocomposites and their correlation with material performance.

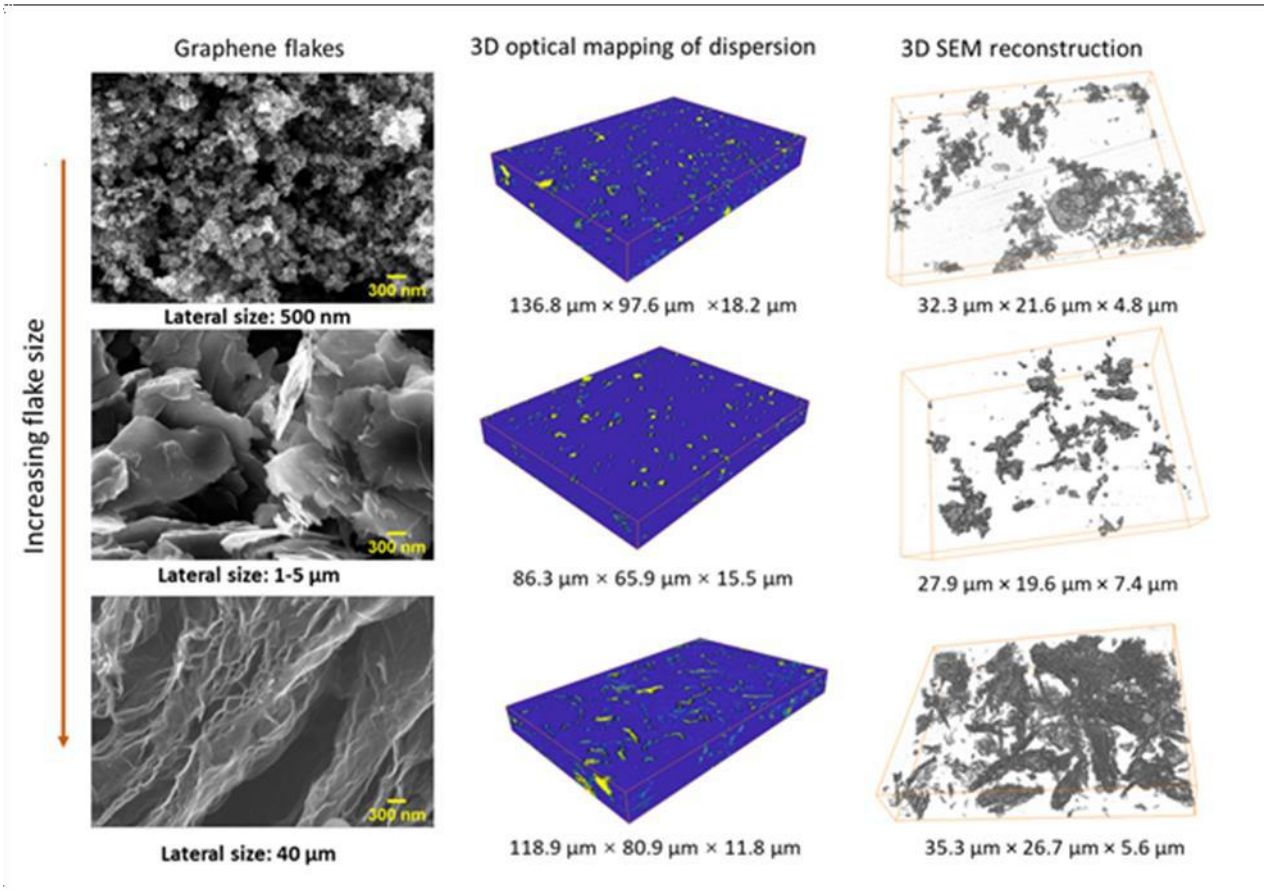

Analysing the SEI Layer Formation and Lithiation Processes of Si Nanowire Based Electrodes by Cryogenic STEM EELS and In-situ Liquid Cell Electrochemistry STEM

Temilade Esther Adegoke, Eoin Moynihan, Alan Harvey, Kevin Ryan, Ursel Bangert, Shelly Michele Conroy

Imperial College London, UK

In-situ transmission electron microscopy (TEM) allows researchers to analyse at the nano-scale and in 'real time' the electrochemical processes of the electrode materials within batteries during device operation. The active interface regions of such electrodes form solid electrolyte interface (SEI) layers during the charge and discharge cycling. The formation and movement of this functional SEI nano-interface is one of the main research fields in battery science, as it directly affects battery performance and lifetime. Of particular interest

is observing the structural and chemical evolution of this lithium-rich, extremely complex polycrystalline interface.

Si nanowires are attractive materials for applications such as lithium battery anodes due to their high theoretical capacity and ultra-low-cost for material sourcing and fabrication. The use of electrochemically active metals such as Sn for the growth of Si nanowires contributes to the overall specific capacity of the electrode. This study explores the phase change in both the Si nanowire metal seed head and the nanowire SEI layer during battery cycling. Our goal is to investigate the effect a chosen seed metal has on the Si electrode. We show the electrochemical behavior of Si based anodes using liquid cell systems is comparable to the results from bulk half-cell systems and ex-situ analysis. We then compare the benefits and drawbacks of liquid cell in-situ electrochemistry to cryogenic STEM and EELS analysis of the same system. Although in-situ electrochemistry STEM offers many advantages over other characterisation techniques, this analysis method is still in its infancy. We discuss in this presentation the benefits of multidimensional electron microscopy, spectroscopy, in-situ and cryogenic approaches to understand the complex and beam sensitive liquid-solid active regions of battery materials.

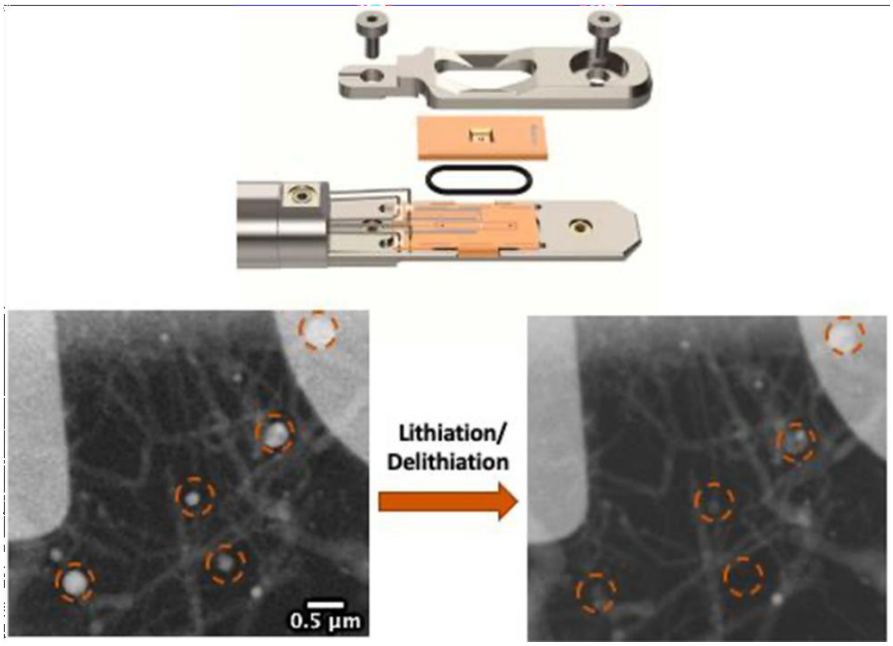

Investigating the Ferroelasticity Governing the Dynamics of Improper Ferroelectric Domain Walls by In-Situ Biasing 4D-STEM

Shelly Conroy, Steven Zeltmann, Benjamin Savitzky, Sinead Griffin, Jim Ciston, Eileen Courtney, Elora McFall, Roger Whatmore, Ursel Bangert, Colin Ophus

Imperial College London, UK

Dynamic conducting ferroelectric domain walls overturn the classical idea that our electronic circuits need to consist of fixed components of hardware.[1] Domain wall topologies in ferroelectrics are an emerging research focus in nano-electronics and potential quantum technologies.[2, 3] However, due to the high energetic cost of creating charged walls in conventional ferroelectrics they are not stable long term. Improper fer-

roelectrics circumvent this issue as their driving force is not a polar instability, but rather the critical dynam- ics of symmetry-breaking of the non-polar primary mode. With these benefits there has been a recent surge in improper ferroelectric topology research.[4]

We focus our studies on the improper ferroelectric boracite material system, known for their stable conducting and insulating domain walls and anomalous motion associated with negative capacitance.[5, 6] Boracite is an improper ferroelectric material where the primary order parameter is the physical quantity spontaneous shear strain. As a ferroelastic material the conductivity of the charged walls is governed by the shear strain direction of the neighbouring domains. Thus, traditional atomic resolution STEM polarity mapping will not give a true picture of the ferroelectric properties. In order to understand the mechanism of the wall movement and the fundamental physics governing their formation, strain analysis was completed using four-dimensional scanning transmission electron microscopy (4D-STEM)[7, 8] strain mapping. This strain analysis was then compared to the atomic resolution STEM imaging and polarity mapping.[9]

The dynamic nature of the topologies was first investigated by utilising the applied electric field of the STEM probe.[10] We show long-ranged re-ordering of shear strain during wall motion that is not present when the walls are stationary, and the complexity of the domain walls' local strain as they move through defects such as twin boundaries. Additionally we used an in-situ biasing holder set up in a parallel contact mode to compare to our previous device level work on negative capacitance measurements.[5] When mobile, the insulating domain walls have a very distinct local change in both strain and symmetry compared to the conducting walls. Finally, we explore the motion of higher order topology junctions such as vertices and vortices. Theoretical calculations confirm the shear strain to polarization vector relationship and charged topology energetics. We will present the benefits of 4D-STEM characterization for wall topologies governed by ferroelasticity, over the use of segmented detectors, where differential phase contrast mapping cannot detangle the strain and polar signals. The opportunities time-resolved 4D-STEM characterization methods can bring to the field of ferroelastic governed polar topology physics will be discussed in detail.

References:

[1] G Catalan, J Seidel, R Ramesh and JF Scott, Reviews of Modern Physics 84 (2012) 10.1103/RevModPhys.84.119
[2] JPV McConville, et al. Advanced Functional Materials 30 (2020) 10.1002/adfm.202000109
[3] D Meier and SM Selbach, Nature Reviews Materials (2021) 10.1038/s41578-021-00375-z
[4] D Meier, et al., Nature Materials 11 (2012) 10.1038/nmat3249
[5] JGM Guy, et al., Advanced Materials 33 (2021) 10.1002/adma.202008068
[6] RGP McQuaid, et al., Nature Communications 8 (2017) 10.1038/ncomms15105
[7] C Ophus, Microscopy and Microanalysis 25 (2019) 10.1017/S1431927619000497
[8] BH Savitzky, et al., Microscopy and Microanalysis 27 (2020) 10.1017/S1431927621000477
[9] E O'Connell, et al., (2021) arXiv:2110.00112
[10] M Conroy, et al., Microscopy and Microanalysis, 26 (2020) 10.1017/S1431927620023594

Acknowledgements:

Work at the Molecular Foundry was supported by the Office of Science, Office of Basic Energy Sciences, of the U.S. Department of Energy, DE-AC02-05CH11231. M.C. acknowledges funding from the Royal Society Tata University Research Fellowship (URF\R1\201318).

Multi-dimensional electron microscopy data analysis assisted by deep learning

Fanzhi Su

University of Cambridge, UK

The study of nanostructured optoelectronic devices by advanced electron microscopy techniques can reveal how morphology, crystallography, and composition affect the behaviour of the individual active components, as well as the response of the composite structure. The new generation of electron microscopes collects several spatially-resolved signals simultaneously, creating datasets that contain rich and exciting information. New data analysis strategies need to be devised and tested, before they can be used to extract and interpret this information. Deep learning neural networks, a type of machine learning designed to process complex non-linear relationships, are a promising class of tools for multi-dimensional electron microscopy analysis. Our research focuses on adapting deep learning methods to imaging, spectroscopic, and diffraction datasets acquired simultaneously, with the aim of harvesting new information on materials and composited for energy applications, such as light-emitting diodes, solar cells, and Li-ion batteries.

Electron microscopy studies on concentration gradient Ni-rich cathodes for lithium-ion batteries

May Ching Lai, Jędrzej Morzy, Dr Nirmalesh N Anthonisamy, Prof Serena Cussen, Prof Caterina Ducati

University of Cambridge, UK

Over the past decades, the drive for a high-capacity, high charge/discharge rate, long cycle-life and superior safety energy storage systems has led to a rapid advancement of cathode materials for lithium-ion batteries (LIBs). Transition-metal oxides such as $LiNi_{0.6}Mn_{0.2}Co_{0.2}O_2$ are widely used in the industry and their more Ni-rich and higher capacity counterparts are considered one of the most promising cathode candidates for next-generation LIBs. However, mechanical integrity issues such as particle cracking are thought to be one of the leading causes of structural deterioration and limited long-term cycle stability for Ni-rich cathode materials. To address these issues, a novel progressive concentration gradient cathode material was synthesised via a co-precipitation strategy. The particle core, $LiNi_{0.8}Mn_{0.1}Co_{0.1}$ oxide (NMC811), can deliver high specific capacity owing to its higher Ni content; meanwhile the surface, is designed to have a higher relative content of Mn and Co (nominally NMC442), to provide enhanced structural and thermal stability.

Macroscopic battery testing shows that the concentration gradient material possesses a higher electrochemical capability compared to pristine NMC811. The concentration gradient material has a good cycling stability, 74.5% capacity after 500 cycles at C/2, retained a discharge capacity of 127 mAh/g at 3.0 - 4.3 V. In comparison, the synthesised pristine NMC811 sample retained 20.8 % capacity under the same loading profile.

In our nanoscale study, we used focused ion beam-scanning electronic microscopy (FIB-SEM) and scanning transmission electron microscopy (STEM) to investigate the structural and compositional evolution of the gradient and pristine cathodes. Energy dispersive x-ray (EDX) mapping of cross sectional specimens was carried out to evaluate the gradient profiling in detail, assisted by machine learning-based quantification. Our results help elucidate the properties of the cathode material at the nanoscale, and contribute to the understanding of electrode stability and performance.

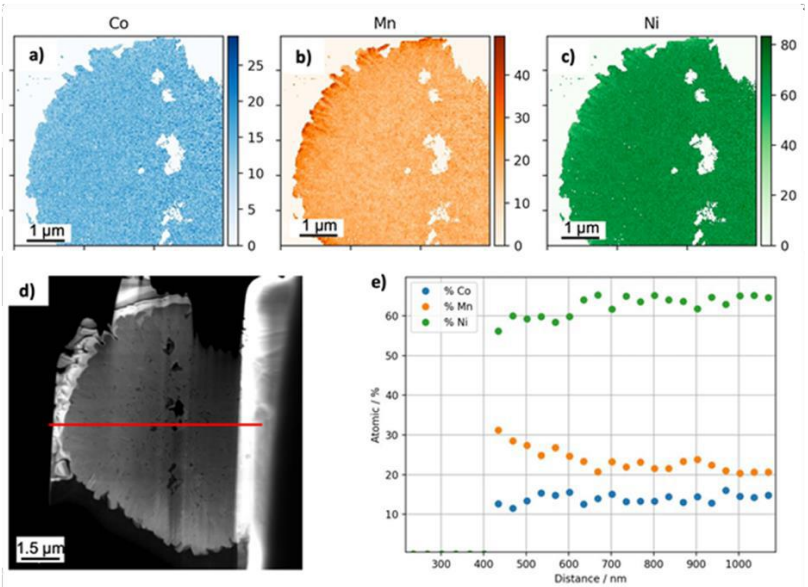

TEM cross-sectional views of concentration gradient NMC811: EDX maps consisting of elements (a) Co, (b) Mn, (c) Ni. (d) STEM HAADF image where the red line highlights the line profile of the composition change shown in (e).

Investigating Avalanche Criticality in $LaAlO_3$: The Effect of Aspect Ratio

John Scott, Blai Casals, King-Fa Luo, Atta Haq, Davide Mariotti, Ekhard Salje, Miryam Arredondo

Queen's University Belfast, UK

Ferroelastics have a variety of standalone applications in memory and acousto-optic devices and in the context of multiferroic materials, which are probably the most attractive materials, ferroelastics play a vital role in the fundamental understanding of multiferroic switching, as a large majority of multiferroics exhibit a ferroelastic component that mediates many of the observed properties, such as (super-)conductivity and magnetoelectricity.

The switching of ferroelastic domains under the application of strain is characterised by a hysteresis loop which typically appears smooth macroscopically, yet are actually formed by small discrete jumps or 'jerks' microscopically.

Most driven systems exhibiting small discrete events as such, cover a broad range of sizes dubbed as 'crackling noise' which collectively form avalanches. Mean-field theory allows for the statistical characterisation of domain wall movement by predicting the power law distribution of jerks as a scale-free process that describes the probability of a jump to some critical exponent that is characteristic of that system, derived from the maximum-likelihood method.

These power-law critical exponents can be implemented to describe the statistics of certain observables, such as the energy released during events(ϵ), and demonstrate a behaviour that is independent of the microscopic properties of that system due to scale invariance (no characteristic size or time scales). As such, other systems of equivalent exponent values are said to be of the same 'universal class', where the statistical behaviour of one class can be utilised to garner insight into another system that macroscopically appears to be much different or more intractable, such as tectonic activity and the crackling of sweet wrappers.

This study presents a new insight into the role that the sample aspect ratio has on the domain dynamics within a ferroelastic, by probing two bulk $LaAlO_3$ sample sets of differing different aspect ratios (high versus low) via in-situ heating microscopy techniques.

It was shown that the aspect ratio influences i) the resultant domain pattern at room temperature with a correlation identified between overall domain orientation and ii) the dynamical behaviour of the sample as it cools from 545°C. Moreover, the dynamics of the high aspect ratio sample set display a rather distinct behaviour where a cascading domain front forms, leading to a global reconfiguration of the microstructure.

Statistical analysis (Figure 1) shows that not only is there a difference in the overall criticality between the two samples, but that the high aspect ratio sample demonstrates a 'mixing' of the critical exponent before and after the global reconfiguration (ϵ = 1.66 to 1.33) highlighting the change in behaviour as a function of the aspect ratio.

We extend this to in situ STEM investigations, heat cycling $LaAlO_3$ lamella within different gas conditions to mirror the environment of the bulk, and explore the effect of aspect ratio by etching shapes into the lamella with AFM techniques.

These findings and the current investigation lends itself to in-situ ferroic studies, with particular regards to the development of in situ active adaptable and thermally activated devices including neuromorphic computing.

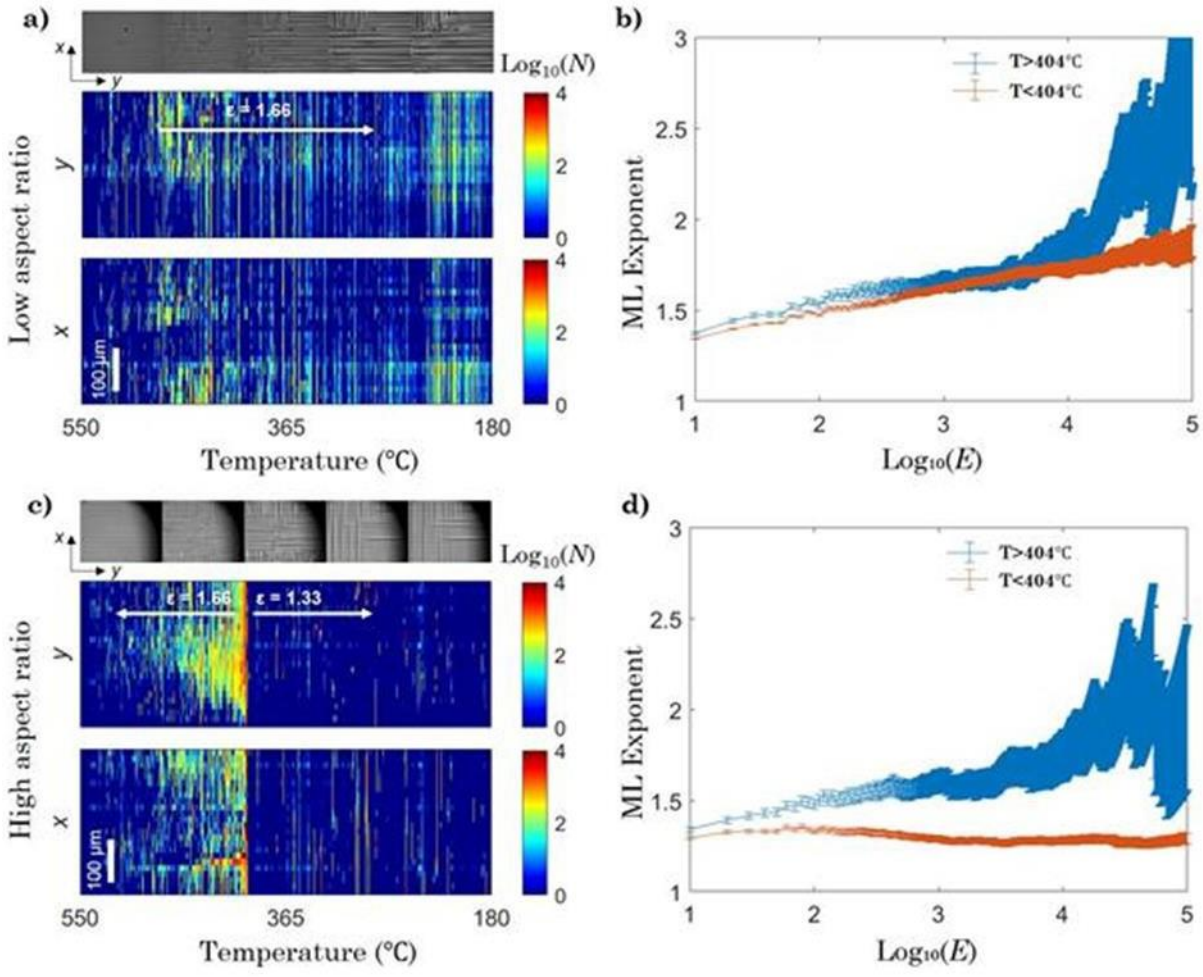

Figure 1. Spatiotemporal evolution of avalanche activity and power-law distribution. Spatiotemporal maps of avalanche activity as a function of temperature and corresponding optical progressions are shown for the a) low aspect ratio sample and c) high aspect ratio sample. The maximum likelihood (ML) exponent is derived from the gradients in the b) low aspect ratio sample and d) high aspect ratio sample, which shows a deviation from the value below 404±5°C corresponding to a mixing of the energy critical exponent. The shadowing of the snapshots in c) are from an overlapping aperture.

Characterising Surface Segregation in Bimetallic Precious Metal Catalysts using Analytical Scanning Transmission Electron Microscopy

Sam Sullivan-Allsop, Rongsheng Cai, Nicholas Clark, homas Slater, Pedro Camargo, Sarah Haigh

University of Manchester, UK

Characterisation of the surface composition of bimetallic nanoparticle catalysts provides key information for uncovering structure-property relationships and the realisation of improved catalytic behaviour. Here, we present comparison of analytical scanning transmission electron microscopy (STEM) methods applied to the characterisation of core-shell gold-platinum and gold-palladium nanoparticles. We focus on identification of elemental surface segregation (layer thickness and composition) for gold nanoparticles with low alloying contents of Pd or Pt (>10 at%). We compare results gained through semi quantitative analysis of STEM high-angle annular dark field imaging (HAADF), energy dispersive x-ray spectroscopy (EDX) and electron energy loss spectroscopy (EELS).

The gold-platinum and gold-palladium core-shell nanoparticles were produced through wet chemical synthesis routes[1] as described in Rodrigues et al. The nanoparticles are ~ 10 nm in diameter and contain a relatively low percentage composition of platinum or palladium in the sample. This introduces challenges for elemental analysis as typically percentage composition of an element below 10 %, becomes increasingly difficult to quantify.[2] Furthermore, for the gold-platinum nanoparticles the similarities in the atomic number between gold and platinum mean that the HAADF contrast will be unable to distinguish between the two elements and characteristic X-ray lines will be close together making their differentiation by EDX spectroscopy challenging. Finally, as the surface segregation is expected to be confined to the outer few monolayers of the sample, this places stringent requirements on the spatial resolution for the spectroscopic analysis (EDX and EELS).

Comparing HAADF, EELS and EDX for samples with low (<10%) and ultra-low (<1%) alloying contents we demonstrate that the combination of the multiple analytical methods was highly valuable to verify the elemental surface segregation, with all techniques having strengths and weaknesses. Advanced data processing via python/hyperspy[3] using methods such as background subtraction, model based fitting and decomposition was shown to be necessary to extract useful compositional information from the low signal to noise EELS and EDX STEM spectrum images. The spatial resolution and compositional uncertainty in the characterisation are at the limit of what is experimentally possible for the EDX analysis.

References:

1. Rodrigues, T. S. et al. Synthesis of Colloidal Metal Nanocrystals: A Comprehensive Review on the Reductants. Chem. - A Eur. J. 24, 16944–16963 (2018).
2. Watanabe, M., Williams, D. B. & Tomokiyo, Y. Comparison of detectability limits for elemental mapping by EF-TEM and STEM-XEDS. Micron 34, 173–183 (2003).
3. Peña;, F. de la et al. Hyperspy v1.6.3. (2021) doi:10.5281/zenodo.4923970.

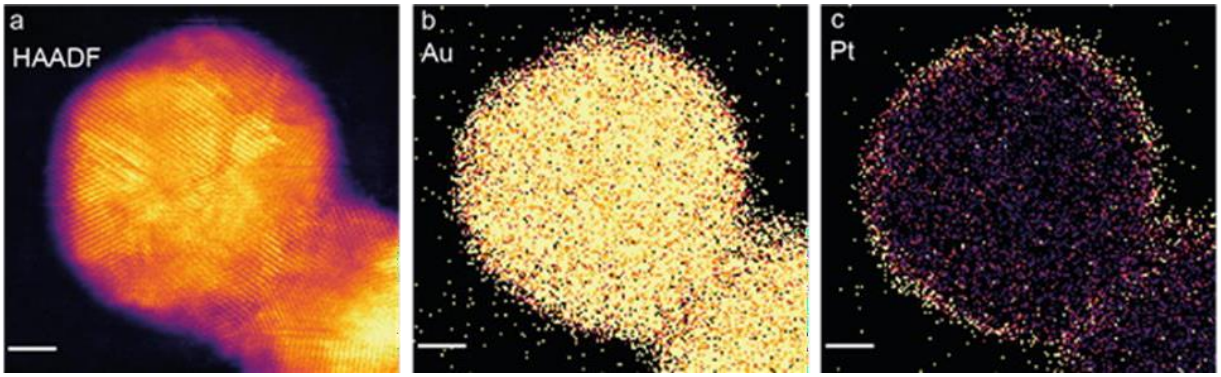

Supporting Image Caption:

(a) HAADF-STEM image of a typical Au-Pt nanoparticle (~ 7 at% Pt). (b-c) EDX elemental maps of the nanoparticle, for Au (b) and Pt (c) from the X-ray lines Au Lα and Pt Lα respectively. Scale bars are all 2 nm.

Atomistic and electronic structures of CuCrMnO4 spinel studied by probe-corrected STEM, EELS, 4DSTEM and DFT modelling.

Trung Dung Tran, Hong Ren, Rachel Kerber, Glenn Jones, Jonathan Booth, Dogan Ozkaya

Johnson Matthey Technology Centre, UK

Multiple microscopy techniques were applied for understanding atomic arrangement and electronic structures of blackbody-type CuCrMnO4 spinel. Using probe-corrected STEM, the [010]-projected atomic image of CuCrMnO4 was compared with variations of DFT-optimised models. The best experiment-fitted model could then be examined in 3D for atomistic geometry which is hinted in the [010] projection image. EELS mapping at high spatial resolution was carried out for atomic distribution of Cu, Cr and Mn. The characterised atomic arrangement is then connected with electronic structure and oxidation states of the three transition metals and oxygen found by high energy-resolution EELS (for ELNES). Variations in unit-cell geometry from bulk to surface, which was found by standard STEM-based atomic imaging, is complemented by 4DSTEM applied for large areas. As 4DSTEM experiment is also performed at the atomic resolution, virtual ABF imaging of oxygen and capability for atomistic strain mapping can also be explored.

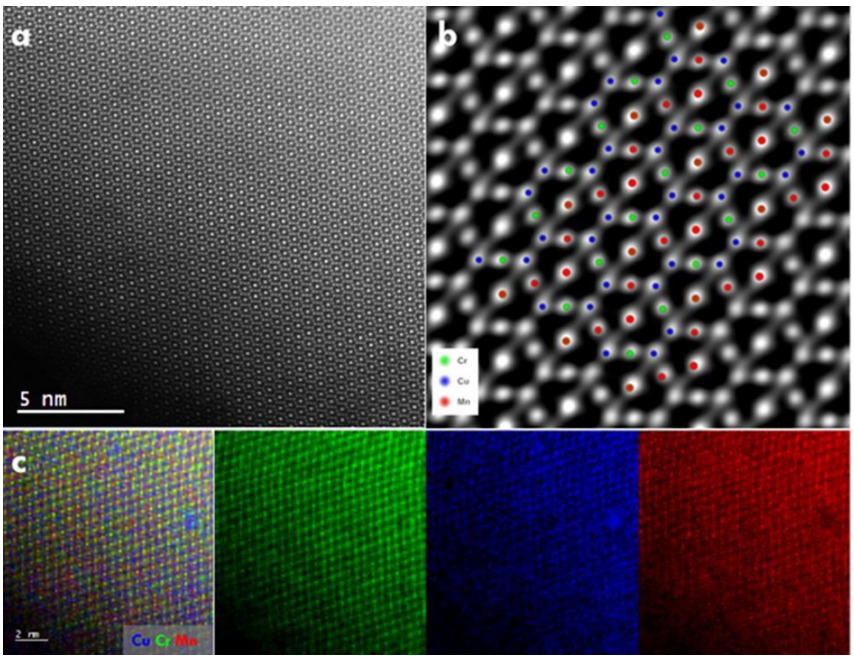

Figure 1. (a) Standard HAADF-STEM imaging of [010]-CuCrMnO4; (b) Experimental image overlayed with DFT-optimised model; (c) High-resolution EELS mapping of Cr (green), Cu (blue) and Mn (red).

Multiscale microscopic characterization of 3D volume and metal-polymer interface using cutting edge multi scale electron microscopy technologies

Min Wu

Thermo Fisher Scientific, Netherlands

Additive particles and agglomerates serve multiple functions in tires such as antioxidants, heat resisting elements, binders and others. The morphology, size and chemical distribution of these additive materials determine overall tire materials properties such as strength, elasticity, fuel efficiency, wear resistance and wet grip, etc. Meanwhile, since construction materials such as steel wires are used for reinforcement in tires, the microstructure of metal cords and adjacent rubber interface has been in significant ongoing research interests because gradual degradation of polymer metal interface fundamentally affects tire lifetime.

In this abstract we present the results of two multi scale electron microscopic characterizations on tire materials using cutting edge instruments including scanning electron microscope (SEM), STEM inside SEM chamber and multiple ion species plasma focused beam system (PFIB) integrated with femtosecond laser beam, the Helios Laser Hydra. In the first dataset we investigated the 3D morphology and chemical distribution of additive particles in tire rubber volume using Helios Laser Hydra. The cut face quality on tire rubber and additive particles using different ion species with various beam parameters is also compared and analysed. In the second dataset the polymer metal interface microstructure has been characterized using Helios Hydra system. A piece of lamella was extracted from the interface and subsequently pre examined by STEM technology inside the Helios Dual Beam chamber, before being transferred and analyzed using transmission electron microscopy (TEM) equipped with energy dispersive X-ray spectroscopy (EDS).

Nanoparticle Feature Analysis for Subsampled Images Using Deep Neural Networks

William Pearson, Nigel Browning, Yalin Zheng, Ke Chen

University of Liverpool, UK

In the field of particle nanoscopy image analysis, the size and shape (morphology) of nanoparticles and their special arrangements (dispersion) are a key analytical measure for conducting chemical experiments. Extracting quantitative information from nanoscale images of materials structures and processes is a repetitive and costly process. Incomplete images in (S)(T)EM nanoscopy presents the question of whether we will be able to make analysis of the morphology of particles before human analysis takes place. Recent strides in deep learning present a strong potential for efficient prediction for particle tracking and morphology analysis. Our aim is to develop models for the segmentation of particles from the background, calculation of their morphology and analysis of their topology. Further to this, subsampled training data can be used to retrain the model for the application of the model in a compressive sensing/ resolution upscaling use-case.

Electron Microscopy research is bottlenecked in part by the manual processing of particle morphology calculations on existing programs. Particles are often difficult to discern with constraints of large disparities in their noise patterns, spatial/temporal resolution, magnification or low signal-to-noise ratio. Park et al have developed computational techniques to analyse images for the extraction of particle information. Their research outlines several techniques for the quantitative analysis of the morphology, location, dispersion analysis and multi-object tracking analysis of nanoparticles. Our work intends to extend upon work such as this by developing a supervised machine learning model for multi-target tracking and segmentation of nanoparticles.

Deep learning models offer strong particle tracking results with fast inference time once the model has been trained. In [2], Convolutional Neural Networks have been leveraged in the analysis of nanoscopy for the identification of local structures leveraging the FCN network architecture. However, there is still need for review of the performance of tracking particles over a temporal dimension and with materials of different chemical compositions. Furthermore, application of different network architectures could offer gains in predictive performance. In our work, a transfer learning approach was applied to the MASK-FCN [3] network using Coco weights for the initial layers. Application of these networks for sub-sampled data also needs to be thoroughly investigated.

In this presentation, supervised machine learning methods such as Convolutional Neural Networks, Recurrent Neural Networks and Adversarial Neural Networks will be discussed for their ability to analyse electron microscopy images. In addition, this presentation seeks to demonstrate the performance of state-of-the-art deep learning models for finding particles in images with varying degrees of background noise.

References:

1. Park, C. and Ding, Y., 2021. Data Science for Nano Image Analysis.
2. Madsen, J., Liu, P., Kling, J., Wagner, J.B., Hansen, T.W., Winther, O. and Schiøtz, J., 2018. A deep learning approach to identify local structures in atomic-resolution transmission electron microscopy images. Advanced Theory and Simulations, 1(8), p.1800037.
3. He, K., Gkioxari, G., Dollár, P. and Girshick, R., 2017. Mask r-cnn. In Proceedings of the IEEE international conference on computer vision (pp. 2961-2969).
4. Lin, T.Y., Maire, M., Belongie, S., Hays, J., Perona, P., Ramanan, D., Dollár, P. and Zitnick, C.L., 2014, September. Microsoft coco: Common objects in context. In European conference on computer vision (pp. 740-755). Springer, Cham.

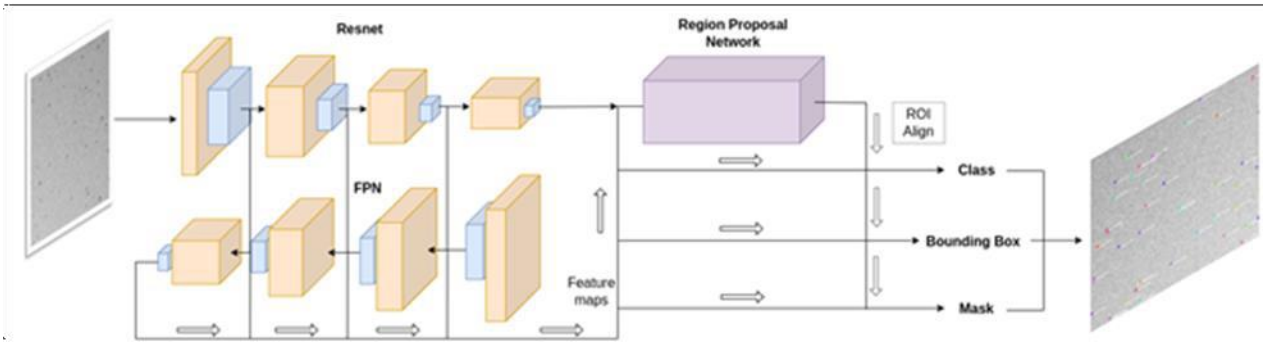

Using atomistic modelling to assist ADF-STEM based strain measurements of nanoparticle alloys

Tom Ellaby, Aakash Varambhia, Dogan Ozkaya

Johnson Matthey Technology Centre, UK

Pt catalysts are used extensively in proton-exchange membrane (PEM) fuel cells, with a particularly important role in the oxygen reduction reaction at the cathode. Improvements to these catalysts increase the efficiency of the fuel cell while reducing the loading of rare and expensive Pt. Efforts so far have led to the development of Pt nanoparticle alloys that include Co or Ni in their composition. Their higher activity is understood to be a result of the induced strain on the Pt surface, though the picture is not entirely clear.

Measuring strain from ADF images is possible for on-axis nanoparticles, though is always limited to an average of atomic columns in the beam direction. This can make it difficult to isolate the effects at the surface,

while facets are hard to identify. For monometallic nanoparticles, the intensity of the columns in the ADF images can be used to determine the number of atoms in each column, and from that reconstruct a 3D nanoparticle, but this is much harder with alloys. The different electron interactions for different elements leads to different intensities in the ADF image makes counting atoms in columns difficult, while the differences in lattice parameters can lead to much less well-defined lattices.

Modelling can be used to produce simulated ADF images of alloyed nanoparticles with arbitrary morphology and composition. This could be used to help identify the features of the real nanoparticles that are hard to distinguish from their ADF images, which we have demonstrated for pure Pt nanoparticles. For alloys, of course, there are effectively endless possible compositions, which makes finding a match difficult. As a first attempt, we have looked at core-shell alloys as well as nanoparticles with a random distribution of elements. We hope to develop this method to improve our ability to measure surface strain, which will require many more compositions to be considered.

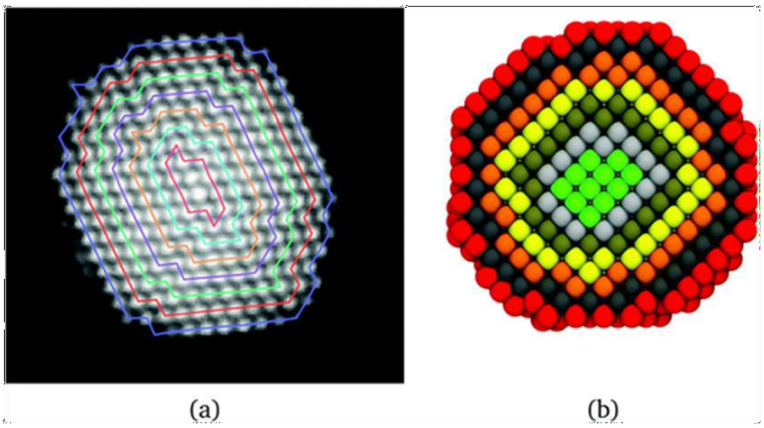

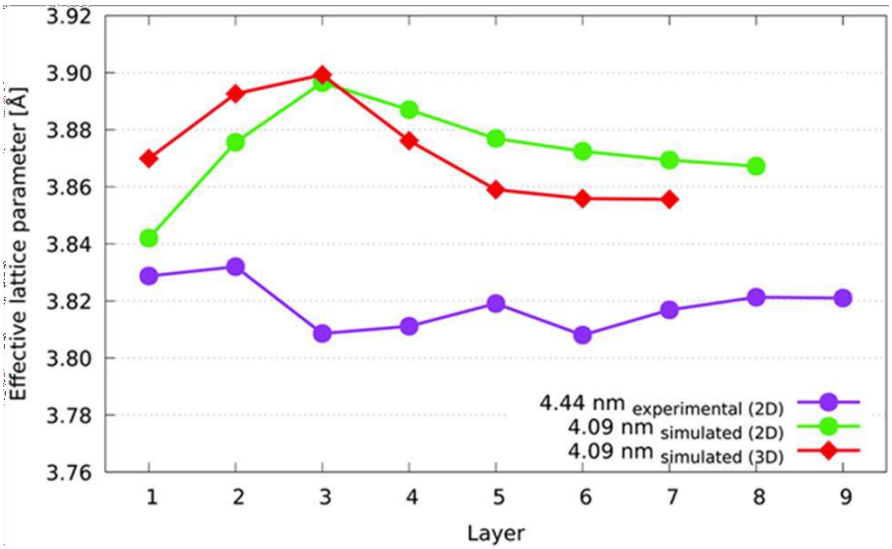

Properties of InGaAs metamorphic buffers on GaAs

Nicholas Stephen, Praveen Kumar, Agnieszka Gocalinska, Emanuele Pelucchi, Miryam Arredondo--Arechavala

Queen's University Belfast, UK

There has been a drive to develop InGaAs QW on GaAs substrate semiconductor lasers that can replace InP

based lasers currently used in telecommunications [1]. However due to the lattice mismatch between InGaAs QW and GaAs substrate, this can introduce defects which can act as non-radiative recombination centres. One approach that has been used to overcome the mismatch is metamorphic growth which involves growing a buffer layer between the substrate and active region. This creates an artificial substrate with a lattice constant of our choosing while maintaining the properties of the original GaAs substrate. This helps in reducing the strain and more importantly the number of performance reducing non-radiative recombination centres.

There are many growth parameters that can be optimised in metamorphic growth which include the growth temperature, the type of grading and the use of surfactant such as Sb [2] [3]. Recently attention has been turned to using a parabolic graded InGaAs metamorphic buffer due its ability to control misfit dislocations that relax the buffer [4]. Muller et al proposed that for a parabolic InGaAs metamorphic buffer of thickness (T)

$$\{\varepsilon_{(||)}=0 \quad 0\leq t\leq t_{o}\}$$

$$\{\varepsilon_{(||)}=-[f(t)-f(t_0)] \quad t_{o}\leq t \leq T)\}$$

where $\varepsilon_{(||)}$ is residual parallel strain, t_0 is distance at which misfit dislocations are confined and f(t) is the lattice misfit [5].

The implication of higher t_0 is lower $\varepsilon_{||}$ at the buffer and vice versa for lower t_0. However few studies focus finding t_0 and the corresponding In concertation and how the inclusion of subsequent layers, such as cladding layers for improving optical confinement, affects t_0. There is also not much known about how the strain in the growth direction (ε_{yy}) propagates at the interface with preceding layers.

Our work investigated different InGaAs/GaAs films with different properties such as orientation towards [1 1 1], inclusion of Strain Balancing layer (SBL) and using AlInGaAs/InGaP superlattice (SL) or InGaP after the InGaAs metamorphic buffer. Experimental work was conducted using a Scanning Transmission Electron Microscope (STEM) with an attached energy dispersive X-ray spectrometer (EDX). ε_{yy} was calculated using Geometric Phase Analysis (GPA) [6], which derives the local strain in a high resolution image relative to a reference region.

Our findings shown further insights into t_0 dependence on the structure and how this links to the surface roughness. Comparing two identical structures (see Supporting Figure a-b) without (A2168 0.2°) and with a SBL (A2192 0.2°), we observed that t_0 decreased and that the top of the InGaP film was rough in the sample with an SBL. This was indicative of high $\varepsilon_{||}$ earlier theoretical strain predictions [5] and corroborates previous Atomic force microscopy work [1].

Furthermore, using a SL (samples A2229 0.2° and A2248 6° in Supporting Figure c) after the InGaAs metamorphic buffer instead of InGaP (A2168 0.2°, A2168 6° and A2192 0.2° in Supporting Figure c) has increased t_0 and in turn reduced $\varepsilon_{||}$. GPA analysis of identified trends such as for A2168 samples, there is lower compressive ε_{yy} strain InGaP layer in the 6° direction compared to 0.2°.

In conclusion, our study has provided further insights into how the strain behaviour is influenced by the design of the structure. This work combined with other studies can help optimising metamorphic growth procedure for GaAs based telecommunication lasers.

References

1. Mura, E. E. et al. Importance of Overcoming MOVPE Surface Evolution Instabilities for >1.3 μm Metamorphic Lasers on GaAs. Cryst. Growth Des. 21, 2068–2075 (2021).
2. Krishnamoorthy, V., Lin, Y. W. & Park, R. M. Application of '"critical compositional difference"' concept to the growth of low dislocation density (<10^4 /cm 2) In x Ga 1− x As (x ≤0.5) on GaAs. J. Appl. Phys. 72, 1752–1757 (1992).

3. Gocalinska, A. M., Manganaro, M. & Pelucchi, E. Unexpected Aspects of Strain Relaxation and Compensation in InGaAs Metamorphic Structures Grown by MOVPE. Cryst. Growth Des. 16, 2363–2370 (2016).
4. Bosacchi, A. et al. Continuously graded buffers for InGaAs/GaAs structures grown on GaAs. J. Cryst. Growth 175–176, 1009–1015 (1997).
5. Müller, B. H. et al. Zn0.85Cd0.15Se active layers on graded-composition InxGa1−xAs buffer layers. J. Appl. Phys. 85, 8160–8169 (1999).
6. Hÿtch, M. J., Snoeck, E. & Kilaas, R. Quantitative measurement of displacement and strain fields from HREM micrographs. Ultramicroscopy 74, 131–146 (1998).

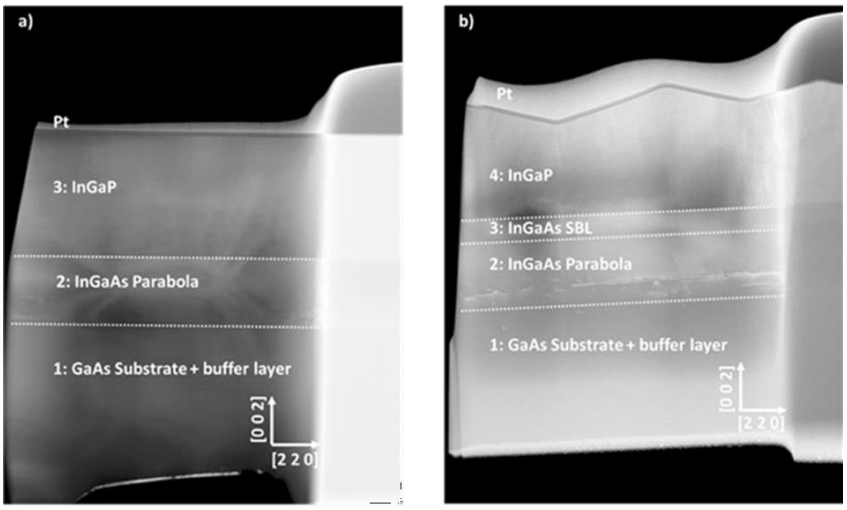

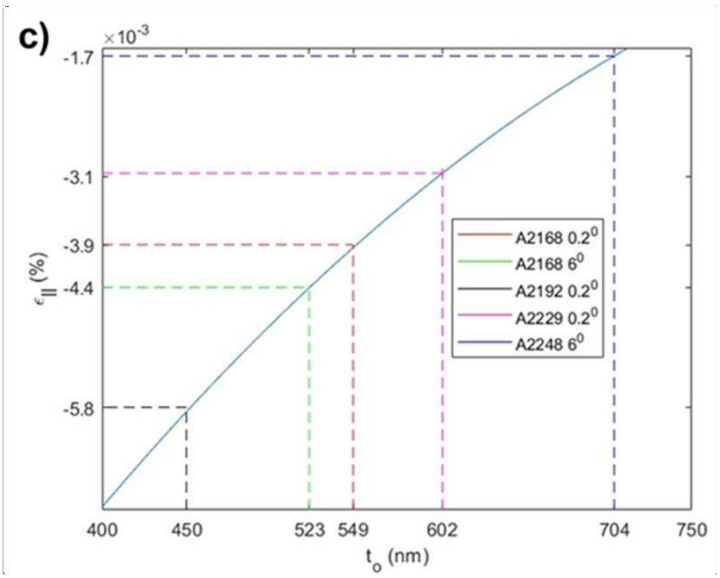

The next generation of in-situ open cell environmental double aberration corrected e-(S)TEM: ARTEMIS

Leonardo Lari, Ed Boyes, Pratibha Gai, Vlado Lazarov

University of York, UK

Atomic resolution electron microscopy is a powerful and increasingly important tool for nanomaterials characterisation that is vital to solutions of key problems in energy, IT, health, safety, transport, the environment and economy.

York is in the process of installation of in-situ open cell environmental TEM/STEM facility based on a JEOL NeoArm cold FEG double corrected instrument (ARTEMIS). Recent progress in vacuum modification and open cell gas injection systems will provide a much-improved version of the current proof-of-principle ETEM/STEM based on the first generation of aberration corrected microscope JEOL 2200FS.

Here we will discuss the wide range of capabilities associated with the machine based on variable voltage, Gas/vapour injection system, diffraction and EDX/EELS spectroscopy, and the new science enabled by this facility.

In addition, we will present in-situ results, that includes oxidation/reduction and H_2O vapour on thin films and nanoparticles in low pressure open cell environment, that were performed on the first generation environmental TEM/STEM where single atom visualisation by HAADF-STEM in an open cell controlled gas reaction environment and temperature was demonstrated.

Acknowledgement: We thank the EPSRC (UK) for funding, through capital infrastructure grant, 'Aberration-Corrected Scanning Transmission Electron Microscope with atomic resolution spectroscopy under controlled environmental conditions: AC-eSTEM'; EP/S033394/1.

Sizing fat globules and casein micelles in Milk using Cryo FIB-SEM

Fraser Laidlaw, Denise Li, Joe Bradley, Wilson Poon

University of Edinburgh, UK

Milk is a colloidal fluid of fat globules and casein micelles, suspended in a mixture of lactose, whey protein and water. The size of fat globules in milk is one of the primary factors affecting the quality of milk, such as creaming rate and texture1, while the casein micelle size is thought to have an effect on the processing of milk into other dairy products, for example in cheesemaking2,3. Knowledge of the particles sizes in milk is therefore important for many aspects of the dairy industry.

Laser diffraction and dynamic light scattering are commonly employed to size fat globules in milk for quality control or research purposes, however the results, and parameters used to describe particle sizes, can differ significantly, and can depend on the processing of the milk sample. Examples of parameters used to describe particles size in milk includes the D[4,3] (volume moment mean), D[3,2] (surface area moment mean), DV10, DV50 and DV90 (volume percentiles where 10%, 50% and 90% of the population is below the volume). The wide range of parameters used to describe the milk leads to a complicated and confusing picture of the size distribution of fat globules and casein micelles in milk.

Differential Dynamic Microscopy (DDM) is being investigated as a cheap, simple and quick method (requiring only a simple optical microscope, white light source and digital camera) to extract the size distributions of both the casein micelles and fat globules in milk. To access the accuracy of DDM, cryo FIB-SEM is being employed to measure the size distribution of both particles as a point of comparison.

Here we will present preliminary data on fat globule and casein micelle sizing using cryo FIB-SEM, discuss the cryo FIB-SEM workflow and potential challenges encountered when trying to accurately measure the size distribution of fat globules and casein micelles in milk.

References

1. Fleming et al., J. Dairy Sci. 100, (2016), 1640-1649

2. Hristov et al. 2016, Measurement of Casein Micelle Size in Raw Dairy Cattle Milk by Dynamic Light Scattering, Milk Proteins, DOI:10.5772/62779
3. Ong et al., Food Science and Technology 44, (2011), 1291 - 1302

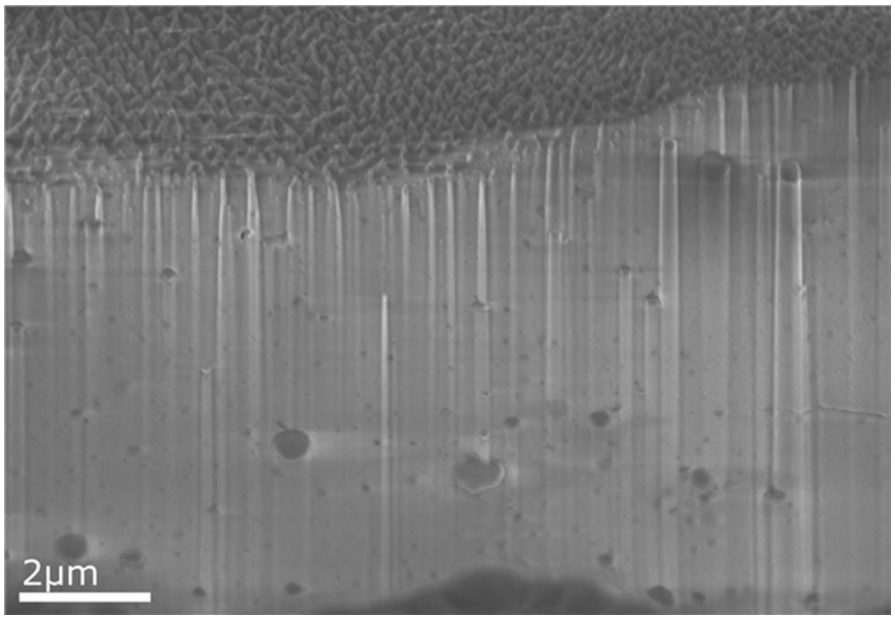

Figure 1: Cross section of whole milk. Both large and small, dark and lighter contrast particles can be seen. Darker contrast particles are thought to be the fat globules while the lighter contrast particles are the casein micelles. Further work is needed to differentiate between the fat and casein micelles.

Multimodal In-Situ Spectrum Imaging with Synchronized and Automated Stimulus Control

Liam Spillane

Gatan Inc., United States

Spectrum imaging (SI) performed in the scanning transmission electron microscope (STEM) is a well-established method for advanced materials characterization, due to the wide variety of electron scattering signals that are provided and which can be collected simultaneously, or near simultaneously, at high spatial resolution from the same specimen region. Morphological and crystallographic information may be determined from imaging and diffraction methods such as 4DSTEM, where composition may be determined from spectroscopic techniques such as energy dispersive (x-ray) spectroscopy (EDS) and electron-energy loss spectroscopy (EELS). EELS has the further capability of probing local electronic structure, enabling local measurement of chemical bonding, changes in oxidation state, phonon and/or electronic band structure characterization. For in-situ STEM analysis, the capability to capture data at: high speed, high dose efficiency, and high in-situ stimulus resolution is critical. A CMOS based transmission electron counting detector incorporated into an optimized post-column energy filter is a well proven platform for performing both STEM EELS and 4DSTEM experiments. Synchronization of an in-situ stimulus to a multiple pass SI experiment has also previously been demonstrated as an effective methodology for maximizing the in-situ stimulus resolution [1]. Here we use copper (II) oxide as a model material system and present in-situ heating results acquired using a CMOS based electron counting EELS spectrometer (GIF Continuum). These results are used to demonstrate recent advances in synchronized in-situ spectrum imaging acquisition. These advances allow automated acquisition of CBED and EDS signals at a given in situ

condition in addition to the EELS signal. Furthermore, datasets are streamed/written to disk instead of held in memory over the course of the in-situ experiment. The combination of these two key advances maximizes the information that can be extracted from a single sample even for irreversible transformations since all data can be acquired in a single experiment, in addition to maximizing the stimulus resolution at which the data can be captured. [1] L. Spillane, et al., Microsc. Microanal. 26 (Suppl 2), (2020)

List of EMAG Committee Members

Chair	Professor Jun Yuan, MInstP
Secretary and Honorary Treasurer	Dr Donald MacLaren, MInstP
Ordinary Member	Dr Miryam Arredondo-Arechavala, FInstP
Ordinary Member	Dr Laura Clark, MInstP
Ordinary Member	Dr Michele Conroy, MInstP
Ordinary Member	Dr Alexander Eggeman, MInstP
Ordinary Member	Dr Sarah Harper, MInstP
Ordinary Member	Dr Emanuela Liberti, MInstP
Ordinary Member	Dr Catriona McGilvery, MInstP
Ordinary Member	Dr Joanne Sharp, MInstP
Ordinary Member	Dr Thomas Slater, MInstP
Co-opted Member	Dr Andy Brown, MInstP

DENS solutions

Your in situ TEM solutions partner

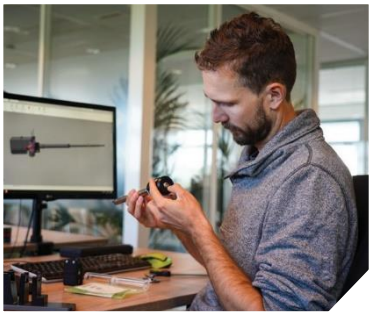

About DENSsolutions

DENSsolutions is your dedicated partner for **in situ electron microscopy research**. We develop and deliver state-of-the-art in situ solutions for **heating, biasing, gas and liquid**, allowing you to perform meaningful research at the nanoscale with a tremendous impact on a global scale.

Using **MEMS-based sample carriers**, DENSsolutions upgrades your TEM into a laboratory for nanotechnology that unveils the evolutionary nanoscale dynamics of your sample. With our dedicated technology, software and service, we support you from **sample management to data analysis**, promising reliability and accuracy every time.

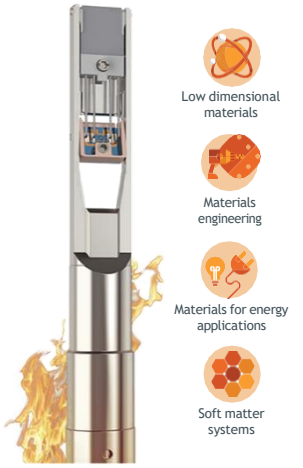

Wildfire

Heat your sample up to **1300°C** with highly accurate temperature control and unprecedented **sample stability** in all directions.

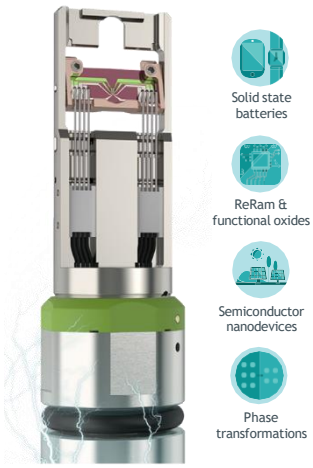

Lightning

Gain **exceptional control** over the temperature and bias of your sample. Achieve electric fields higher than **300 kV/cm** at **900°C**.

Climate

Expose your samples to a **controlled gas environment** with pressures up to **2 bar** and switch gasses in **seconds**.

Stream

Take full control over your liquid environment. Independently tune the **flow rate and liquid thickness** while heating or biasing your sample.

Curious to learn more about our advanced systems?
Then **get in touch** with us or your **local distributor** right away.

CONTACT US
www.denssolutions.com/contact

FIND YOUR LOCAL DISTRIBUTOR
www.denssolutions.com/distributors